Oligomerization and Protein-Protein Interactions of the Sensory Histidine Kinase DcuS in *Escherichia coli*

Dissertation

Zur Erlangung des Grades

Doktor der Naturwissenschaften

Am Fachbereich Biologie

der Johannes Gutenberg-Universität Mainz

Yun-Feng Liao

geb. in Taipeh, Taiwan

Mainz, 2008

Dekan:
1. Berichterstatter:
2. Berichterstatter:
Tag der mündlichen Prüfung: Feb. 11, 2009

Contents

Abstract **vii**

1 Introduction **1**
1.1 Two-component Regulatory Systems 1
1.2 DcuS and Functionally Relevant Proteins 3
1.3 Fluorescence Spectroscopy 6
1.4 Specific Aims 7

2 Theory **9**
2.1 Fluorophores 9
2.1.1 Organic Dyes 10
2.1.2 Cloned Fluorophores 10
2.2 Fluorescence Spectroscopy 11
2.3 Fluorescence Resonance Energy Transfer (FRET) 12
2.3.1 Principles of FRET 13
2.3.2 FRET Measurements 15
2.3.3 Quantitative FRET 17
2.4 Degree of Oligomerization 19

3 Materials and Methods **21**
3.1 Materials 21
3.2 Sample Preparation 24
3.2.1 Protein Preparation for *in vitro* Measurements 24
3.2.2 Cell Preparation for *in vivo* Measurements 25
3.3 Spectroscopy 27
3.3.1 Absorption Spectroscopy 27
3.3.2 Fluorescence Spectroscopy 27
3.3.3 Software 28

4 Results **29**
4.1 Samples 29

4.1.1 DcuS-FP Fusions for *in vivo* Measurements 31
4.1.2 Labeled DcuS for *in vitro* Measurements 38
4.2 Quantitative FRET Analysis 45
4.2.1 Step 1: Spectral Correction and Background Subtraction . . 46
4.2.1.1 Spectral Correction 47
4.2.1.2 Background Problems 48
4.2.1.3 Concept of Flexible Background Subtraction 49
4.2.1.4 Monte Carlo Simulation of Background Subtraction 52
4.2.1.5 Experimental Validation of Background Subtraction 57
4.2.2 Step 2: Gordon's Equation 62
4.2.2.1 Adaptation for Fluorescence Spectroscopy 62
4.2.2.2 Experimental Validation by PDI-TDI Dyad 68
4.2.3 Combining steps 1 and 2 72
4.2.3.1 Applicability and Accuracy (*in vitro*) 73
4.2.3.2 Applicability and Accuracy in living cells 73
4.2.4 Combining steps 1, 2 and 3 79
4.2.5 Conclusion 80
4.3 Oligomerization and Protein-Protein Interaction of DcuS 82
4.3.1 Oligomerization (*in vivo*) 82
4.3.1.1 Oligomeric State of DcuS in Living Cells 82
4.3.1.2 Effect of Fumarate on the Oligomeric State 83
4.3.2 Oligomerization (*in vitro*) 86
4.3.2.1 Oligomeric State of DcuS 86
4.3.2.2 Effect of Fumarate on the Oligomeric State 88
4.3.2.3 Oligomeric State of a Binding-defect Mutant . . . 92
4.3.2.4 Effect of Protein Amount on the Oligomeric State . 92
4.3.3 Protein-Protein Interactions of DcuS (*in vivo*) 95
4.3.3.1 Interaction between DcuS and CitA 95
4.3.3.2 Interaction between DcuS and DctA 96
4.3.3.3 Interaction between DcuS and Tar 97

5 Discussion **101**
5.1 Method: Quantitative FRET Analysis 101
5.2 Interaction between CFP and YFP 105
5.3 Oligomerization / Protein-Protein Interactions of DcuS 106
5.4 Outlook 108

Abbreviations **109**

Bibliography **111**

Publications and Presentations **123**

Abstract

DcuS is a membrane-integral sensory histidine kinase involved in the DcuSR two-component regulatory system in *Escherichia coli* by regulating the gene expression of C_4-dicarboxylate metabolism in response to external stimuli. The periplasmic sensory domain and cytoplasmic kinase domain of DcuS are located on opposite sites of the cell membrane. How DcuS mediates the signal transduction across the membrane remains little understood. For a more detailed understanding, this study focused on the oligomerization and protein-protein interactions of DcuS by using quantitative Fluorescence Resonance Energy Transfer (FRET) spectroscopy.

A quantitative FRET analysis for fluorescence spectroscopy has been developed in this study, not only solving the background problems in cells but taking into account the spectral crosstalk between fluorophores and the variation in the fluorophore concentrations. This analysis consists of three steps: (1) flexible background subtraction based on a multi-parameter fitting was verified theoretically and experimentally to prepare background-free spectra for further FRET quantification, (2) a FRET quantification method combining the correction for spectral crosstalk with the normalization for variations in fluorescence concentrations to accurately and robustly determine FRET efficiency (E) and donor fraction ($f_D = \frac{[D]}{[D]+[A]}$) from the corrected spectra, and (3) determining the degree of oligomerization (interaction stoichiometry) in the protein complexes by fitting a model of oligomeric states to the plot of FRET efficiency (E) against donor fraction (f_D). The accuracy and applicability of this analysis was validated by theoretical simulations and independent experimental systems with test series containing different donor-to-acceptor stoichiometries (f_D = 0-1). Because FRET efficiency depends on the ratio of donor to acceptor, this analysis allows intra- and inter-experiment comparisons by combining FRET efficiency with donor fraction. These three steps were integrated into a computer procedure as an automatic quantitative FRET analysis which is easy, fast, and allows high-throughout to quantify FRET accurately and robustly, even in living cells.

The method was subsequently applied to investigate oligomerization and protein-protein interactions of DcuS, in particular in living cells. To rule out false-positive FRET results due to interaction between CFP and YFP, different controls of CFP and YFP fusions were tested. A 1:1 CFP-YFP tandem fusion was constructed as a positive control of FRET occurrence. Analysis with our method yielded $E = 0.6 \pm 0.1$ and $f_D = 0.5 \pm 0.02$. To evaluate the direct interaction of CFP and YFP in the membrane, a non-interacting membrane-bound protein was co-expressed with DcuS. The chemotaxis receptor Tar in its truncated form (Tar^{1-331}-YFP) was used and revealed a minor FRET signal ($E = 0.06 \pm 0.01$ for $f_D = 0.39 \pm 0.02$). This signal can be regarded as an estimate of direct interaction between CFP and YFP moieties of fusion proteins co-localized in the cell membrane (false-positive). To confirm if the FRET occurrence is specific to the interaction of the investigated proteins, their FRET efficiency should be clearly above $E = 0.06$.

The oligomeric state of DcuS was examined both *in vivo* and *in vitro* by three independent experimental systems. FRET efficiency observed *in vivo* between DcuS-CFP and DcuS-YFP ($E = 0.19 \pm 0.02$ for $f_D = 0.41 \pm 0.01$) was clearly above the background of $E = 0.06$, suggesting DcuS exists as an oligomer. Only a minor effect of fumarate on the oligomerization level ($E = 0.12 \pm 0.01$ for $f_D = 0.40 \pm 0.01$) was observed. However, the range of f_D was too limited for determining the degree of oligomerization. Therefore, labeled DcuS mixtures with a full range of donor fraction (f_D = 0-1) were used *in vitro*. Consistent results from two independent FRET pairs (Alexa Fluor 488/Alexa Fluor 594, or IAF/TMRIA) *in vitro* revealed that DcuS is mainly a dimer. No effect of fumarate on oligomerization could be observed. The consistent FRET occurrence *in vitro* and *in vivo* provides evidence for homo-dimerization of DcuS as full-length protein for the first time.

Moreover, novel interactions (hetero-complexes) between DcuS and its functionally related proteins, citrate-specific sensor kinase CitA ($E = 0.15 \pm 0.02$ for $f_D = 0.41 \pm 0.01$) and aerobic dicarboxylate transporter DctA ($E = 0.28 \pm 0.03$ for $f_D = 0.48 \pm 0.01$) respectively, have been identified for the first time by intermolecular FRET *in vivo*.

In conclusion, an automatic quantitative FRET analysis was developed and successfully applied to study the oligomerization and protein-protein interactions of DcuS. This analysis can be widely applied as a robust method to determine the interaction stoichiometry of protein complexes for other proteins of interest labeled with adequate fluorophores *in vitro* or *in vivo*.

1 Introduction

1.1 Two-component Regulatory Systems

Two-component Regulatory systems in *E. coli* Metabolic regulation in bacterial cells is adaptive to environmental changes. For the metabolism of numerous substrates, *Escherichia coli (E. coli)* comprises a variety of cellular signaling pathways, in which the sensors (mostly on the cell membrane) recognize the extracellular or intracellular stimuli of substrates, the carriers on the cell membrane uptake substrates across the membrane into the cytoplasm, and enzymes or specialized proteins subsequently metabolize these substrates and regulate the expression of relevant genes in response to the external stimuli. Most metabolic pathways in *E. coli* are regulated by various two-component regulatory systems, in which a membranous sensory histidine protein kinase (HK) receives the extracellular stimuli, and a cytoplasmic response regulator protein (RR) regulates the expression of downstream target genes. Upon the signal perception (i.e. ligand binding) of the periplasmic sensory domain, the sensor kinase mediates transmembrane signal transduction (i.e. signal transmitted across the membrane) by triggering autophosphorylation at a histidine residue in its own kinase domain and by subsequent phosphotransfer to an aspartate residue in its cognate response regulator. The phosphorylation of the response regulator may induce a change in the conformation or the oligomeric state to expose its DNA binding domain to the promoter of its target genes, and consequently regulates the expression of its target genes [1–3]. Because many kinases contain more than one sensory domain to integrate different extracellular or intracellular signals, the diversity and complexity of cross-regulation in the cellular metabolic network may beyond current understandings of typical two-component regulatory systems. Not only responds to external stimuli and transmits signal to its cognate response regulator, the sensor kinase may interact with other intracellular sensor kinase(s) or carrier(s) to form various combinations of heteromeric complexes for the regulation of cellular metabolism [4, 5].

DcuSR *E. coli* can utilize C_4-dicarboxylates under aerobic or anaerobic conditions. The two-component regulatory system DcuSR (dicarboxylate uptake sensor and regulator, Fig. 1.1) in *E. coli*, consists of a membranous sensor kinase (DcuS) and a cytoplasmic response regulator (DcuR). The DcuSR system regulates the expression of genes of C_4-dicarboxylate metabolism in response to extracellular C_4-dicarboxylates (i.e. fumarate, succinate, and so on) as well as tricarboxylate (i.e. citrate) [6].

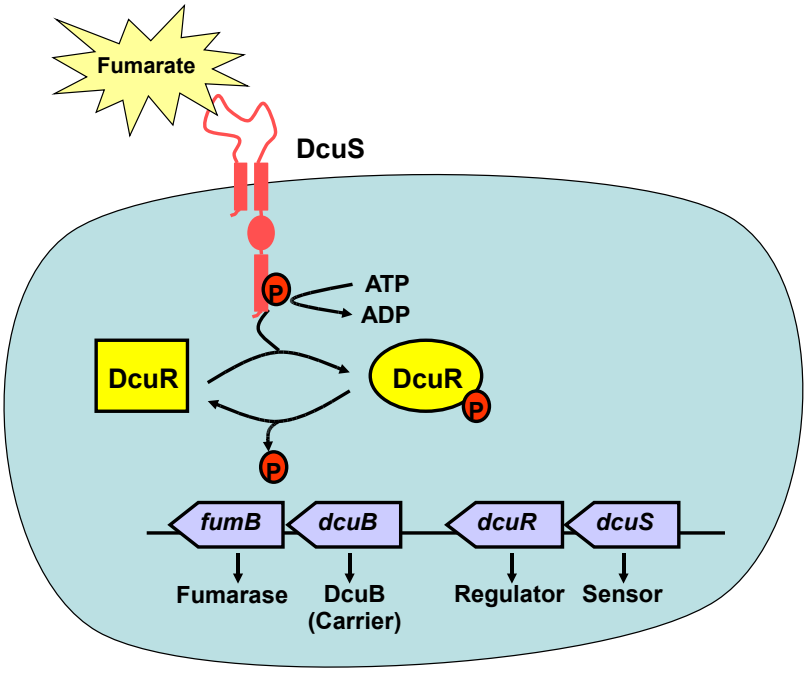

Figure 1.1: Model of the two-component regulatory system DcuSR.

Sensor kinase DcuS is located on the membrane for sensing C_4-dicarboxylates. Upon the signal perception of C_4-dicarboxylates, DcuS autophosporylates the histidine residue of its cytoplamic kinase domain, and subsequently transfers the phosphoryl group to activate its cognate response regulator DcuR. The phosphorylated DcuR is activated to regulate the gene expression (transcriptional activation or repression) to synthesize relevant proteins involved in C_4-dicarboxylate metabolism, such as fumarase FumB (*fumB* gene) to metabolize fumarate, dicarboxylate carrier DcuB (*dcuB* gene) to transport fumarate into cell, sensor DcuS (*dcuS* gene) and regulator DcuR (*dcuR* gene). Phosphorylation and DNA binding of DcuR was reported *in vitro*. Isolated DcuR protein was phosphorylated by the sensory histidine kinase DcuS, and subsequently phospho-DcuR induces expression of genes such as the *dcuB-fumB* operon, the *frdABCD* operon, and the *dctA* gene [7, 8].

1.2 DcuS and Functionally Relevant Proteins

DcuS: structure DcuS consisting of 543 amino acids (molar mass $\sim$ 61 kDa) is a membranous sensory histidine protein kinase in response to extracellular C_4-dicarboxylates and citrate [9]. Based on the predicted model of DcuS structure (Fig. 1.2) [9], the periplasmic sensory domain (PD) for signal perception is enclosed by two transmembrane helices (TM1 and TM2). Following the second transmembrane helix (TM2) are the cytoplasmic Per-Arnt-Sim (PAS) domain for putative signal perception [10, 11], and the kinase domain with a conserved histidine residue (H349) for autophosphorylation.

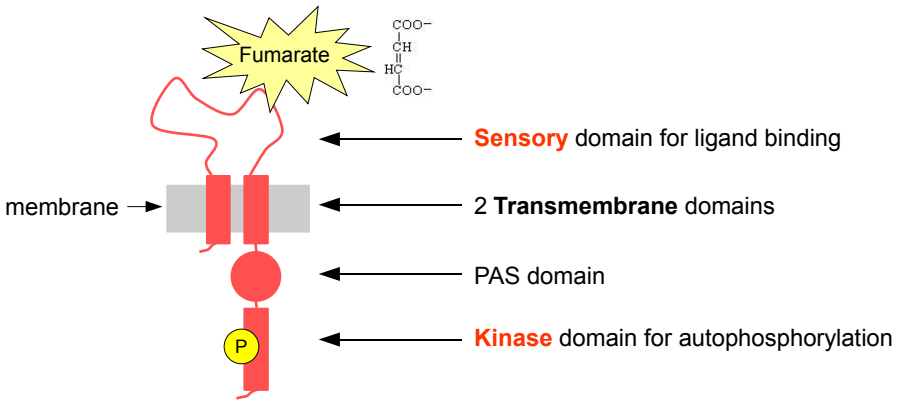

Figure 1.2: Schematic diagram of DcuS structure.

Structural and functional studies on DcuS mainly focused on the role of periplasmic sensory domain (PD or PAS_P) in signal perception [3]. NMR and crystal structures were reported for the sensory domain of DcuS [12–14]. The binding site in the periplasmic sensory domain was characterized by using various mutants of the DcuS protein [15, 16]. With respect to the cytoplasmic kinase domain of sensory histidine kinase in two-component systems, even fewer structures were elucidated [17, 18]. Recently, the structure of DcuS-PD/PAS (39.6 kDa multidomain, PAS_P-$TM_{1,2}$-PAS_C) domains in liposomes were characterized by solid state NMR [15, 19]. However, structural studies are still limited to truncated domain(s) of DcuS instead of the full-length DcuS protein.

DcuS: oligomerization DcuS is a membrane-integral sensory histidine protein kinase. The periplasmic sensory domain and cytoplasmic kinase domain of DcuS are located on the opposite sides of the cell membrane. For the signal perception, the periplasmic sensory domain of DcuS recognizes not only fumarate, but a broad range of C_4-dicarboxylates and citrate. The binding affinity of DcuS with

various C_4-dicarboxylate was examined by testing the induction of downstream gene expression *in vivo* [15]. Signal perception is suggested to depend on not only sensory domain, but PAS domain as well. In some studies, C_4-dicarboxylate sensing requires C_4-dicarboxylate carriers. The carrier-dependent regulation may be mediated by PAS domain [20]. In the presence of ATP, purified DcuS reconstituted into liposome retains the kinase activity for autophosphorylation and transfer of phosphate to DcuR *in vitro*, and an increase in kinase activity of DcuS upon adding fumarate or other effectors [9]. However, the transmembrane signal transduction, from the signal perception of the periplasmic sensory domain to the kinase activity of the cytoplasmic kinase domain, remains little understood.

Based on *in vitro* assay, the reconstituted DcuS in liposomes behaves differently from the monomeric DcuS in solution. DcuS existing as monomers in detergent showed no phosphorylation activity, whereas DcuS reconstituted in liposome possesses the phorphorylation activity. The functional state of DcuS was assumed as dimer or higher oligomer which may be essential for its kinase function [9]. Sensory domain of DcuS ($DcuS^{42-181}$) was reported to be monomeric by gel filtration chromatography at low concentration in the presence or absence of ligand, but a monomer-dimer equilibrium could be observed at millimolar protein concentrations by sedimentation equilibrium analytical ultracentrifugation at a physiological pH and ionic strength [14]. Even sensory domain of DcuS were observed as dimers in crystal structure (44 mM protein concentration), the structural studies on overexpressed recombinant protein (at mM range) may not correspond to its native conformation in living cells, because DcuS exists as a membrane protein typically low in natural abundance. So far, the oligomeric state of full-length DcuS has not been elucidated by structural studies yet.

DcuS: protein-protein interactions Protein-protein interactions among numerous proteins are ubiquitous and essential in biological metabolic network. Different two-component regulatory systems may be cross-regulated, thus the sensor kinase or response regulator of a two-component regulatory system may interact not only with its cognate partner, but also with other components from different two-component systems [21]. Besides, trans-phosphorylation between non-cognate HK-RR pairs also raise the possibility of cross-talk in signal transduction between two-component systems [22]. However, the interaction between DcuS and other structurally-correlated (histidine sensor kinase) or functionally-relevant (dicarboxylate carrier or transporter) proteins remains little understood. Only

transcription regulation of DcuSR at gene level was reported, such as repression by NarXL two-component system [23] or regulation by transcriptional regulator CRP-cAMP [24].

Citrate-specific sensory kinase: CitA The two-component DcuSR system of *E. coli* is closely related to the citrate-specific two-component CitAB system. C_4-dicarboxylate sensor DcuS is classified into the CitA family based on the sequence and structural similarity to the citrate sensor CitA [6, 25]. Citrate sensor CitA is involved in the citrate-sensing CitAB two-component regulatory system. The sensor kinase CitA of *E. coli* functions as a high-affinity citrate receptor [26, 27], whereas DcuS possessing a broader range of ligand specificity which can recognize not only many different C_4-dicarboxylates but also tricarboxylates (e.g. citrate). Crystal structures of the periplasmic sensory domain of CitA from *Klebsiella pneumoniae* reveal the first extracellular PAS domain [28], both in the citrate-free and citrate-bound state. A comparison of the two structures shows that ligand binding causes a considerable contraction of the sensor domain. This contraction may represent the molecular switch that activates transmembrane signaling in the receptor [29]. Sequence alignment of the sensory domains of the DcuS and PhoQ are homologous to CitA and are subjects of parallel structural studies [12]. A few structures were elucidated for the structural homologues of DcuS (CitA [28, 29], PhoQ [30], DctB [14, 31]), but whether DcuS may interact with other two-component system sensors/regulators is little understood.

Dicarboxylate carrier: DctA C_4-dicarboxylate sensors control the synthesis of enzymes or specialized proteins for C_4-dicarboxylate metabolism [20]. Uptake of C_4-dicarboxylates is achieved by aerobic DctA system or by anaerobic DcuAB and DcuC systems. The *dctA* gene encoding the aerobic C_4-dicarboxylate carrier (DctA) is weakly induced by the DcuSR system in response to C_4-dicarboxylate and citrate [6, 25, 32]. DctA was supposed to regulate its own synthesis through an interaction with DcuS [33], but no post-transcriptional regulation of DctA by DcuSR system was reported yet.

1.3 Fluorescence Spectroscopy

To study oligomerization and interaction of proteins, several techniques can be used, such as native gel electrophoresis [34], chemical crosslinking [35], analytical ultracentrifugation [34], affinity chromatography [36], gel-filtration chromatography [34], coimmunoprecipitation (coIP) [37], dynamic light scattering [35], atomic force microscopy [35], surface plasmon resonance (SPR) [34, 36], electron paramagnetic resonance (EPR) [38], electron microscopy (EM) [39], and so on. However, the hydrophobic nature of membrane proteins increases the technical difficulties in expression and purification of membrane proteins *in vitro*. Therefore, assays on membrane proteins are more challenging than those on soluble proteins. Besides, the natural abundance of membrane proteins is typically low. The over-expression of recombinant membrane proteins may result in higher expression levels than the physiological level of endogenous proteins, and tend to form artificial aggregates (inclusion bodies). To circumvent these problems, fluorescence techniques were used here to study DcuS. The sufficient sensitivity of fluorescence for detecting lower concentrations allows experiments at close to physiological level of native proteins. Among numerous fluorescent probes (organic fluorescent dyes, quantum dots/nanocrystals, and fluorescent proteins), the genetically-generated fusions with fluorescent proteins ensure site-specific labeling *in vivo* [40]. In contrast to the protein purification required for biochemical assays, the fluorescent protein fusions allow noninvasive and nondestructive measurements in living cells. To investigate oligomerization and protein-protein interaction, inter-molecular Förster/Fluorescence resonance energy transfer (FRET) has been widely applied.

1.4 Specific Aims

This project is a cooperation of the workgroups of Prof. Dr. Basché (Institute of Physical Chemistry, Mainz University, Germany) and Prof. Dr. Unden (Institute of Microbiology and Wine Research, Mainz University, Germany). For a more detailed understanding of the role of DcuS in the transmembrane signal transduction, two specific biological aims were addressed in this study (Fig. 1.3):

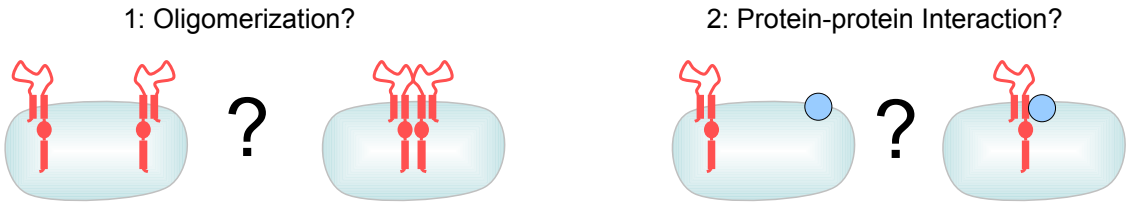

Figure 1.3: Specific biological aims: structure-functional relationships of DcuS.

1. Oligomeric State of DcuS Because isolated DcuS monomers in detergent solution revealed no function, the intermolecular interactions (homocomplex) of DcuS might be functionally related. Therefore, the oligomeric state of DcuS was investigated both *in vitro* and in living *E. coli* cells.

2. Interaction of DcuS with Functionally Relevant Proteins In addition to homo-oligomerization, protein-protein interactions (hetero-oligomerization) between DcuS and functionally relevant proteins (citrate-specific sensor kinase CitA or dicarboxylate carrier DctA) were investigated by fluorescence spectroscopy in living cells.

Prerequisite To address the biological aims 1 and 2, a fluorescence spectroscopy-based method was developed to determine FRET efficiency (E) and donor fraction (f_D) even in living cells.

2 Theory

2.1 Fluorophores

To perform fluorescence measurements, molecules of interest need to be fluorescent or labeled with fluorophores. Proteins can be labeled by extrinsic fluorophores, e.g. small organic fluorescent dyes or genetically ligated fluorescent proteins. Extrinsic fluorophores offer a wide range of fluorescence signals which can be detected in the visible range. When the fluorescence signal is shifted in the red region, it can be less interfered by background or autofluorescence. In this study, the potential labeling sites on DcuS include (1) labeling sites for extrinsic fluorescent labeling, and (2) fusion sites for genetically tagged fluorescent proteins (Fig. 2.1). For *in vitro* fluorescence measurements, DcuS possesses two cysteine (C199 and C471) residues which can be specifically labeled by thiol-reactive fluorophores (e.g. maleimide and iodoacetamide). For *in vivo* fluorescence measurements, DcuS can be genetically tagged with green fluorescent protein (GFP) variants, cyan fluorescent protein (CFP) or yellow fluorescent protein (YFP), at N- or C-terminus.

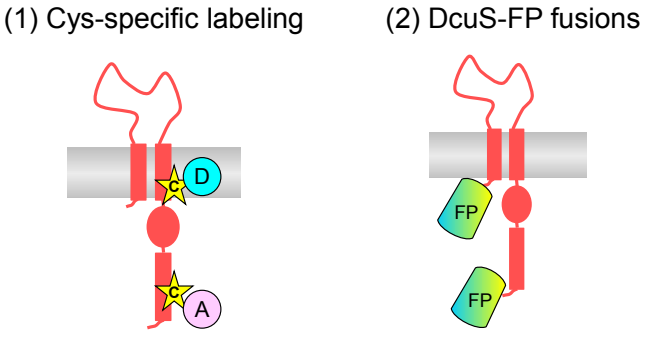

Figure 2.1: Potential labeling sites on DcuS: (1) Cysteine (Cys, C) for thiol-reactive labeling with donor (D) or acceptor (A) fluorophores; (2) terminus for fusion with fluorescent protein (FP).

2.1.1 Organic Dyes

Organic fluorescent dyes are available with different reactive groups which can selectively label amino-containing amino acid (lysine) or thiol-containing amino acid (cysteine). An alternative way of protein labeling is non-covalent bonding. Commonly used fluorescent dyes usually have high molar extinction coefficient and high quantum yield. Cysteine residue is not very common in most proteins, and therefore can be labeled with high selectivity by thiol-reactive probes. Moreover, the optimal pH for reaction of cysteine-specific labeling is at physiological pH. In this study, DcuS contains two cysteine residues: a membranous cysteine (C199) and a cytosolic cysteine (C471). For cysteine-specific labeling of DcuS with fluorescent dyes, two categories of thiol-reactive groups were used, including (1) maleimide and (2) iodoacetamide.

1. Maleimide: Alexa Fluor 488 C_5-maleimide (hereafter cited as Alexa 488) is a spectrally similar alternative of Fluorescein containing thiol-reactive maleimide group. Alexa Fluor 594 C_5-maleimide (hereafter cited as Alexa 594) is spectrally similar to Texas Red dye, and can be used as a FRET acceptor of Alexa 488.

2. Iodoacetamide: 5-IAF (5-iodoacetamidofluorescein) is a 5-isomer of fluorescein derivative. 5-TMRIA (Tetramethylrhodamine-5-iodo-acetamide dihydroiodide) is a 5-isomer of TMR (tetramethylrhodamine) derivative. 5-IAF and 5-TMRIA can be used as a FRET pair.

2.1.2 Cloned Fluorophores

In addition to conventional fluorescent dyes, DcuS can also be genetically fused with green fluorescent protein (GFP) or its variants. The 2008 Nobel Prize in Chemistry rewards the initial discovery of GFP and a series of important developments which emphasizes the role of GFP as a tagging tool in bioscience [41–43]. GFP was first observed in the jellyfish *Aequorea victoria* in 1962. As a non-invasive labeling in living cells, GFP and its genetically engineered spectral variants from the blue to red spectrum (blue: BFP; cyan: CFP; yellow: YFP; or red: RFP) are recently widely used to study proteins of interest in living cells [43]. Wild-type GFP contains 238 amino acids, folding as a 11-stranded β-barrel cylinder threaded by an α-helix running up the axis of the cylinder. The fluorescent moiety of GFP protein is a Ser-Tyr-Gly derived chromophore buried deeply in the center of the

β-barrel [44, 45]. In this study, the enhanced cyan fluorescent protein (ECFP containing mutations F64L, S65T, Y66W, N146I, M153T, V163A) is used as the donor fluorophore, coupled with enhanced yellow fluorescent protein (EYFP including S65G, V68L, Q69K, S72A, and T203Y) as the acceptor in living cells. The Förster distance between CFP and YFP pair is 4.92 nm $\pm$ 0.10 nm[46]. To examine the protein-protein interactions in living cells, DcuS or protein of interest was genetically fused with either CFP or YFP to generate fusion proteins. Subsequently, CFP-tagged and YFP-tagged protein fusions were co-expressed in *E. coli* cells as a FRET pair for *in vivo* measurements.

2.2 Fluorescence Spectroscopy

In this study, fluorescence spectroscopy was performed by recording fluorescence spectra to obtain the fluorescence intensity (F) and emission maximum (λ_{max}) for further quantification of interaction stoichiometry. A brief introduction to fluorescence spectroscopy is given as follows [47]. A molecule can absorb light which brings it to an electronically excited state. Fluorescence is the emission of light from the excited singlet state. The spectral distribution of fluorescence can be measured with a spectrofluorometer by recording the fluorescence excitation or emission spectra. An excitation spectrum is recorded when the emission wavelength (λ_{em}) is fixed, and an emission spectrum is recorded when the excitation wavelength (λ_{ex}) is fixed. A spectrofluorometer (Fig. 2.2) generally contains an excitation light source, excitation monochromater, sample holder, emission monochromater, and detector.

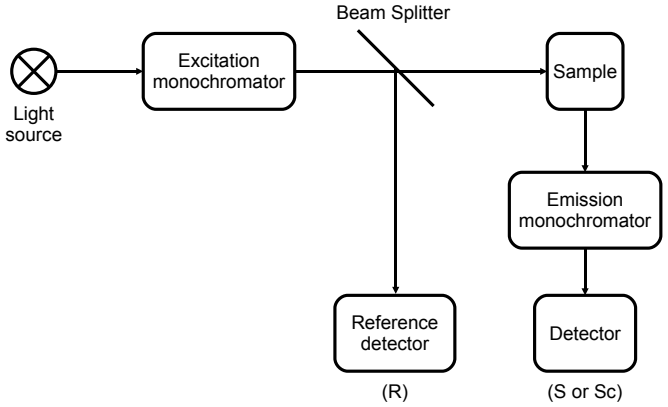

Figure 2.2: Schematic diagram of a spectrofluorometer

Split by a beam splitter between excitation monochromater and sample holder,

most of the light travels through the sample holder and a minor fraction of the light to the reference detector. The fluorescence signal (S) is recorded by the detector after the emission monochromator. Fluorescence is usually detected at a right-angled geometry relative to the excitation light source to reduce the interference of scattered excitation light. A reference signal (R) is simultaneously recorded by the reference detector to correct the time-dependent fluctuation of the light source and the wavelength-dependence of the excitation monochromator. For recording excitation spectra, the S signal is corrected by R signal to yield $\frac{S}{R}$. For recording emission spectra, the S signal is corrected by an instrument-dependent correction factor for the detector (c) to yield $\frac{S \times c}{R}$. The concentration of the fluorophore should be kept diluted to avoid the inner filter effects.

The fluorescence emission spectra depends on the chemical structure and the solvent surrounding of the fluorophore. Because the fluorophore always emits fluorescence from the lowest excited state, the shape of emission spectrum is generally independent of the excitation wavelength, known as Kasha's rule.

The fluorescence quantum yield (QY) is the number of emitted photons relative to the number of absorbed photons (ranging from 0 to 1). The relaxation process of a fluorophore is either though emission (rate k_F) or non-radiative decay (rate k_{nr}). The fraction of fluorophores that decay through emission (k_F) is the fluorescence quantum yield:

$$QY = \frac{k_F}{k_F + k_{nr}} \tag{2.1}$$

2.3 Fluorescence Resonance Energy Transfer (FRET)

In this study, fluorescence resonance energy transfer (FRET) measurements were performed to study the oligomerization of DcuS (aim 1) and protein-protein interactions between DcuS and relevant proteins (aim 2). To address these questions with respect to interaction relationships, this study focuses on the occurrence of FRET when the donor and acceptor are in close proximity, instead of determining accurate distances between donor and acceptor. Interaction between donor- and acceptor-labeled proteins can bring the FRET pair (donor and acceptor fluorophores) within the distance for FRET to occur. Therefore, self-association or binding interaction can be inferred by the occurrence of FRET between the donor-acceptor pair of fluorophores. The distance-dependence of FRET efficiency at nanometer scale is applicable to detect the interaction between two fluorophores

on two different proteins (inter-molecular FRET) which can be used to probe protein-protein interactions or co-localization between proteins.

2.3.1 Principles of FRET

Fluorescence (Förster) Resonance Energy Transfer (FRET) is the distance-dependent transfer of excitation energy from a donor fluorophore (D) to an acceptor (A) in a non-radiative process (without the emission of photons) through long-range dipole-dipole interactions. The rate of energy transfer (k_T) is given by [47]

$$k_T = \frac{1}{\tau_D}\left(\frac{R_0}{r}\right)^6 \tag{2.2}$$

where r is the distance between donor and acceptor, and R_0 is the Förster distance, the distance at which the FRET efficiency is 50%. In other words, R_0 is the distance between donor and acceptor at which 50% of the excitation energy of the donor is transferred to the acceptor and 50% deactivates in other radiative and nonradiative processes.

Energy transfer competes with the spontaneous decay of the donor ($\frac{1}{\tau_D}$). The transfer rate (k_T) is dependent on the inverse sixth power of the distance (r) between donor and acceptor fluorophores. The efficiency of energy transfer is the ratio of energy transfer rate (k_T) to the total decay rate of the donor [47].

$$E = \frac{k_T}{k_T + k_{nr} + k_F} = \frac{k_T}{k_T + 1/\tau_D} \tag{2.3}$$

Taken together, the FRET efficiency (E) can be described by Eq. (2.4).

$$E = \frac{R_0^6}{R_0^6 + r^6} = \frac{1}{1 + (\frac{r}{R_0})^6} \tag{2.4}$$

In other words, the FRET efficiency (E) depends on the distance between donor and acceptor (r) and the Förster distance (R_0). Fig. 2.3 illustrates the distance dependence of FRET efficiency. The FRET efficiency (E) is strongly dependent on the distance between donor and acceptor (r) when the distance between donor and acceptor is around the Förster distance (R_0). Therefore, FRET method is especially suitable to detect interactions of biomolecules, e.g. conformational changes or protein-protein binding.

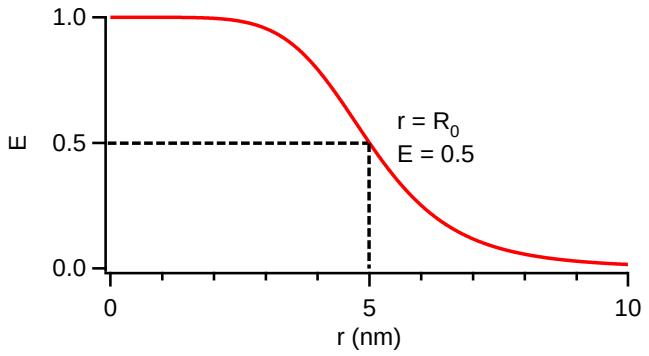

Figure 2.3: Distance dependence of fluorescence resonance energy transfer. R_0 is the Förster distance, the distance at which the FRET efficiency (E) is 50%. According to Equation (2.4), here R_0=5 nm.

Förster distance (R_0) depends on the quantum yield of the donor (Q_D) in the absence of acceptor, the orientation factor (κ^2) describing the relative orientation between dipoles of donor and of acceptor, the refractive index of the medium (n), and the extent of spectral overlap ($J(\lambda)$) of the emission spectrum of donor with the absorption spectrum of acceptor [47]:

$$R_0 = 8.79 \times 10^3 \left[QY_D \kappa^2 n^{-4} J(\lambda) \right]^{1/6} \tag{2.5}$$

FRET efficiency increases with the spectral overlap ($J(\lambda)$) of the spectrum of donor with the absorption spectrum of acceptor. The extent of spectral overlap is given by [47]

$$J(\lambda) = \frac{\int_0^\infty F_D(\lambda)\varepsilon(\lambda)\lambda^4 d\lambda}{\int_0^\infty F_D(\lambda) d\lambda} \tag{2.6}$$

where $F_D(\lambda)$ is the fluorescence intensity of the donor, $\varepsilon(\lambda)$ is the molar extinction coefficient of the acceptor at λ.

The efficiency of energy transfer between donor and acceptor also depends on the dipole-dipole orientation. The orientation factor (κ^2) represents the relative orientation between donor and acceptor dipoles. The value of κ^2 ranging from 0 to 4. Because both dipoles of donor and acceptor can rotate much faster than the occurrence of FRET in most cases, κ^2 is commonly assumed to be an averaged value of 2/3 [47].

2.3.2 FRET Measurements

Upon excitation of the donor fluorophore, the occurrence of FRET leads to a decrease in donor emission intensity (quenching of the donor fluorescence or quenched donor emission). If the acceptor is a fluorophore, the quenched donor emission is simultaneously accompanied by an increase in acceptor emission intensity (sensitized acceptor emission). FRET efficiency can be experimentally determined by quenched donor emission or sensitized acceptor emission (steady-state spectra as Fig. 2.4) or by a decrease of donor fluorescence lifetime in the presence of the acceptor (time-resolved measurements).

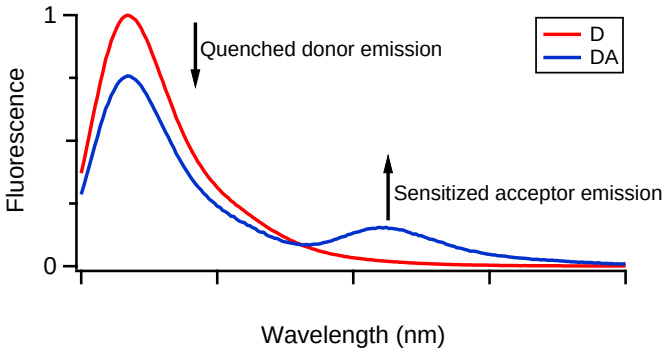

Figure 2.4: Intensity-based FRET (steady-state spectra): reduced donor emission coupled with sensitized acceptor emission.

Reduced Donor Emission Intensity-based FRET measurement determines FRET efficiency by analyzing steady-state spectra of donor by Eq. (2.7). FRET efficiency can be measured by a decrease in the quantum yield of donor measured in the presence of acceptor (QY_{DA}) compared with that in the absence of acceptor (QY_D), or by the decrease in the fluorescence intensity of donor measured in the presence of the acceptor (F_{DA}) compared with that in the absence of the acceptor (F_D) [47].

$$E = \frac{QY_D - QY_{DA}}{QY_D} = \frac{F_D - F_{DA}}{F_D} = 1 - \frac{F_{DA}}{F_D} \tag{2.7}$$

To calculate the FRET efficiency by analyzing fluorescence intensities from steady-state spectra, the concentrations of donor and acceptor should be taken into account.

Sensitized Acceptor Emission The spectral overlap between acceptor absorption and donor emission is required for the occurrence of FRET, but the acceptor in

a FRET pair is not necessarily fluorescent. If the acceptor is a fluorophore, the occurrence of FRET can lead to an increase in acceptor emission intensity (sensitized acceptor emission) which simultaneously accompanies with a decrease in donor emission intensity (reduced donor emission). The FRET efficiency calculated from sensitized acceptor emission without direct excitation of donor at acceptor excitation wavelength is given by [47]

$$E = \frac{\varepsilon_A(\lambda_D^{ex})}{\varepsilon_D(\lambda_D^{ex})}[\frac{F_{AD}(\lambda_A^{em})}{F_A(\lambda_A^{em})} - 1](\frac{1}{f_D}) \tag{2.8}$$

where $\varepsilon_A(\lambda_D^{ex})$ and $\varepsilon_D(\lambda_D^{ex})$ are the extinction coefficients (or absorbance) of the donor and acceptor at the donor excitation wavelength (λ_D^{ex}). $F_A(\lambda_A^{em})$ is the acceptor intensity measured at an acceptor emission wavelength (λ_A^{em}) in the absence of donor, $F_{AD}(\lambda_A^{em})$ is the acceptor intensity measured in the presence of donor. f_D is the fractional labeling with the donor. To determine the FRET efficiency from the sensitized acceptor emission is more complicated than from reduced donor emission, because the measured acceptor intensity contains not only FRET signal but also the signals from direct excitation of donor ($F_D(\lambda_A^{em})$) and acceptor ($F_A(\lambda_A^{em})$) at acceptor excitation wavelength (λ_A^{ex}). The measured acceptor intensity must be corrected for these spectral crosstalk (bleed-through) for calculating FRET from sensitized acceptor emission by Eq. (2.8).

Reduced Donor Lifetime The occurrence of FRET shortens the average lifetime of a donor. Lifetime-based FRET measurements determines FRET efficiency by analyzing the reduced donor lifetime (τ) in the presence and absence of an acceptor (Eq. (2.9)) [47].

$$E = \frac{\tau_D - \tau_{DA}}{\tau_D} = 1 - \frac{\tau_{DA}}{\tau_D} \tag{2.9}$$

where τ_D is the fluorescence lifetime of the donor measured in the absence of the acceptor, and τ_{DA} is the fluorescence lifetime measured in the presence of the acceptor. The fluorescence lifetime is a concentration-independent parameter of the fluorophore. However, specialized instrumentation for lifetime measurements is more complex and more expensive than steady-state spectrofluorometer, and therefore not widely used in biological laboratories.

2.3.3 Quantitative FRET

FRET efficiency In this study, Eq. (2.10) (hereafter cited as Gordon's equation) reported in Gordon *et al.* (1998) [48] was applied to calculate the FRET efficiency from the measured spectra. Gordon's equation was originally developed for fluorescence microscopy. Spectral crosstalk is a common problem and may result from several aspects, such as the direct excitation of acceptor at donor excitation wavelength, and the detection of donor emission at acceptor emission wavelength. Besides, the FRET efficiency (E) depends on the fluorophore expression levels of the donor ([D]) and the acceptor ([A]). By combining reduced donor emission with sensitized acceptor emission, Gordon's equation aims to correct the spectral crosstalk and to normalize the FRET efficiency by fluorophore concentrations. In this study, the FRET efficiency (E) were calculated by Gordon's equation.

$$
\begin{aligned}
E &= 1 - \frac{QY_{DA}}{QY_D} \\
&= \frac{F_f - D_f \cdot \frac{F_d}{D_d} - \frac{A_f - F_f \cdot \frac{A_d}{F_d}}{1 - \frac{F_a}{A_a} \cdot \frac{A_d}{F_d}} \left[\frac{F_a}{A_a} - \frac{F_d}{D_d} \cdot \frac{D_a}{A_a} \right]}{G \left[1 - \frac{D_a}{F_a} \cdot \frac{F_d}{D_d} \right] \left[D_f + \frac{F_f - D_f \cdot \frac{F_d}{D_d} - \frac{A_f - F_f \cdot \frac{A_d}{F_d}}{1 - \frac{F_a}{A_a} \cdot \frac{A_d}{F_d}} \left[\frac{F_a}{A_a} - \frac{F_d}{D_d} \cdot \frac{D_a}{A_a} \right]}{G \left[1 - \frac{D_a}{F_a} \cdot \frac{F_d}{D_d} \right]} \left[1 - G \cdot \frac{D_a}{F_a} \right] - \frac{A_f - F_f \cdot \frac{A_d}{F_d}}{1 - \frac{F_a}{A_a} \cdot \frac{A_d}{F_d}} \cdot \frac{D_a}{A_a} \right]}
\end{aligned}
\tag{2.10}
$$

Nomenclature: Filter Sets and Samples In Gordon's equation, three filter sets were used, termed by capital letters (Table. 2.1): Donor (D), FRET (F), and Acceptor (A). Three types of samples were prepared, represented by lower case letters (Table. 2.2) containing donor (d), acceptor (a), or a mixture of donor and acceptor (f).

Filter Set	Excitation Wavelength	Emission Wavelength
D (Donor Filter Set)	excite donor	detect donor
A (Acceptor Filter Set)	excite acceptor	detect acceptor
F (FRET Filter Set)	excite donor	detect acceptor

Table 2.1: Filter sets (D, A, F) in Gordon's equation.

Sample	Fluorophore(s)
d	donor only
a	acceptor only
f	both donor and acceptor

Table 2.2: Fluorophore(s) in samples (d,a,f) in Gordon's equation.

Experimental values For the calculation of FRET efficiency by Gordon's equation, two fluorescence emission spectra were recorded (excited at donor excitation wavelength and at acceptor excitation wavelength, respectively) for each sample. From these two measured spectra, three fluorescence intensities were obtained: two fluorescence intensities (Donor signal and FRET signal) were obtained from the spectrum excited at donor excitation wavelength, and one intensity (Acceptor signal) from the spectrum excited at acceptor excitation wavelength. Combining 3 filter sets (D,A,F) with 3 samples (d,a,f), 9 signals can be obtained (Table. 2.3), including: 3 from the sample containing donor only (D_d, A_d, F_d), 3 from the sample containing acceptor only (D_a, A_a, F_a) and 3 from the sample containing both donor and acceptor (D_f, A_f, F_f).

	d	a	f
D	D_d	D_a	D_f
A	A_d	A_a	A_f
F	F_d	F_a	F_f

Table 2.3: 9 experimental values obtained by combining 3 filter sets (D,A,F) with 3 samples (d,a,f)

The energy transfer efficiency (E) was subsequently calculated with Eq. (2.10) from these nine values. Non-FRET signals are from the direct excitation of the acceptor at the donor excitation wavelengths. The G factor used in Eq. (2.10) represents the ratio between the decrease of donor signal due to FRET and the increase of acceptor signal due to FRET.

$$G = \frac{QY_a}{QY_d} \times \frac{\Phi_a}{\Phi_d} \times \frac{T_F}{T_D} \tag{2.11}$$

where QY is the fluorescence quantum yield of donor (d) or acceptor (a), Φ is the fraction of the fluorescence transmitted by the detection set, and T is the detection efficiency for a given wavelength pair (for more details see p.65).

In addition to FRET efficiency (E) by Eq. (2.10), two measures of donor ($\overline{Dfd}$) and acceptor ($\overline{Afa}$) concentrations can also be calculated by Eq. (2.12) and Eq. (2.13) respectively [48]. These two fluorophore concentration indexes, $\overline{Dfd}$ and $\overline{Afa}$,

refers to individual fluorescence intensities of donor and acceptor in the mixture of donor and acceptor when no FRET would occur (theoretical quantities, not measurable). $\overline{Dfd}$ is the donor signal that would take place if no FRET occurred in the mixture sample and is therefore proportional to the total concentration of donor. $\overline{Afa}$ is the acceptor signal that would take place if no FRET occurred in the mixture sample and is therefore proportional to the total concentration of acceptor.

$$\overline{Dfd} = Df + \frac{Ff - (Fd/Dd)Df - \dfrac{Af - (Ad/Fd)Ff}{1-(Fa/Aa)(Ad/Fd)}[Fa/Aa - (Fd/Dd)(Da/Aa)]}{G[1-(Da/Fa)(Fd/Dd)]} \tag{2.12}$$

$$\overline{Afa} = \frac{Af - (Ad/Fd)Ff}{1-(Fa/Aa)(Ad/Fd)} \tag{2.13}$$

2.4 Degree of Oligomerization

In this study, the degree of oligomerization (subunit stoichiometry) was examined by inter-molecular FRET, i.e. donor- and acceptor-labeled proteins were mixed *in vitro* or expressed *in vivo* at various donor fractions. FRET efficiency (E) and donor fraction (f_D based on the concentration indexes of fluorophores) can be obtained from spectra by using Gordon's Equation. The degree of oligomerization was determined by fitting to a model of oligomeric state [49, 50]. The number of subunits in the oligomer complex (subunit stoichiometry) is described by (E) and donor fraction ($f_D = \frac{[D]}{[D]+[A]}$) as:

$$E = E_{max} * (1 - f_D^{(oligo-1)}) \tag{2.14}$$

where E is the apparent FRET efficiency, E_{max} is the maximal FRET efficiency, f_D is donor fraction, and $oligo$ is the number of subunits in an oligomer complex.

Based on Eq. (2.14), FRET efficiency (E) as a function of donor fraction (f_D) and degree of oligomerization ($oligo$) revealed a linear model for dimers as well as non-linear models for higher-order oligomers (Fig. 2.5).

The relationship between FRET efficiency (E) and donor fraction (f_D) is related to the degree of oligomerization (oligomeric structure) in the molecular mixtures/complexes of donor and acceptor. No FRET efficiency ($E = 0$) can be ob-

served in monomers ($oligo = 1$), i.e. the FRET efficiency in monomers is independent of the donor fraction. In contrast, FRET efficiency depends on the donor fraction in dimers or higher-order oligomers ($oligo \geq 2$), where each donor has more possibilities to transfer energy to more surrounding acceptors in higher-order oligomers compared with lower-order oligomers with the same donor fraction.

Monomer	$E = 0$
Dimer	$E = E_{max} * (1 - f_D)$
Trimer	$E = E_{max} * (1 - f_D^2)$
Tetramer	$E = E_{max} * (1 - f_D^3)$
Oligomer	$E = E_{max} * (1 - f_D^{(oligo-1)})$

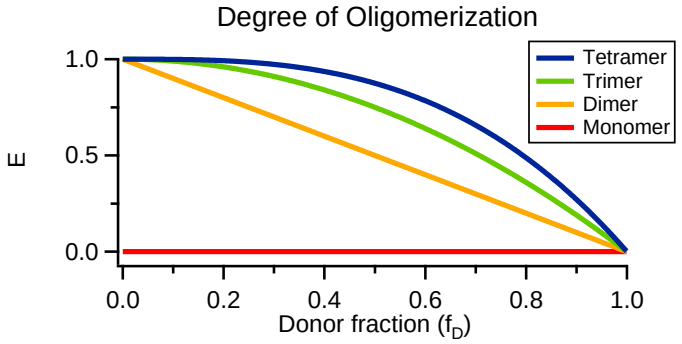

Figure 2.5: FRET efficiency (E) as a function of donor fraction (f_D)

3 Materials and Methods

3.1 Materials

Chemicals (Table. 3.1) were purchased from Fluka (Neu-Ulm, Germany), Gibco (Eggenstein, Germany), Roth (Karlsruhe, Germany), Serva (Heidelberg, Germany) or Sigma-Aldrich (Deisenhofen, Germany) at the highest purity available. Organic dyes (Table. 3.2) were supplied by workgroup of Prof. Dr. Klaus Müllen (Max Planck Institute for Polymer Research, Mainz, Germany) [51] or purchased from AnaSpec (San Jose, CA, USA) or Invitrogen (Carlsbad, CA, USA). All are of analytical grade or better and used without further purification. Double-distilled water (ddH_2O) was used for the reagent setup. Bacterial strains and expression plasmids were listed in the Table. 3.3. The contents of buffer and solution were summarized in Table. 3.4.

Chemical	**Company**
Casein (Select Pepton Nr. 140)	Gibco BRL
Fumarate	Fluka
Glycerol	Roth
HCl	Fluka
Imidazole	Roth
KCl	Roth
KH_2PO_4	Roth
LDAO (Lauryldimethylamine oxide)	Fluka
NaCl	Roth
Na_2HPO_4	Roth
Toluene	Sigma-Aldrich
Tris	Roth
Yeast Extract (Servabacter 24540)	Serva

Table 3.1: Chemicals used in this study.

Fluorophore	Source
PDI [perylenediimide]	[51]
TDI [terrylenediimide]	[51]
Dyad (PDI-TDI)	[51]
Alexa Fluor 488-C_5-Maleimide	Invitrogen
Alexa Fluor 594-C_5-Maleimide	Invitrogen
5-IAF [5-Iodoacetamidofluorescein]	AnaSpec
5-TMRIA [Tetramethylrhodamine-5-iodoacetamide]	AnaSpec

Table 3.2: Organic dyes used in this study.

	Bacterial strain or expression plasmid	Reference
***E. coli* K-12**		
JM109	wild-type *E. coli* strain	[52]
IMW237	*E. coli* strain containing $dcuB' -' lacZ$	[15]
IMW244	DctA-deleted *E. coli* strain	[32]
IMW262	DcuS-deleted *E. coli* strain	[6]
IMW280	CitA-deleted *E. coli* strain	[53]
Plasmids		
pDK108	Tar^{1-331}-YFP; pTrc99a derivative (Ap^r)	[54]
pECFP	CFP (Ap^r)	Clontech
pEYFP	YFP (Ap^r)	Clontech
pMW151	DcuS; pET28a derivative (Kan^r)	[9]
pMW324	DcuS (C199S); pET28a derivative (Kan^r)	This study
pMW325	DcuS (C471S); pET28a derivative (Kan^r)	This study
pMW336	DcuS (C471S, C471S); pET28a derivative (Kan^r)	This study
pMW446	DcuS (R147A, C199S); pET28a derivative (Kan^r)	This study
pMW407	DcuS-YFP; pBAD30 derivative (Ap^r)	[53]
pMW408	DcuS-CFP; pBAD18 derivative (Kan^r)	This study
pMW442	CitA-YFP; pBAD30 derivative (Ap^r)	[53]
pMW523	CFP-DctA; pBAD30 derivative (Ap^r)	This study
pMW524	DctA-CFP; pBAD30 derivative (Ap^r)	This study
pMW525	YFP-DctA; pBAD30 derivative (Ap^r)	This study
pMW526	DctA-YFP; pBAD30 derivative (Ap^r)	This study
pMW762	CFP; pBAD18 derivative (Kan^r)	This study
pMW763	YFP; pBAD18 derivative (Kan^r)	This study
pMW764	CFP; pBAD30 derivative (Ap^r)	This study
pMW765	YFP; pBAD30 derivative (Ap^r)	This study
pMW766	CFP-YFP; pBAD18 derivative (Kan^r)	This study
pMW767	YFP-CFP; pBAD18 derivative (Kan^r)	This study
pMW768	CFP-YFP; pBAD30 derivative (Ap^r)	This study
pMW769	YFP-CFP; pBAD30 derivative (Ap^r)	This study

Table 3.3: Strains and plasmids used in this study.

Buffer and Solution		Contents
Luria-Bertani (LB) medium	10 g/L	Casein
	5 g/L	Yeast Extract
	5 g/L	NaCl
Homogenization buffer	50 mM	Tris-HCl
	10%	glycerol
		pH 7.7 HCl
DcuS-labeling-buffer	50 mM	Tris-HCl
	0.5 M	NaCl
	5 mM	Imidazole
	5 %	Glycerol
	0.04 %	LDAO
		pH 7.2 HCl
Tris/HCl buffer	50 mM	Tris
		pH 7.7 HCl
PBS buffer	137 mM	NaCl
	2.7 mM	KCl
	10 mM	Na_2HPO_4
	2 mM	KH_2PO_4
		pH 7.5 HCl
P1 buffer	50 mM	Tris
	10 mM	$MgCl_2$
		pH 7.7 HCl

Table 3.4: Buffer and solution used in this study.

3.2 Sample Preparation

3.2.1 Protein Preparation for *in vitro* Measurements

The preparation of recombinant proteins was done by Patrick Scheu (WT, C471S, C199S, Cys^-, R147A), Dr. Holger Kneuper (WT, C471S, R147A), and Verena Bock (C199S and Cys^-) in the workgroup of Prof. Dr. Unden (Institute of Microbiology and Wine Research, Mainz University, Germany).

Protein Expression and Purification Plasmid construction of DcuS mutants was performed by site-directed mutagenesis with a kit (Qiagen) according to the manufacturer's instructions. Expression of the recombinant DcuS proteins were performed by standard procedures [55]. Membrane fraction containing DcuS protein was obtained by removing cell debris by centrifugation and subsequently pelleted by ultracentrifugation. The pellet containing DcuS was homogenized in homogenization buffer (50 mM of Tris-HCl, 10% of glycerol, pH 7.7), and stepwise solubilized by adding 2% (w/v) of Empigen BB (30% solution, Calbiochem). The solubilized protein was stored by shock-freezing in liquid N_2 and storing at -80°C before use. Solubilized His-tagged DcuS protein was purified by using Ni^{2+}-NTA column (Qiagen). Eluated DcuS was dialyzed against imidazole-free buffer to avoid potential interference of imidazole in the steps of labeling and spectroscopy. Protein concentrations were determined by Bradford assay kit (Bio-Rad) using bovine serum albumin (BSA) as a standard.

Fluorescent Labeling of Proteins Fluorescent dyes were dissolved in DMSO to yield a 10 mM stock solutions, and freshly diluted by DcuS-labeling-buffer (50 mM Tris-HCl buffer (pH 7.2) containing 500 mM NaCl, 5% glycerol, and 0.04% LDAO) for further labeling reactions. The reaction mixture, 16 μM (1 mg/ml) purified DcuS protein and 50 μM or 160 μM thiol-reactive fluorescent dyes (Invitrogen or AnaSpec) in DcuS-labeling-buffer, was incubated in the dark for 2 h at room temperature or overnight at 4°C. While labeled for 2 h at room temperature, the labeling reaction was terminated by adding 20 mM of cysteine dissolved in DcuS-labeling-buffer to a volume of 800 μL for 30 min. Excess unbound dyes were removed by PD-10 column (Sephadex^{TM}G-25, Amersham Biosciences). Labeled protein was purified and concentrated in a Vivaspin concentrator (Vivascience) with a cut-off (MWCO) of 30 kDa at 4°C to a volume of 1 ml. The extent of label-

ing was estimated spectrophotometrically according to the absorption spectrum of labeled DcuS by measuring dye absorbance and protein concentration, using a UV-vis spectrophotometer. Final labeled DcuS were kept on ice or stored at 4°C before further fluorescence measurements.

Reconstitution of DcuS into Liposomes Labeled DcuS proteins were reconstituted at a phospholipid:protein ratio 20:1 (w/w) in *E. coli* phospholipids (Avanti Polar Lipids Inc.) as described [15]. Reconstituted DcuS was frozen in liquid N_2, and stored at -80°C before use.

3.2.2 Cell Preparation for *in vivo* Measurements

The preparation of fluorescent fusion proteins was in cooperation with Prof. Dr. Unden′s group (Institute of Microbiology and Wine Research, Mainz University, Germany). The plasmid construction and protein expression of XFP (XFP: CFP or YFP) fusions were prepared by Patrick Scheu (DcuS and CitA) and Julia Bauer (DctA and controls).

Preparation of cells with DcuS-FP Fusion proteins DNA sequence of DcuS (*dcuS*) was genetically fused with that of CFP (*ecfp*) or YFP (*eyfp*) to generate *dcuS-cfp* or *dcuS-yfp* fusion constructs (both C′ and N′ fusions). The *dcuS-yfp* fusion (pMW407) was cloned into pBAD30-Amp [53], and the *dcuS-cfp* fusion (pMW408) was constructed into pBAD18-Kan. The sequences of resulting constructs were verified by sequencing. Plasmids of DcuS-FP fusions were transformed into *E. coli*. Co-expression of FP fusions in cells was generally induced by 133 μM or 333 μM L-arabinose at 30°C. After harvest, *E. coli* cells were washed twice by spin-centrifugation with PBS buffer and then resuspended in PBS buffer. Cells resuspended in PBS were used immediately for fluorescence measurements. The DcuS activity of DcuS-XFP fusions was confirmed by inducing *dcuB'-'lacZ* expression. *E. coli* containing *dcuB'-'lacZ* and DcuS-XFP fusions was grown anaerobically at 37°C in M9 mineral medium (Miller, 1992) with glycerol and dimethyl sulfoxide as energy substrates and with fumarate (20 mM) as an effector. Samples were withdrawn at OD_{578nm}=0.5-0.7 for measurement of $\beta-$galactosidase activity. Fluorescence of DcuS-XFP fusions was confirmed by fluorescence spectroscopy.

Western blot analysis of DcuS-FP expression levels *E. coli* cells induced by different arabinose concentrations were sedimented by centrifugation and dissolved in SDS-containing sample buffer [56]. The dissolved whole cell proteins were separated by SDS-PAGE and transferred to nitrocellulose membranes [57]. Membranes were treated with rabbit polyclonal antiserum (Eurogentec) raised against the periplasmic domain of DcuS and detected with secondary IgG antibodies coupled to peroxidase (Sigma-Aldrich).

Cell fractionation Arabinose-induced bacteria were harvested by centrifugation at 6,300 g for 10 min. All further steps were done at 4°C. Washed cells from 400 ml medium were resuspended in 8 ml buffer (50 mM Tris/HCl, pH 7.7, 10 mM $MgCl_2$). The bacteria were broken using a French press (3x at 8,274 kPa) and then centrifuged at 8,600 g for 10 min to sediment debris and potential inclusion bodies (low-speed pellet) and to separate them from the soluble fraction and cytoplasmic membranes contained in the supernatant (low-speed supernatant). Proteins from the low-speed pellet and the low-speed supernatant were detected by Western blot analysis with mouse polyclonal antibodies (Qiagen, Hilden) against the His_6-tag of the fusion protein. Protein bands were detected with secondary IgG antibodies coupled to peroxidase (Sigma-Aldrich). Protein bands of three independent preparations were visualized and quantified by using the KODAK Image Station 440CF and the KODAK Molecular Imaging software. To sediment the membrane fraction, the low-speed supernatant was centrifuged at 200,000 g for 65 min. The membrane pellet was washed twice (1 mM Tris/HCl, pH 7.7, 3 mM EDTA), homogenized in buffer (50 mM Tris/173 HCl, pH 7.7, 10% (w/v) glycerol), and solubilized by adding 2% (w/v) of Empigen BB (30% solution, Calbiochem) as described [9]. The low-speed supernatant fraction was fractionated in a sucrose step-gradient (0%, 10%, and 40% sucrose) by ultracentrifugation at 200,000 g for 2 h. Fractions of 1 ml were collected and 20 μl of each fraction was subjected to SDS-PAGE to examine banding of DcuS-YFP in the protein/membrane fraction and in the protein aggregate fraction. Isolated and purified DcuS-YFP was used as a standard.

Purified FP of Reference Spectra Reference spectra of CFP (donor) and YFP (acceptor) were purified from *E. coli* cells expressing donor or acceptor, respectively. CFP or YFP protein was expressed from a 20 mL culture of *E. coli* cells grown in Luria-Bertani (LB) after 1% inoculation of the overnight culture. Cells were har-

vested by centrifugation and resuspended in 20 mL of Tris buffer pH 7.7 and 10 mM $MgCl_2$. Cell supernatant was prepared by 3 cycles of French Press and cleared by centrifugation to remove the cell debris, and subsequently by ultracentrifugation to separate cytosolic (soluble protein) fraction from membrane fraction. The supernatant containing cytosolic fraction was subjected to vivaspin concentrator (MWCO: 10,000 Da) to separate FP proteins from small fluorescent molecules. The measured spectra of purified FP were normalized to unity as the reference spectra of donor and acceptor.

3.3 Spectroscopy

3.3.1 Absorption Spectroscopy

Absorption spectra of samples were measured in a 1-ml quartz cuvette (semi-microcuvette) by using a dual-beam UV-VIS spectrophotometer (OMEGA 20, Bruins Instruments, Germany). The absorption spectra were recorded at a wavelength range (250 nm to 700 nm) with an increment 0.5 nm by using a slit width of 0.5 mm.

3.3.2 Fluorescence Spectroscopy

Fluorescently labeled samples were measured at room temperature in a 1-ml quartz cuvette (semi-microcuvette) by using a FluoroMax-2 spectrofluorometer (Jobin Yvon-Spex). To ensure a linear relationship between fluorescence intensities and fluorophore concentrations, the samples were always kept dilute to record spectra within the linear range of the signal detector, and corrected measured spectra for the detector saturation. The emission spectra were recorded at an excitation wavelength and a range of emission wavelength according to the fluorophore respectively (Table. 3.5) [58]. The slit bandwidth for excitation and emission was 5 nm. Fluorescence spectra were corrected for the wavelength dependence of the fluorometer (Sc/R).

DcuS-FP Fusions Cells expressing DcuS-FP fusion proteins were washed twice by spin-centrifugation with PBS buffer. Absorption spectra were recorded before fluorescence measurements. Cells were diluted to an absorbance of 0.1 at 400

Fluorophore	Abs (nm)	Em (nm)	M.W.	Ec ($cm^{-1}M^{-1}$)
Alexa 488-Maleimide	493	516	720.66	72,000
Alexa 594-Maleimide	588	612	908.97	96,000
5-IAF	492	515	515.26	78,000
5-TMRIA	543	567	825.22	87,000

Table 3.5: Spectral properties of organic fluorophores used in this study.

nm to avoid inner filter effect and signal saturation. The emission spectra were recorded, by excitation of CFP (λ_{ex}= 433 nm) or of YFP (λ_{ex}= 488 nm), respectively, with an increment of 1 nm and an integration time of 0.2 s.

3.3.3 Software

All of the experimental data (absorption spectra, fluorescence spectra, fluorescence decay curves, and images obtained by confocal microscope) were analyzed by using IGOR Pro software (WaveMetrics, Lake Oswego, OR, USA).

4 Results

Sec. 4.1 describes the samples prepared to address different aims in this study. A quantitative FRET analysis developed in Sec. 4.2 was applied to study oligomerization of DcuS and protein-protein interactions between DcuS and relevant proteins (Sec. 4.3).

4.1 Samples

Fig. 4.1 gives an overview of the fluorescence signals and the experimental environments of DcuS samples in this study. The fluorescence signals (under different experimental environments) are originated from three categories of DcuS samples: (1) DcuS fusion with fluorescent protein in living cells (*in vivo*), (2) labeled DcuS in detergent or in liposomes (*in vitro*), and (3) intrinsic fluorescence of DcuS (*in vitro*).

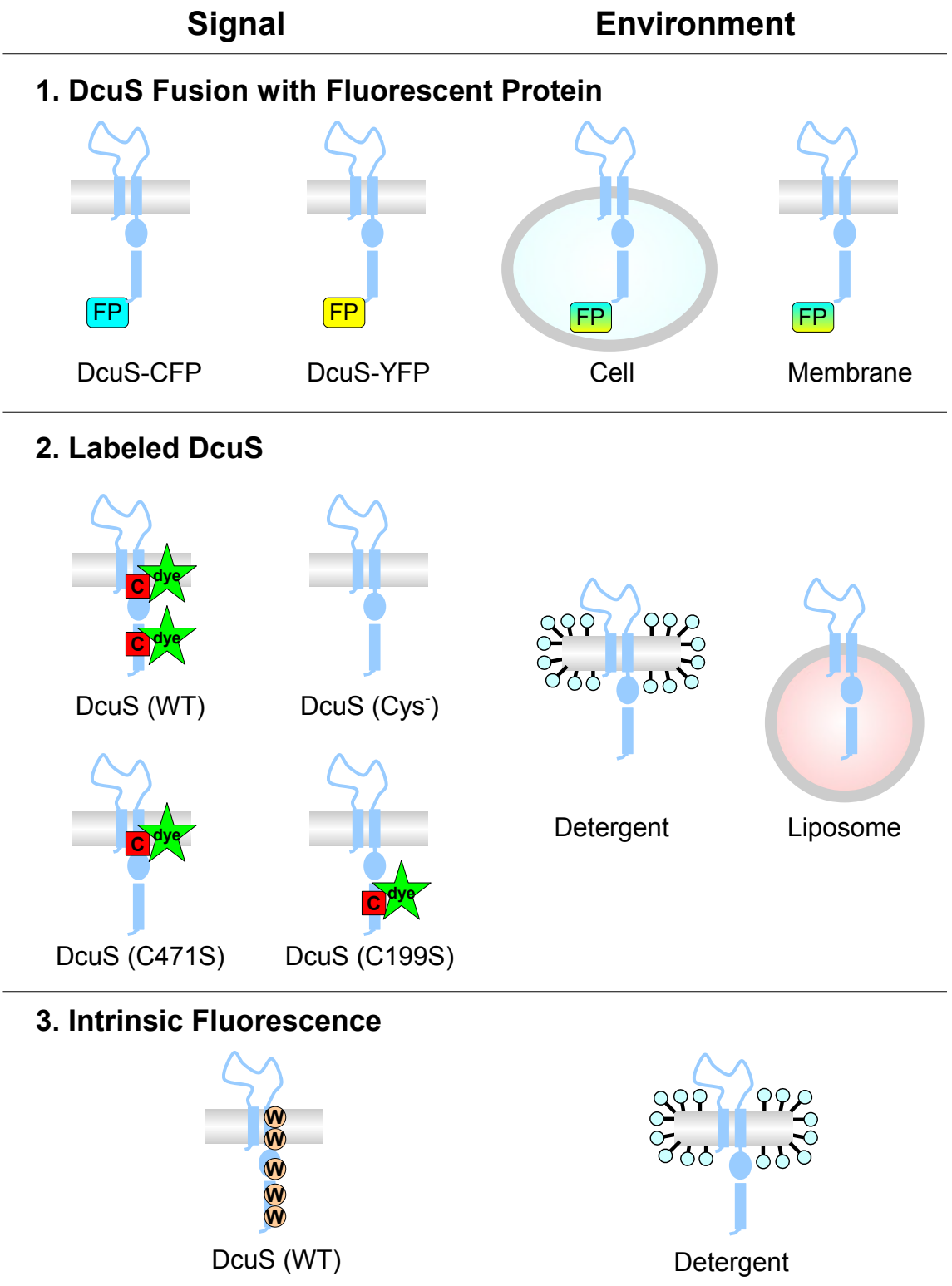

Figure 4.1: Signals and experimental environments of DcuS samples in this study. Abbreviations: C, cysteine; FP, fluorescent protein (CFP or YFP); S, serine; W, tryptophan; WT, wild-type.

4.1.1 DcuS-FP Fusions for *in vivo* Measurements

Fluorescent-protein Pair (CFP and YFP) Cyan fluorescent protein (CFP as donor) and yellow fluorescent protein (YFP as acceptor) were used as FRET pair for *in vivo* measurements (Fig. 4.2). To avoid the interference of the excitation light in the detection of emission light, CFP and YFP were not excited exactly at their absorption maxima but at relatively shorter wavelengths.

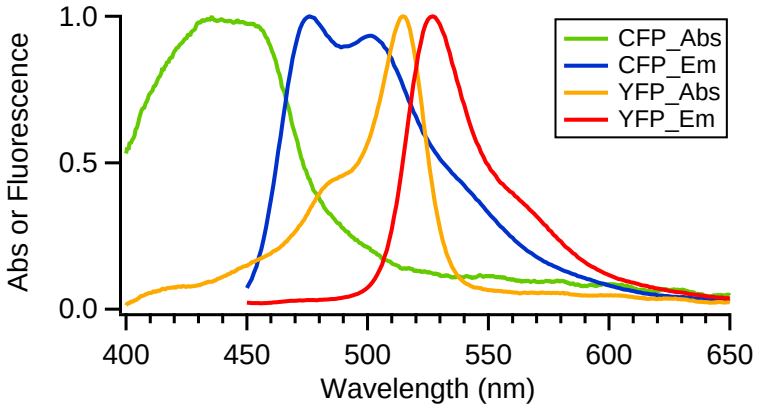

Figure 4.2: Absorption and emission spectra of purified CFP and YFP (Sec. 3.2.2). CFP was excited at 433 nm, and YFP was excited at 488 nm. All spectra were normalized to unity.

To examine the functionally-relevant oligomeric state of DcuS *in vivo* (Sec. 4.3), DcuS was genetically fused with CFP or YFP at the N- or C-terminus of DcuS to yield chimeric fusion proteins, DcuS-CFP or DcuS-YFP (Fig. 4.3). To examine the protein-protein interactions of DcuS *in vivo* (Sec. 4.3.3), other relevant proteins (CitA, DcuB, and DctA) were also genetically tagged with CFP or YFP.

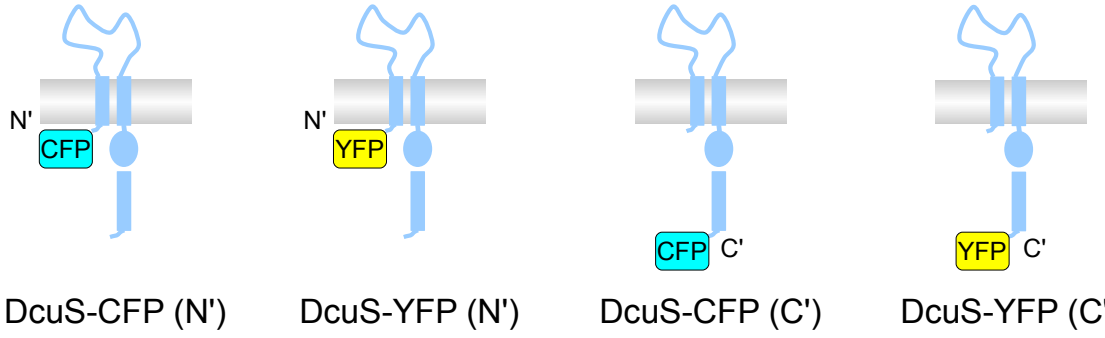

Figure 4.3: DcuS genetically tagged with CFP or YFP at N- or C-terminus.

CFP and YFP fusions of DcuS (and relevant proteins) were co-expressed in living cells (Fig. 4.4) to examine the inter-molecular interactions by detecting the occurrence of FRET between CFP and YFP. To avoid the artifacts of FRET occurrence

due to over-expression of FP fusions, an expression vector pBAD (under the control of the *araBAD* promoter responding to arabinose as an inducer) was used for a moderate expression at physiological level of FP fusions. For the co-expression of CFP and YFP fusions in the same cell, two different but similar pBAD vectors were used (pBAD18 vector for CFP fusion, and pBAD30 vector for YFP fusion) to achieve relative similar expression level of CFP and YFP fusions in the same cell.

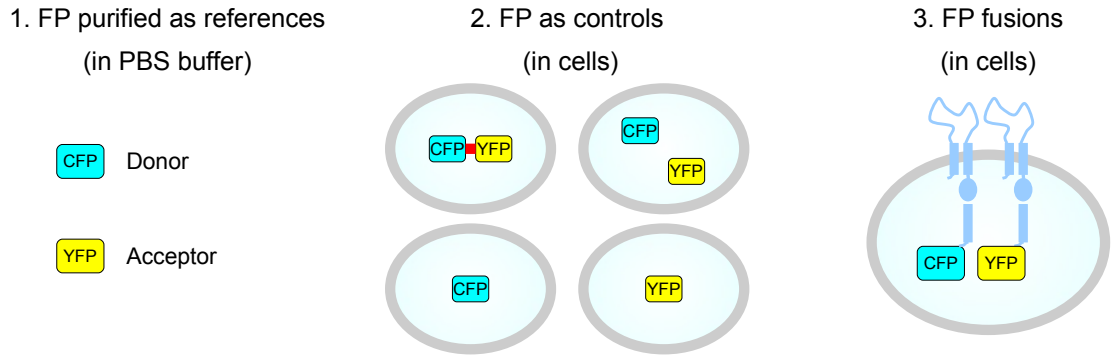

Figure 4.4: DcuS-FP fusions system investigated: (1) CFP and YFP as FRET pair; (2) FP in cells as controls; (3) CFP and YFP fusions co-expressed in cells.

Functionality of DcuS-FP Fusions (FP fluorescence) The fluorescence of DcuS-CFP and DcuS-YFP fusions was confirmed by fluorescence spectroscopy (Sec. 3.3.2), and the spectral shape and peak position were compared with reference spectra of CFP or YFP (Fig. 4.5). The emission spectrum of cells expressing DcuS-CFP fusion revealed typical major peak of CFP (477 nm). However, the strange spectral shapes without typical minor peak of CFP (504 nm) demonstrate background subtraction by either buffer spectrum or *E. coli* spectrum was not adequate to remove existing background in living cells. Similarly, the emission spectrum of cells expressing DcuS-YFP fusion appeared a typical YFP peak at 527 nm. Buffer-subtracted spectrum of DcuS-YFP fusion was much broader than the YFP reference spectrum, indicating background subtraction by buffer spectrum is not competent to remove all of the background. Taken together, DcuS-CFP and DcuS-YFP fusions were proved to retain the function of wild-type CFP and YFP. Besides, both cases demonstrated the effect and importance of background subtraction, in particular for the spectra in living cells (for details see 4.2.1).

Functionality of DcuS-FP Fusions (DcuS activity) To test if DcuS-FP fusions are as functional as endogenous DcuS, the *dcuS-cfp* plasmid encoding DcuS-CFP or *dcuS-yfp* plasmid encoding DcuS-YFP was expressed in DcuS-deficient *E. coli* strain

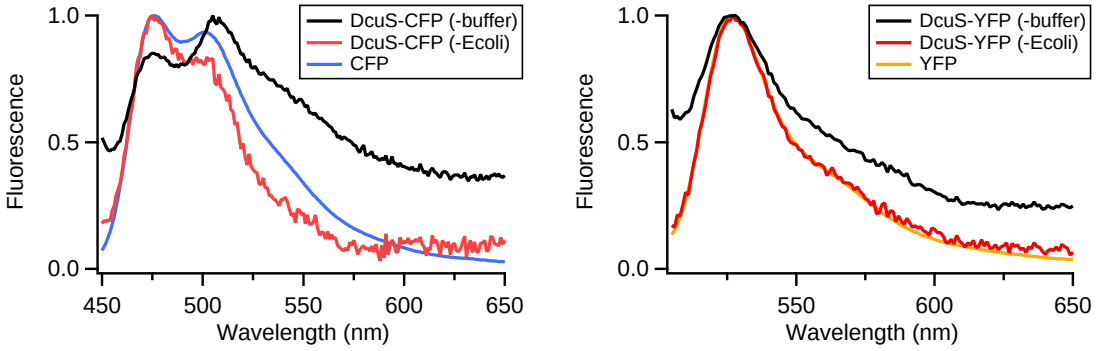

Figure 4.5: Emission spectra of cells expressing either DcuS-CFP or DcuS-YFP fusion. Left: emission spectra (λ_{ex}= 433 nm) of cells expressing DcuS-CFP fusion (black: buffer-subtracted; red: *E. coli*-subtracted) in comparison with CFP reference spectrum (blue). Right: emission spectra (λ_{ex}= 433 nm) of cells expressing DcuS-YFP fusion (black: buffer-subtracted; red: *E. coli*-subtracted) in comparison with YFP reference spectrum (yellow). Spectra were normalized by peak intensity.

(IMW260). Both *dcuS-cfp* and *dcuS-yfp* plasmids complemented the anaerobic growth of the DcuS-deficient *E. coli* strain. In addition, the functional activities of DcuS-FP fusions compared to wild-type DcuS proteins were also examined by inducing *dcuB′-′lacZ* expression (Fig. 4.6). Based on the β-galactosidase assay, all of the DcuS-FP fusions remain functional *in vivo*. C-terminal DcuS-FP fusions function as well as wild-type DcuS, and N-terminal DcuS-FP fusions shows relatively lower activity than wild-type DcuS. DcuS-FP fusions were verified to retain the function comparable to wild-type DcuS. Taken together, DcuS and FP were both functional upon fusion.

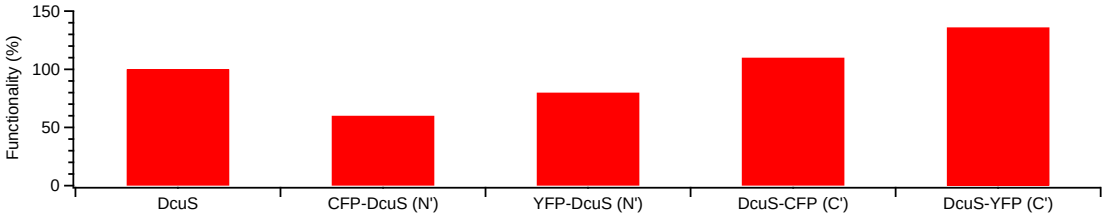

Figure 4.6: Functionality of DcuS-FP fusions by inducing *dcuB′-′lacZ* expression (details see Sec. 3.2.2). All functional activities were normalized to that of wild-type DcuS.

Test of Inclusion Bodies To rule out the potential artifacts due to inclusion bodies, the presence of DcuS-YFP inclusion bodies and their contribution to the fluorescence of the cells was examined. The potential artifact of inclusion bodies was excluded for DcuS-YFP by cell fractionation (Table. 4.1) and Western blot (Fig. 4.7) analysis. Less than 32% of DcuS-YFP protein and maximally 10% of the total

fluorescence of the cells reside in inclusion bodies. Based on the small contribution of the inclusion bodies (<10%), it can be concluded that the fluorescence in the bacteria corresponds to membrane-integral DcuS-YFP.

Fraction	Western blot	Fluorescence
Low speed supernatant (soluble proteins and membranes)	68 %	90 %
Low speed pellet (debris and inclusion bodies)	32 %	10 %

Table 4.1: Distribution of DcuS-YFP fusion protein and fluorescence in cellular compartments of *E. coli*. The cell homogenate of *E. coli* IMW262 (dcuS$^-$) induced with 333 μM arabinose for 4 h was separated into supernatant and pellet fraction by low speed centrifugation. Quantitative Western blot analysis (average of 3 independent preparations) was performed with both fractions. Fluorescence of low-speed supernatant and low-speed pellet fraction was detected after excitation at 488 nm.

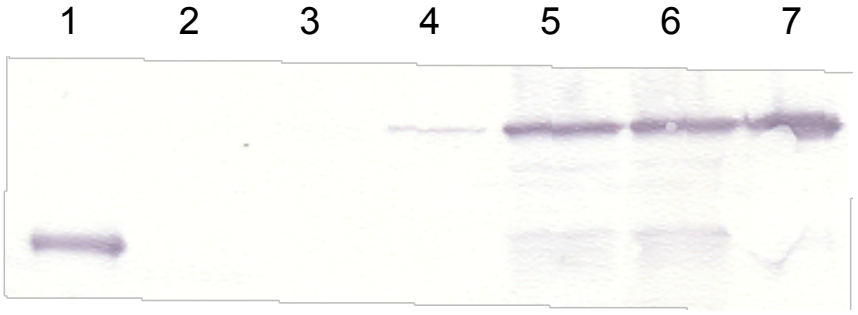

Figure 4.7: Detection of DcuS-YFP in *E. coli* cell lysates by Western blot with antiserum against the periplasmic domain of DcuS. Cells expressing DcuS or DcuS-YFP were sedimented and the pellet was dissolved in SDS sample buffer. 60 μg (lanes 3 to 6) or 120 μg (lane 2) of cell lysates were subjected to SDS-PAGE. After blotted onto a nitrocellulose membrane, DcuS and DcuS-YFP were detected by immunostaining with antiserum against the periplasmic domain of DcuS. Lane 1, purified DcuS (1 μg); lane 2: DcuS (WT, JM109) grown anaerobically in M9 mineral medium with 50 mM glycerol and 20 mM fumarate; lanes 3-6: *E. coli* (JM109) cells expressing DcuS-YFP (pMW407, pBAD 30 derivative) grown under aerobic conditions in LB broth in the presence of 0 μM (lane 3), 10 μM (lane 4), 133 μM (lane 5) or 333 μM arabinose (lane 6); lane 7, purified DcuS-YFP (1 μg).

YFP fusion of citrate sensor CitA To study the interaction between DcuS and CitA *in vivo*, CitA was genetically fused with YFP to yield CitA-YFP fusion. To determine if the CitA-YFP fusion is as functional as endogenous CitA, the *citA-yfp* plasmid encoding CitA-YFP was expressed in CitA-deficient *E. coli* strain (IMW280). The *citA-yfp* plasmid complemented the growth of the CitA-deficient *E. coli* strain. In addition, the plasmid encoding CitA-YFP fusion proteins restored expression of

the *dcuB′-′lacZ* reporter gene fusion to approximately the same level as plasmid encoding wild-type CitA. CitA-YFP retained 97% of the functional activity comparable to wild-type CitA (Fig. 4.8, left). After subtraction by either buffer or *E. coli* background, the emission spectrum of cells expressing CitA-YFP fusion revealed comparable spectral shape and peak position to that of YFP reference spectrum (Fig. 4.8, right).

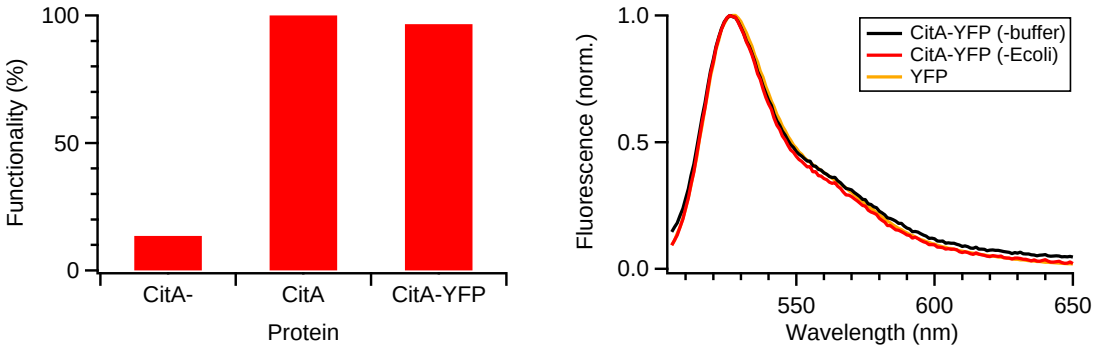

Figure 4.8: Functional tests of CitA-YFP fusion. Left: functional assay of CitA-YFP by inducing *dcuB′-′lacZ* reporter gene expression. Functionality was normalized to unity compared to wild-type CitA (100%). CitA$^-$: CitA-deficient *E. coli* strain. CitA: *E. coli* expressing wild-type CitA. CitA-YFP: *E. coli* cells expressing CitA-YFP. Right: emission spectra (λ_{ex}= 488 nm) of cells expressing CitA-YFP fusion (black: buffer-subtracted; red: *E. coli*-subtracted) in comparison with YFP reference spectra (yellow). Spectra were normalized by peak intensity.

FP fusions of aerobic dicarboxylate transporter DctA To study the interaction between DcuS and DctA in living cells, DctA was genetically tagged with CFP or YFP at N- or C-terminus. The *dctA-cfp* or *dctA-yfp* plasmids complemented the growth of the DctA-deficient *E. coli* strain (IMW244). The CFP or YFP fluorescence was examined among these DctA-FP fusions. DctA-YFP (C') shows higher intensity than other fusions (Fig. 4.9). Therefore, the DctA-YFP (C') fusion was used for further experiments. After subtraction of buffer or *E. coli* background, the emission spectrum of cells expressing DctA-YFP fusion revealed identical peak position to the YFP reference spectrum (Fig. 4.10), and the spectral shape was a little broader than YFP reference spectrum due to inadequate background subtraction by either buffer spectrum or *E. coli* spectrum. To test the induction-time dependence of the expression of DctA-YFP (C') protein, *E. coli* cell expressing DctA-YFP (C') was incubated in the presence of 333 μM arabinose. Emission spectra of DctA-YFP (C') was measured hourly from 3 hr to 8 hr. DctA-YFP (C') revealed time-dependent increase in fluorescence intensity (Fig. 4.11).

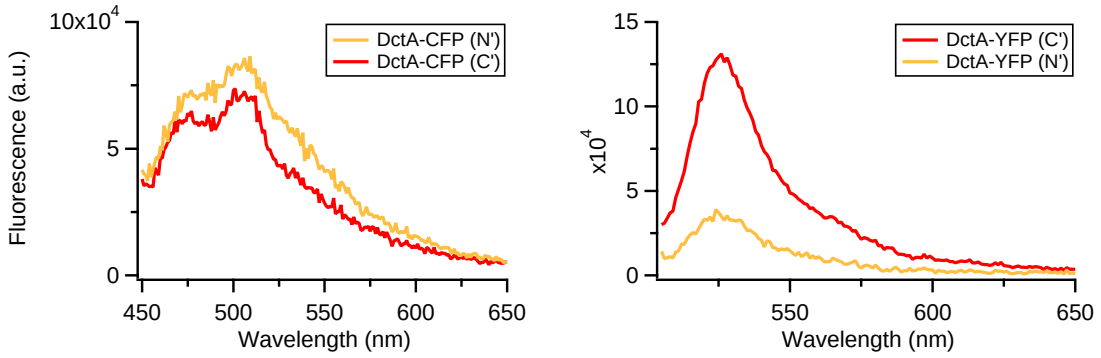

Figure 4.9: Emission spectra of DctA-FP fusions. Left: DctA-CFP fusions (λ_{ex}= 433 nm). Right: DctA-YFP fusions (λ_{ex}= 488 nm). All spectra were buffer-subtracted.

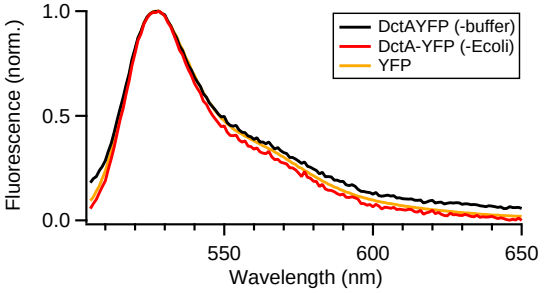

Figure 4.10: YFP fluorescence of DctA-YFP. Emission spectra (λ_{ex}= 488 nm) of cells expressing DctA-YFP fusion (black: buffer-subtracted; red: *E. coli*-subtracted) in comparison with YFP reference spectrum (yellow).

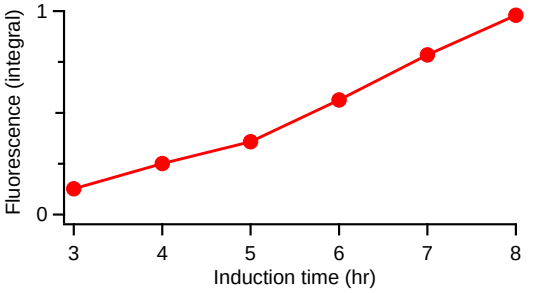

Figure 4.11: Time-dependent induction of DctA-YFP. DctA-YFP fusion was induced by 333 μM arabinose from 3 hr to 8 hr. Emission spectra (λ_{ex}= 488 nm) were recorded hourly. Integrated emission spectra were plotted versus induction time, and then normalized to unity.

Conclusion Upon fusion with CFP or YFP, FP-fusions of DcuS, CitA or DctA revealed comparable functional activities and fluorescence characteristics to their wild-type counterparts. These fusions were adequate and competent to study the protein-protein interactions of DcuS with CitA or DctA in living cells.

4.1.2 Labeled DcuS for *in vitro* Measurements

Cysteine mutants for fluorescent labeling Wild-type DcuS protein, DcuS (WT), contains two endogenous cysteine residues (C199 and C471) for thiol-reactive labeling at neutral pH (similar to physiological conditions). C199 residue is the membranous cysteine located in the end of the second transmembrane domain (TM2). C471 residue is the cytosolic cysteine located in the C-terminal kinase domain. For extrinsic fluorescent labeling, wild-type and cysteine mutants of DcuS were prepared. Fig. 4.12 demonstrates the wild-type and cysteine mutants of DcuS used in this study.

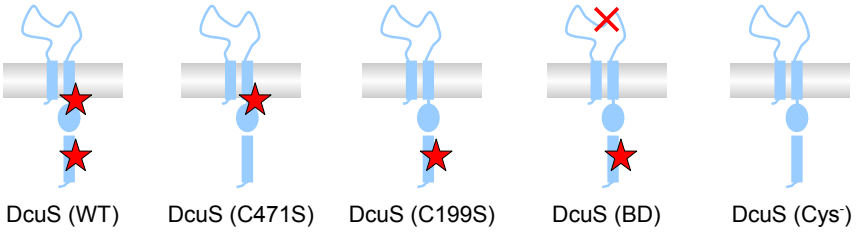

Figure 4.12: Recombinant DcuS proteins used in this study: wild-type (WT) and cysteine mutants. DcuS (BD) is a binding-defect mutant (R147A) with single cysteine mutation (C199S).

To preserve the function of DcuS mutants, cysteine mutants of DcuS were prepared by site-directed mutagenesis (Table. 4.2) to replace cysteine (Cys, C) with serine (Ser, S). To create single labeling site on DcuS, single cysteine mutants, DcuS (C199S) and DcuS (C471S), were genetically generated by mutation of either C199S or C471S. To create no labeling site on DcuS as a negative control to rule out the non-specific labeling, a cysteine-less mutant, DcuS (Cys^-), was generated by mutations of both C199S and C471S. In addition, a binding-defect mutant with single labeling site, DcuS (BD), was generated by mutations of both R147A and C199S.

DcuS mutant	Mutation	Cysteine residue(s)
DcuS (WT)	Wild-type	2 (C199 & C471)
DcuS (C471S)	C471S	1 (C199)
DcuS (C199S)	C199S	1 (C471)
DcuS (BD)*	R147A (binding-defect) & C199S	1 (C471)
DcuS (Cys^-)	C199S & C471S	0 (no cysteine)

*BD: binding-defect

Table 4.2: Recombinant DcuS proteins: wild-type (WT) and cysteine mutants.

Functionality Based on the structural similarity of cysteine and serine residues, cysteine-to-Serine mutation usually preserves the functional activity of protein. The functional activity of DcuS mutants was examined by inducing *dcuB′-′lacZ* expression compared to wild-type DcuS (Fig. 4.13). The functional activity of DcuS (C199S) mutant is comparable to that of wild-type DcuS. DcuS (C471S) and DcuS (Cys$^-$) mutants retain around 80% of functional activity compared to wild-type DcuS. R147A mutation of DcuS leads to nearly complete loss of stimulation of *dcuB′-′lacZ* expression (Fig. 4.13). The binding-defect DcuS mutant retains the same kinase activity as DcuS (WT) for autophosphorylation and phosphor transfer to DcuR, but the kinase activity was no longer stimulated by C4-dicarboxylates [15].

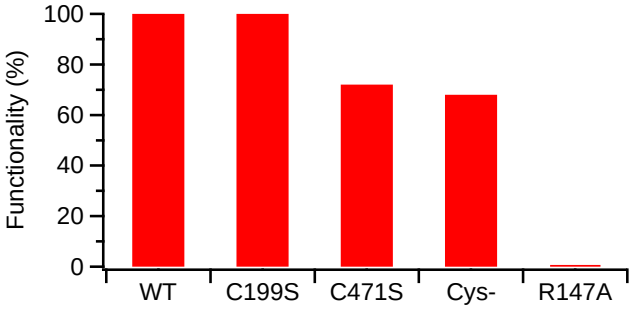

Figure 4.13: Functionality of DcuS: wild-type and cysteine mutants. (details see 3.2.1)

Labeling of DcuS with thiol-reactive fluorophores For site-specific labeling of DcuS, two categories of thiol-reactive groups (Fig. 4.14) were tested, including (1) maleimide (Alexa Fluor 488 and Alexa Fluor 594) and (2) iodoacetamide (IAF and TMRIA). DcuS (Cys$^-$ mutant) was used as a negative control to check the specificity of different thiol-reactive dyes (Fig. 4.15). To purify labeled DcuS, different purification techniques were applied, such as size-exclusion chromatography (PD-10 column) or concentrator (Vivaspin). All free dyes were successfully removed by purification (Fig. 4.15, left). DcuS (wild-type) could be successfully labeled with all dyes (Fig. 4.15, right). However, DcuS (Cys$^-$) mutant was also labeled by different so-called thiol-specific reactive groups (maleimide and iodoacetamide). Even no specific labeling of DcuS could be achieved, maleimide-based (Alexa 488 and Alexa 594) and iodoacetamide-based (IAF and TMRIA) fluorophores can still be used for the oligomerization of DcuS by inter-molecular FRET.

1. Maleimide

Alexa 488 C_5-maleimide

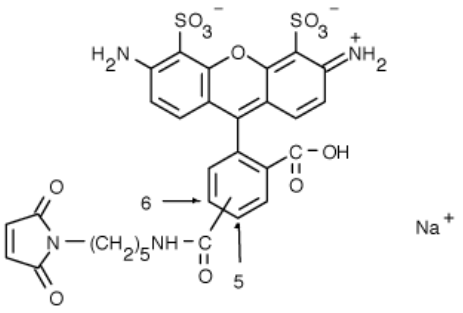

Alexa 594 C_5-maleimide

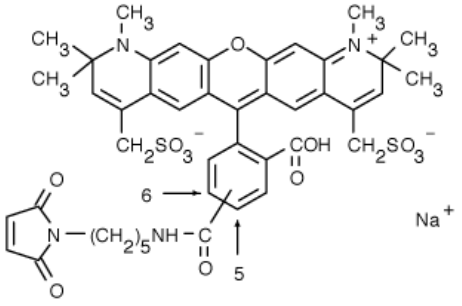

2. Iodoacetamide

5-IAF

[5-Iodoacetamidofluorescein]

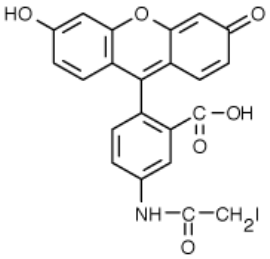

5-TMRIA

[Tetramethylrhodamine-5-iodoacetamide]

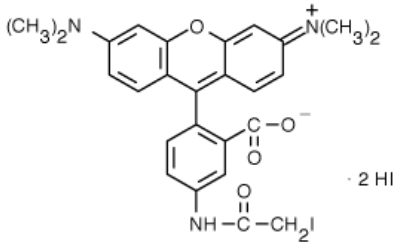

Figure 4.14: Chemical structures of thiol-reactive fluorescent dyes used in this study

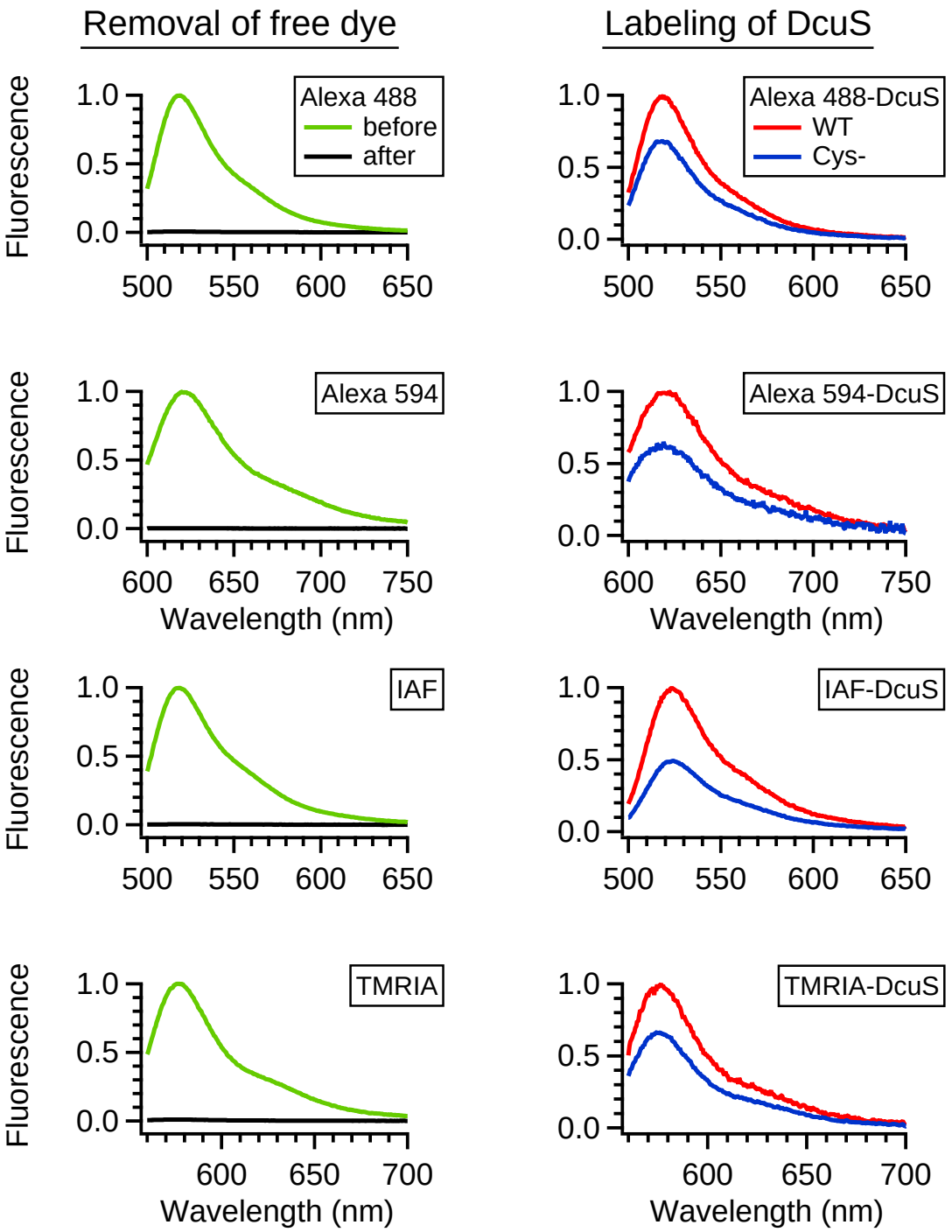

Figure 4.15: Purification and labeling of thiol-reactive dyes. Left: free dyes (1 μM) before or after purification (combining PD-10 column and vivaspin). Right: labeling of DcuS, WT and Cys$^-$ mutant, after purification (details see 3.2.1).

FRET pairs for *in vitro* measurements Two independent FRET pairs (Fig. 4.16), maleimide-based pair (Alexa 488 and Alexa 594) or iodoacetamide-based pair (IAF and TMRIA), were used respectively for *in vitro* FRET measurements (Sec. 4.2 and 4.3). All dyes were excited at shorter wavelengths than their absorption maxima to avoid the interference of excitation light in the detection of emission light.

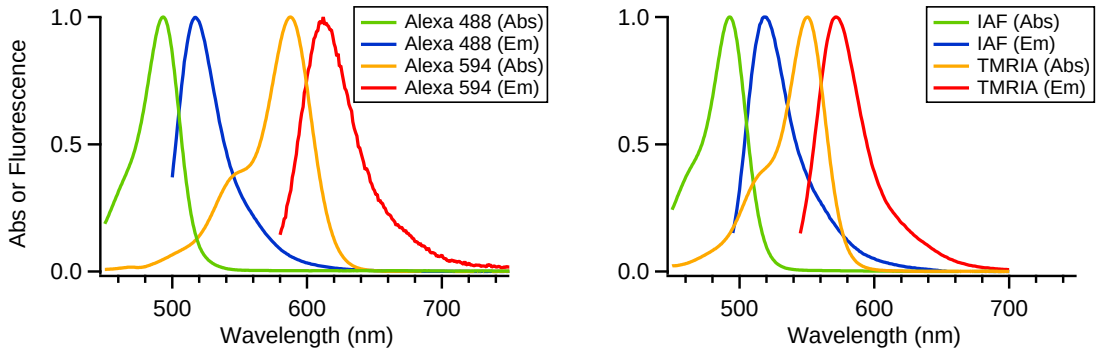

Figure 4.16: Absorption and emission spectra of two independent FRET pairs. Left: Alexa Fluor 488-5-maleimide (donor) and Alexa Fluor 594-5-maleimide (acceptor). Alexa 488 was excited at 480 nm. Alexa 594 was excited at 580 nm. Right: IAF (donor) and TMRIA (acceptor). IAF was excited at 480 nm. TMRIA was excited at 530 nm. All spectra were normalized to unity.

Three types of samples were examined for *in vitro* FRET (Fig. 4.17): (1) mixture of donor and acceptor (free dyes) in detergent, (2) mixture of labeled DcuS in detergent, and (3) mixture of labeled DcuS reconstituted into liposomes. Aliquots of DcuS were labeled with either donor or acceptor. Labeled DcuS batches were mixed and then measured in detergent or functionally reconstituted into liposomes to examine the functionally-relevant oligomeric state of DcuS.

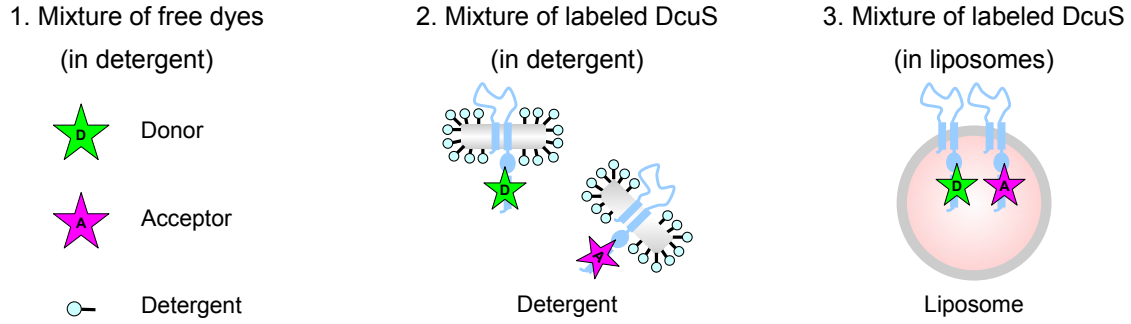

Figure 4.17: Samples for *in vitro* FRET measurements: (1) mixture of donor and acceptor (free dyes) in detergent; (2) mixture of donor- and acceptor-labeled DcuS in detergent; (3) mixture of donor- and acceptor-labeled DcuS reconstituted into liposomes.

Intrinsic Fluorescence and Protein Stability The protein stability of DcuS was monitored by intrinsic fluorescence *in vitro*, in the absence or presence of extrinsic labeling (Fig. 4.1, 3. Intrinsic fluorescence). The emission maximum (λ_{max}) of intrinsic tryptophan fluorescence of DcuS was monitored as an indicator of protein stability or folding during storage (Fig. 4.18, red circle). While excited at 280 nm, DcuS protein showed an emission maximum (λ_{max}) at 335 nm. If the protein unfolds or denatures during storage, the emission maximum will shift to a longer wavelength due to exposure to a more polar environment. In this study, DcuS protein was stored at -20 °C before use. The emission maxima (λ_{max}) of DcuS proteins remain steady at 335 nm during storage (Fig. 4.18, red circle), indicating that DcuS proteins remain stable for a short-term storage of at least two weeks.

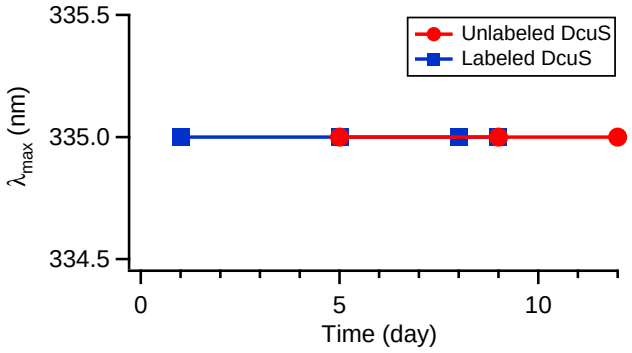

Figure 4.18: Protein stability of DcuS monitored by intrinsic fluorescence. DcuS proteins, unlabeled (red circle) and labeled (blue square), were excited at 280 nm. Wavelength of emission maxima (λ^{em}_{max}) were recorded as a function of time (day).

In the presence of extrinsic fluorescent labeling, the tryptophan emission maximum (λ_{max}) of labeled DcuS (Fig. 4.18, blue square) were still at 335 nm, comparable to that of unlabeled DcuS (Fig. 4.18, red circle). Therefore, the labeling of fluorophores on DcuS protein had no effect on the protein folding and native conformations. Moreover, the emission maxima (λ_{max}) of labeled DcuS remained steady at 335 nm during storage (Fig. 4.18, blue square), indicating that labeled DcuS remained stable for a short-term storage of at least one week. Since protein samples were always measured immediately after labeling without long-term storage, measured DcuS proteins are supposed to fold correctly to their native conformations in this study.

Conclusion Wild-type and cysteine mutants of DcuS were generated and labeled with thiol-reactive fluorophores. However, DcuS (Cys^-) mutant was considerably labeled by different thiol-specific reactive groups (maleimide and iodocac-

etamide). Even no specific labeling of DcuS could be achieved, oligomerization of DcuS *in vitro* (Sec. 4.3.2) can still be examined by inter-molecular FRET.

4.2 Quantitative FRET Analysis

The degree of oligomerization of DcuS was aimed to be determined by fitting with a model of oligomeric states (2.4). This model requires the FRET efficiency (E) as a function of the donor fraction (f_D). FRET efficiencies are often determined by reduced donor fluorescence or sensitized acceptor fluorescence (2.3.2). For this, the fluorescence intensity of one fluorophore (donor or acceptor) in the complex is compared with the fluorescence intensity in the absence of the other fluorophore. This comparison requires that the fluorophore concentrations are either constant or known. However, in living cells constant fluorophore concentrations are hard to achieve. Therefore, the fluorophore concentrations have to be determined. This is usually done by absorption spectroscopy. However, this cannot be done with samples which scatter light strongly, e.g. cells or samples containing liposomes or detergent micelles. Scattering problem is a common issue in our samples. Take the Alexa 488-labeled DcuS reconstituted in liposomes as an example. A typical absorption of Alexa 488 (Fig. 4.19, black) was completely masked in the absorption spectrum of Alexa 488-labeled DcuS in liposomes (Fig. 4.19, red). Because of the scattering originated from the liposomes, the concentration of Alexa 488 cannot be determined by absorption. Similarly, it is also difficult to determine the fluorophore concentrations in DcuS-FP expressing *E. coli* cells because of the scattering originated from the cell particles.

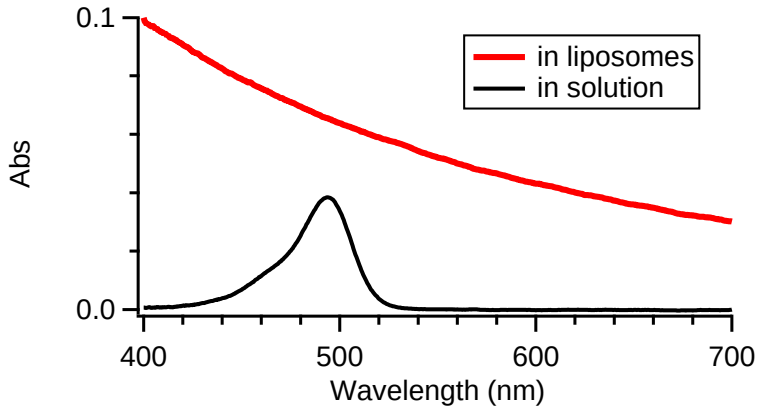

Figure 4.19: Two absorption spectra of Alexa 488-maleimide (Alexa 488) with different background. Red: Alexa 488-labeled DcuS protein reconstituted into liposomes ($\approx$ 0.5 μM estimated from emission spectrum). Black: Alexa 488 (0.5 μM) dissolved in DcuS-labeling-buffer exhibits absorption maximum at 494 nm.

To deal with the general problem of scattering, a method was developed in this study, without the requirement of known fluorophore concentrations for the de-

termination of both FRET efficiency and donor fraction. For this, we modified a method described by Gordon *et al.* [48], which is based on fluorescence emission spectra and does not use absorption. The method yields not only FRET efficiencies but also a measure for the fluorophore concentrations to determine the donor fraction. However, this method presumes background-free fluorescence signals of donor, acceptor, and complex of both. Because measured fluorescence spectra, at least in our case, were strongly contaminated with background originated from different sources, the background must be removed before applying this method.

In summary, our quantitative FRET analysis consists of three steps as described in Fig. 4.20. The first step, spectral correction and background subtraction, is to prepare background-free spectra for further FRET quantification. The second step, Gordon's equation, is to determine FRET efficiency (E) and donor fraction (f_D) from the corrected spectra. The third step is to determine the degree of oligomerization (n) by fitting a model of oligomeric states to the plot of FRET efficiency against donor fraction. By integrating these three steps into a computer procedure, an automatic quantitative FRET analysis was developed which is easy, fast, and high-throughout to quantify FRET accurately and robustly, even in living cells.

4.2.1 Step 1: Spectral Correction and Background Subtraction

The first step of our FRET analysis is to prepare background-free corrected spectra for further FRET quantification. All measured spectra were first processed by a general series of spectral corrections (4.2.1.1). The preliminarily-corrected spectra were than subjected to further background subtraction (4.2.1.2). For a reliable subtraction of potential background, a flexible background subtraction (FBS) was developed based on a multi-parameter fitting function (4.2.1.3) which can remove the background individually, instead of subtraction by a fixed background. The accuracy and consistency of FBS was theoretically validated by Monte Carlo simulation (4.2.1.4), then tested the accuracy and applicability of FBS experimentally by defined dilution series and mixture series in living cells (4.2.1.5). FBS was verified to yield background-free spectra for further FRET quantification, even in living cells.

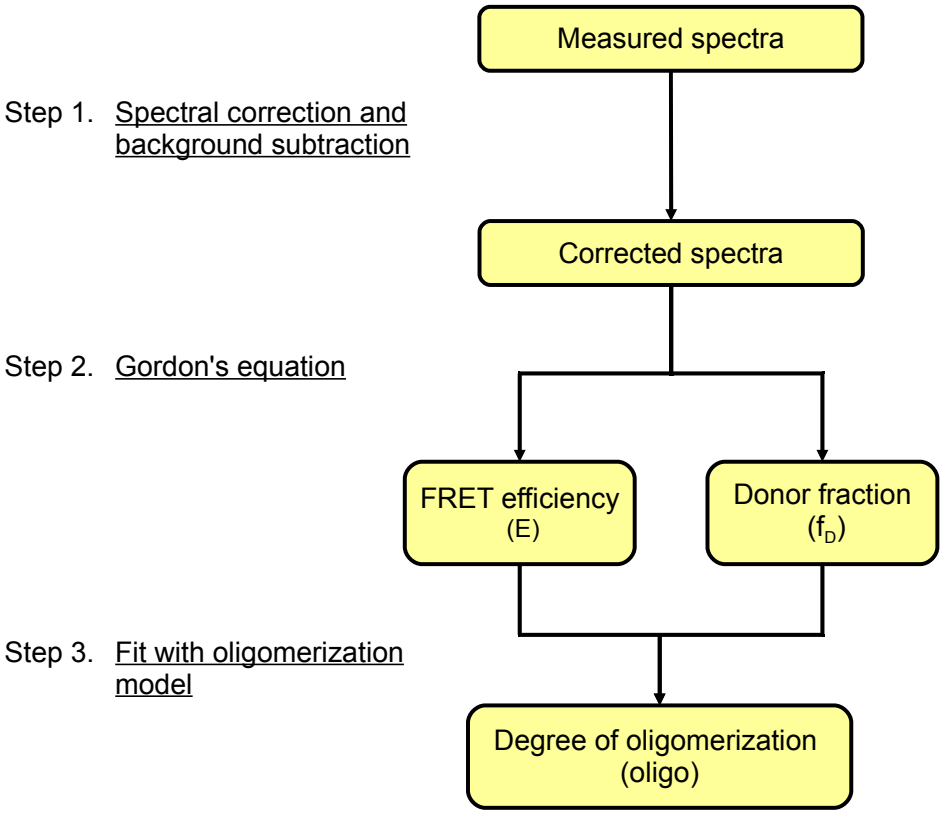

Figure 4.20: Workflow scheme: quantitative FRET analysis.

4.2.1.1 Spectral Correction

The measured fluorescence spectra were processed by a general series of spectral corrections as follows:

1. **Fluorescence intensity of the signal detector** was corrected for the dead-time of the detector by Eq. (4.1) [59], [60]:

$$F_{corr} = \frac{F}{1 - \frac{F}{Saturation}} \tag{4.1}$$

where F is the observed fluorescence intensity, F_{corr} is the corrected fluorescence intensity, $Saturation$ is the detection limit of the signal detector. According to the instruction manual, the signal detector (Fig. 2.2) saturates at 2×10^7, and the fluorescence signal is non-linear above 2×10^6. An empirical value ($2 \times 10^7 \times 1.66$) for $Saturation$ obtained after trials was used.

2. **Reference detector** The temporal fluctuations of the light source were corrected by building the ratio:

$$F_{corr} = \frac{F}{R} \tag{4.2}$$

where R is the reference signal (Fig. 2.2) simultaneously recorded by the reference detector to correct the time-dependent fluctuation of the light source and the wavelength-dependence of the excitation monochromator.

3. **Wavelength dependence of the detector** was corrected by multiplying with the manufacturer's correction factor $c(\lambda)$ for our FluoroMax-2 spectrofluorometer (Jobin Yvon-Spex), Fig. 4.21):

$$F_{corr} = F \times c(\lambda) \tag{4.3}$$

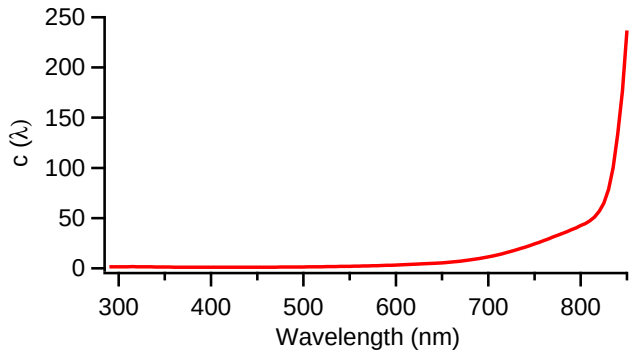

Figure 4.21: The manufacturer's correction factor ($c(\lambda)$) to correct for variations in the spectral detector sensitivity.

4.2.1.2 Background Problems

After these general spectral correction, the spectra were subjected to individual processes to remove potential background signals. Take *E. coli* cells expressing both donor (D) and acceptor (A) as an example (Fig. 4.22), the measured spectrum (DA, black) contains not only signals from donor (blue) and acceptor (yellow), but background signals including:

- Cellular autofluorescence from *E. coli* cells (red)
- Rayleigh scattering from *E. coli* cell particles (purple)
- Raman scattering from buffer (green)
- Offset from instrumental noise (grey)

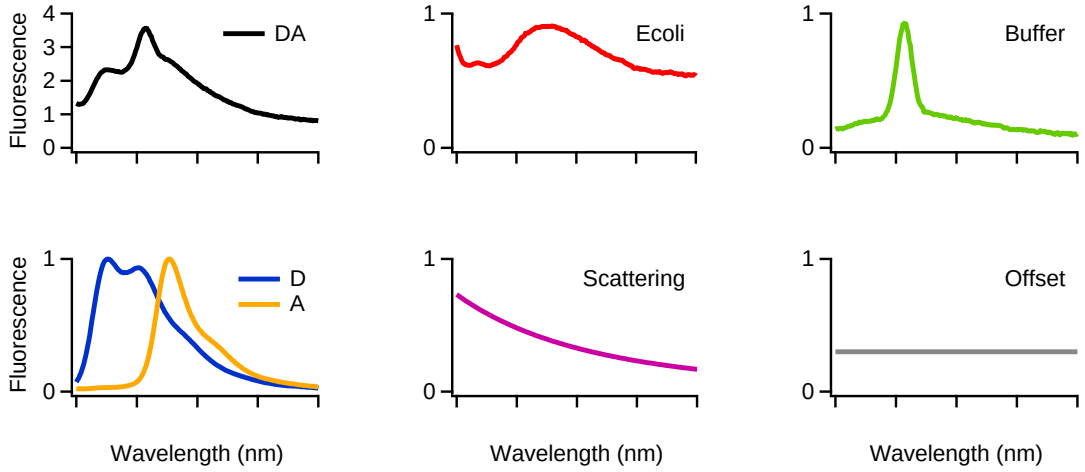

Figure 4.22: Spectral Components. Measured spectrum (black) of *E. coli* cells containing both donor and acceptor. In addition to signals from donor (blue) and acceptor (yellow), measured spectrum contains background signals such as: (1) *E. coli* (red): cellular autofluorescence, (2) buffer (green): Raman scattering, (3) cell particles (purple): Rayleigh scattering, (4) offset (grey): instrumental noise.

E. coli cellular autofluorescence causes inevitable background problems for *in vivo* fluorescence measurements. *E. coli* cells contain endogenous fluorophores, such as nicotinamide adenine dinucleotide (NADH)and flavin adenine dinucleotide (FAD) [61]. The Rayleigh scattering in our experiments is originated from lipid or detergent micelles (*in vitro*) or from cell particles (*in vivo*). The extent of scattering depends on the size and the amount of particles. Larger particles, such as liposome or *E. coli* cells, scatter stronger than smaller ones. The more particles cause the stronger scattering. In addition, a Raman scattering from water (buffer) and an offset from the instrumental noise are also observable. Because the background signals varies from cell to cell, it is not adequate to subtract an individual sample signal by a universal background. Therefore, a flexible background subtraction (FBS) was developed to eliminate the heterogeneous background signals among cells or liposomes.

4.2.1.3 Concept of Flexible Background Subtraction

Take again the measured spectrum obtained from *E. coli* cells expressing both CFP donor (D) and YFP acceptor (A) as an example. The measured spectrum (Fig. 4.23, left) can be regarded as a linear superposition of all fluorescence signals (spectra of donor and acceptor) and background signals (spectra of scattering, autofluorescence, and so on).

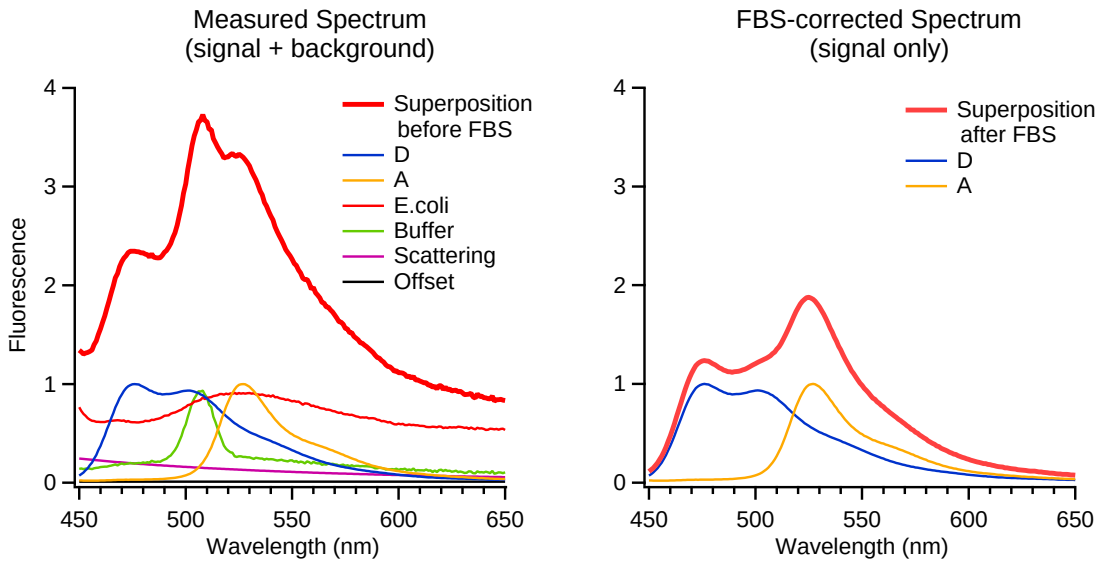

Figure 4.23: Concept of multi-parameter fitting function. Left: measured spectrum as a superposition of all signals and background signals. Right: FBS-corrected spectrum as a superposition of all signals without background. The spectral components in the multi-parameter fitting function include: offset (a), scattering ($\frac{b}{x^4}$), Raman scattering ($c*Buffer(x)$), *E. coli* autofluorescence ($d*Ecoli(x)$), CFP fluorescence ($e*D(x)$), and YFP fluorescence ($f*A(x)$).

To remove the background signals and to extract the pure fluorescence signals from the measured spectrum, a multi-parameter fit was applied (Eq. (4.4)). This equation describes the measured spectrum as a sum of all fluorescence signals and background signals (Fig. 4.23, left), including offset (a), scattering ($\frac{b}{x^4}$), Raman scattering ($c*Buffer(x)$), *E. coli* autofluororescence ($d*Ecoli(x)$), CFP fluorescence ($e*D(x)$), and YFP fluorescence ($f*A(x)$).

$$FI(x) = a + \frac{b}{x^4} + c*Buffer(x) + d*Ecoli(x) + e*D(x) + f*A(x) \tag{4.4}$$

Each signal has an individual prefactor (a-f). The measured spectra were fitted with Eq. (4.4) in order to obtain the individual contributions of each signal. By removing the background, the signals of donor and acceptor can be extracted (Fig. 4.23, right).

Reference Spectra The accuracy and reliability of the multi-parameter fitting function depends on the quality of the spectral components (reference spectra). Before applying the multi-parameter fit to our measured spectra, reference spectra were recorded (Fig. 4.22).

a. **Offset:** assumed as a weak constant detector noise.

b. **Rayleigh scattering:** The intensity is proportional to $\frac{1}{\lambda^4}$ [47]

c. **Raman scattering:** Instead of a standard spectrum, individual reference spectrum from the buffer spectrum was recorded at the same day and under the same conditions for each test series.

d. **Cellular autofluorescence:** Instead of a standard spectrum, individual reference spectrum was recorded from the *E. coli* spectrum grown in parallel to the FP-expressing cell samples under the same conditions for each test series.

e. **CFP donor:** cytosolic CFP (without fusion, details see Sec. 3.2.2) was purified to obtain reference spectra (Fig. 4.24). Autofluorescence spectra (Fig. 4.22) are usually broader than the CFP spectra. The scattering and autofluorescence were obviously removed during purification steps (Fig. 4.24, arrows). No more narrower spectra were observed after the second and third steps, suggesting no more autofluorescent molecules to be removed. The constant spectral shape suggests an almost background-free reference spectrum (Fig. 4.22). The major peak position (476 nm) of purified CFP was in good agreement with the literature values.

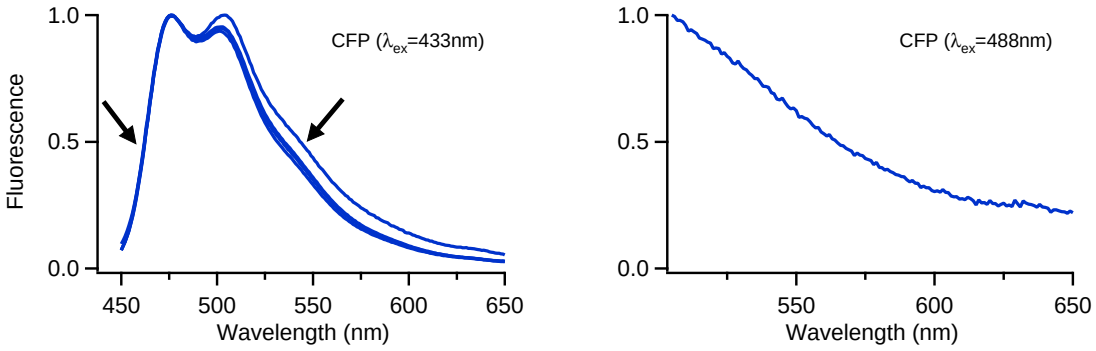

Figure 4.24: Reference spectra of CFP. CFP was purified from cell lysates to remove the autofluorescence components by purification steps, including centrifugation, ultracentrifugation, and three runs of concentration by vivaspin (3.2.2). For each run of vivaspin concentration, emission spectra were recorded at an excitation wavelength of 433 nm or 488 nm respectively. Autofluorescence and scattering were gradually removed during purification steps (left, arrows).

f. **YFP acceptor:** Reference spectrum of purified YFP was prepared in the same way as CFP (Fig. 4.25). The peak position (527 nm) and spectral shape of purified YFP was in good agreement with the literature values.

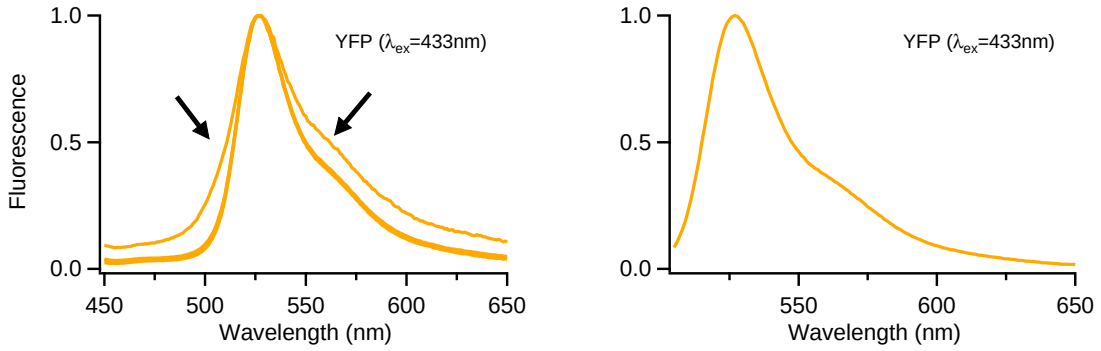

Figure 4.25: Reference spectra of YFP. For more details see Fig. 4.24.

4.2.1.4 Monte Carlo Simulation of Background Subtraction

Concept: Simulation and Analysis Before applying flexible background subtraction (FBS) to our experimental data, the accuracy and consistency of our multi-parameter fitting function for FBS was theoretically examined by a numerical test based on Monte Carlo simulation. The concept of our Monte Carlo Simulation test is as follows:

1. Generated a spectrum (Fig. 4.26, red) by creating random values for the parameters (a-f) of Eq. (4.4)

2. Analyzed the spectrum with our FBS routine (Fig. 4.26, black dashed), i.e. used Eq. (4.4) for a second time, to determine the fitting parameters (a'-f')

3. Built the difference between values from the fit and the created spectrum ($\Delta a = a' - a$, ...)

By repeating **steps 1-3** for 10,000 times, the differences as histograms were plotted for all parameters (Δa-Δf) and built the average and standard deviation for each parameter.

Two examples of Monte Carlo simulation and analysis are shown in Fig. 4.26, and the results of 10,000 repeats are shown in Fig. 4.27. The fitting results are in perfect agreement with the simulated spectra.

To test the accuracy and consistency of our fitting function, the Monte Carlo simulation and analysis were performed under different conditions, such as adding spectral noise, changing the starting values, or both modifications.

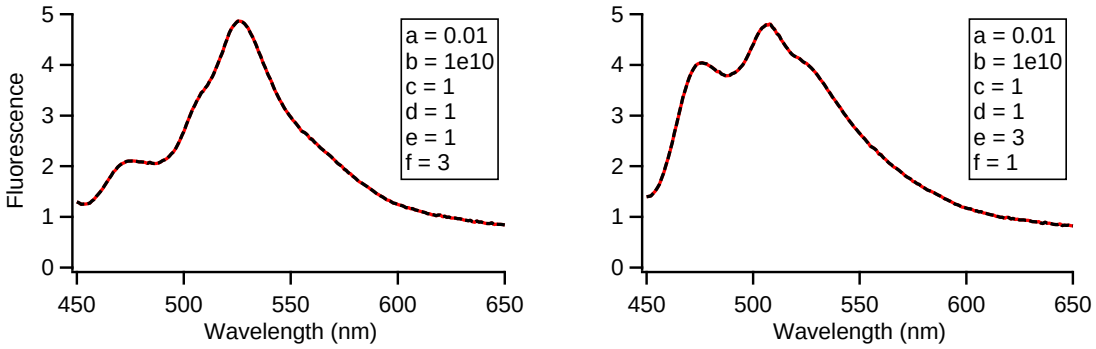

Figure 4.26: Two examples of simulated spectra. Spectra (red solid line) were created by arbitrary values of a-f and Eq. (4.4), and then treated by the FBS routine (black dashed line).

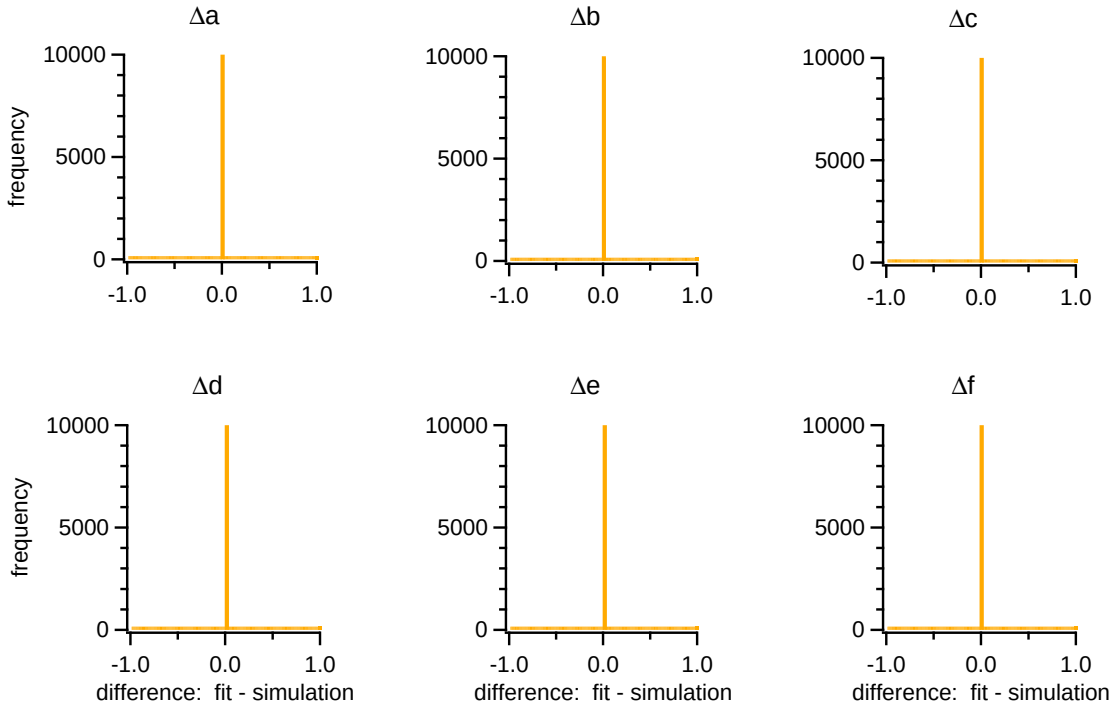

Figure 4.27: An example of results of Monte Carlo simulation and analysis. 10,000 spectra were generated with Eq. (4.4) and random values for the parameters a-f. Subsequently, the spectra were analyzed by FBS routine yielding a'-f' and the differences (Δa-Δf) were plotted as histograms.

Spectral Noise To test if the relatively low signal-to-noise ratio in biological samples (in particular in living cells) may affect the performance of the fitting function, the fitting function was examined by adding extrinsic noise to the simulated spectra as follows:

1. Generated a spectrum by creating random values for the parameters (a-f)
2. **Added extrinsic noise (from 0% to 10% relative to the peak value of each generated spectrum, respectively) to the new spectrum**
3. Analyzed the new spectrum to determine the fitting parameters (a'-f')
4. Built the difference (fit-simulation)

For each extent of extrinsic noise (0%∼10%) in the step 2, **steps 1-4** were repeated for 10,000 times. The results of the test containing noise (1%) were shown in Fig. 4.28. The widths of the distribution indicate the errors in the determination of each fitting parameters. Even the errors in the histograms were larger compared with the test without noise (Fig. 4.27), the accuracy of averages were still comparable to those obtained from the test in the absence of noise. Note, that the most important values of D and A reveal the smallest errors (Δe and Δf). Moreover, the averages of differences (Δe and Δf) were plotted as a function of added noise (Fig. 4.29). For the contributions of donor (Fig. 4.29, left, Δe) and acceptor (Fig. 4.29, right, Δf), the average values of the differences (Δe and Δf) are always 0, only the errors of the differences increased with the noise added to the simulated spectra. While the actual spectral noise of our experimental data is around 1% (Fig. 4.29, arrows), the fitting function can determine the fitting parameters of donor (parameter e) and acceptor (parameter f) with an error of only 2% and 4% respectively. In conclusion, the fitting performance should be reliable for our experimental data despite of the spectral noise.

Starting values To test if different starting values may affect the performance of our fitting function, the fitting function was then examined by using randomly generated sets of starting values as follows:

1. Generated a spectrum by creating random values for the parameters (a-f)
2. **Created random values for the starting values for parameters (a_s-f_s). The starting values for each parameters were set in the following ranges: a ($-0.1 \sim 0.1$), b ($-1\times^{10} \sim 3\times 10^{10}$), c (-1∼3), d (0∼3), e (0∼3), f (0∼3)**
3. Analyzed the new spectrum to determine the fitting parameters (a'-f')

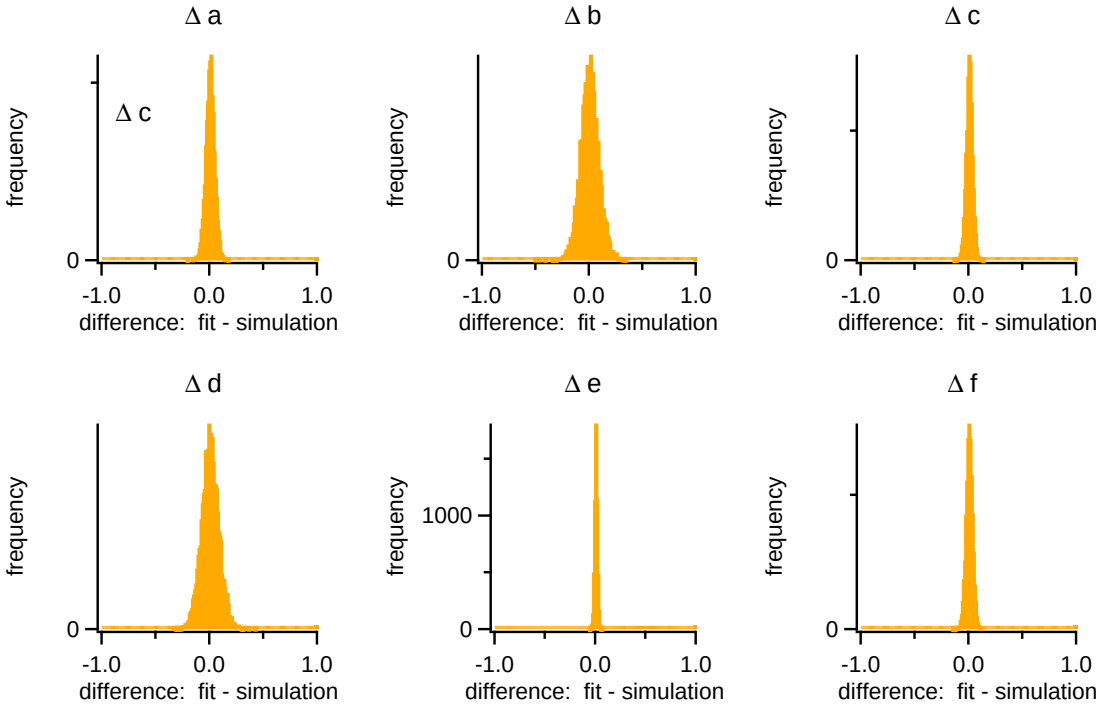

Figure 4.28: The effect of spectral noise on the accuracy of our FBS routine for the individual contributions of donor and acceptor. 10,000 spectra were generated with Eq. (4.4) and random values for the parameters a-f. 1% of noise (relative to the peak intensity of each spectrum) was added to these spectra. The simulated spectra were then analyzed by FBS routine, and the differences (Δa-Δf) were plotted as histograms.

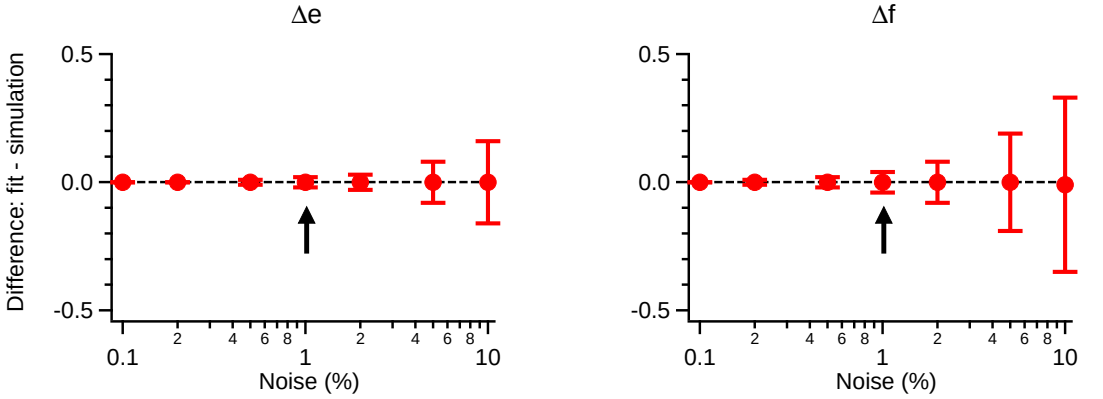

Figure 4.29: The effect of spectral noise on our FBS routine. Simulated spectra were generated by adding various noise (0%, 0.1%, 0.2%, 0.5%, 1%, 2%, 5%, 10% of the peak intensity of each spectrum). The simulated spectra containing different levels of noise were analyzed by the FBS routine. The average values of the differences with their standard deviations were plotted as a function of noise. The arrow indicates the actual noise level (1%) in our measured spectra.

4. Built the difference (fit-simulation)

Steps 2-4 were repeated for 10,000 times. The results looked exactly the same as Fig. 4.27. The fitting results (fit) matched perfectly with the original spectral data (simulation). The accuracy and consistency of our FBS routine was verified despite of various starting values, i.e. FBS dos not depend on the choice of the starting values.

Spectral Noise and Starting Values Moreover, Monte Carlo simulation was performed on noise-added simulated spectra by using various sets of starting values as follows:

1. Generated a spectrum by creating random values for the parameters (a-f)
2. **Added 10% noise to the spectrum**
3. **Created random values for the starting values for parameters (a_s-f_s)**
4. Analyzed the new spectrum to determine the fitting parameters (a'-f')
5. Built the difference (fit-simulation)

By repeating **steps 1-2** for 10 times to generate 10 simulated spectra and repeating **steps 3-5** for 1,000 times for each spectra, the results were very similar to Fig. 4.28. In particular, the standard deviations for Δe and Δf did not change very much and still in the range of 2%-4%. The accuracy and consistency of the fitting function was verified despite of various starting values, even in the presence of 10% of spectral noise. Since the actual spectral noise of our experimental data is around 1%, the fitting performance is almost independent of the starting values.

Conclusion The robustness of our background subtraction algorithm was tested by generating random spectra, and by adding spectral noise, changing the starting values and by applying both modifications. The values obtained by the fitting procedure were in good agreements with the initial values of the parameters used for creating the spectra. This means that signal and background could be determined with high accuracy, and the background can be removed from the raw data efficiently. In conclusion, the applicability of our multi-parameter fitting function was successfully proved by Monte Carlo simulation.

4.2.1.5 Experimental Validation of Background Subtraction

The accuracy of our fitting function was also evaluated experimentally by using defined mixtures of CFP and YFP in living cells. To check if the decrease of fluorophore concentration may affect the performance of our fitting function, various dilution series and mixture series were tested as follows:

1. Dilution by substitution with *E. coli*
   a. CFP-expressing cells
   b. YFP-expressing cells
2. Mixtures of CFP- and YFP-expressing cells
3. Mixtures of *E. coli* cells (no D/A), CFP- and YFP-expressing cells
   a. fixed amount of *E. coli* cells
   b. fixed amount of CFP-expressing cells
   c. fixed amount of YFP-expressing cells

All test series have been analyzed with Eq. (4.4) to remove background and to determine the contributions of donor and acceptor.

Dilution by substitution with *E. coli* To check if the decrease of CFP fluorescence may affect the performance of our fit, a dilution series of CFP-expressing *E. coli* cells was tested (Fig. 4.30, left) by substitution with *E. coli* cells (no FP). Upon serial dilution of the CFP-expressing cells, a linear decrease in fluorescence of CFP was expected to pass through the origin. The linear fit of fitting results of parameter e (CFP) (Fig. 4.30, right) demonstrated that the decrease in CFP concentration had no effect on the accuracy of the fit.

Similarly, a dilution series of YFP-expressing *E. coli* cells was also tested (Fig. 4.31, left) to check if the decrease of YFP fluorescence may affect the performance of our fit. Upon serial dilution of the YFP-expressing cells, a decrease in fluorescence of YFP was expected to pass through the origin. The linear fit of fitting results of parameter f (YFP) as a function of relative cell concentration (Fig. 4.31, right) demonstrated that the decrease in YFP concentration had no effect on the accuracy of the fit.

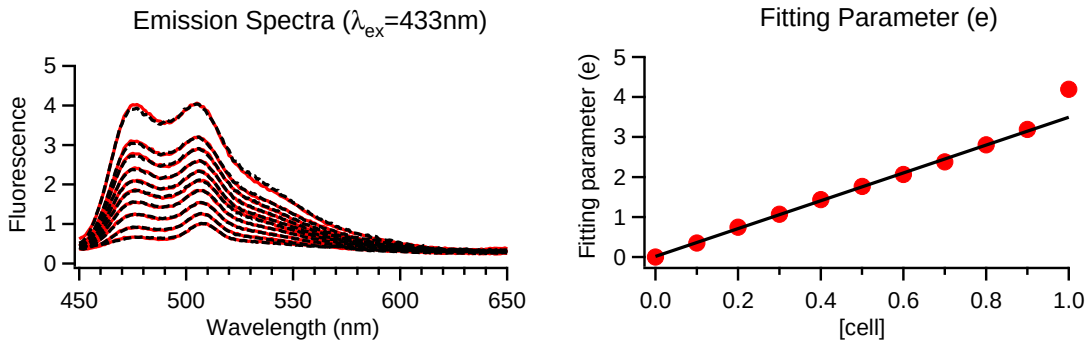

Figure 4.30: Dilution Series of CFP-expressing cells to examine the effect of fluorophore concentration on the accuracy of multi-parameter fitting. CFP-expressing *E. coli* cells were serially diluted by substitution with *E. coli* cells. Emission spectra were measured at excitation wavelength of CFP (433 nm) in PBS buffer. Measured spectra (red) were analyzed by FBS routine yielding fitted spectra (black dashed). The fitting results for parameter e (the contribution of CFP) were plotted against relative CFP-expressing cell concentration (red dot). The initial concentration of CFP-expressing cells was set as 1.0. The linear fit to the data was indicated by a black solid line.

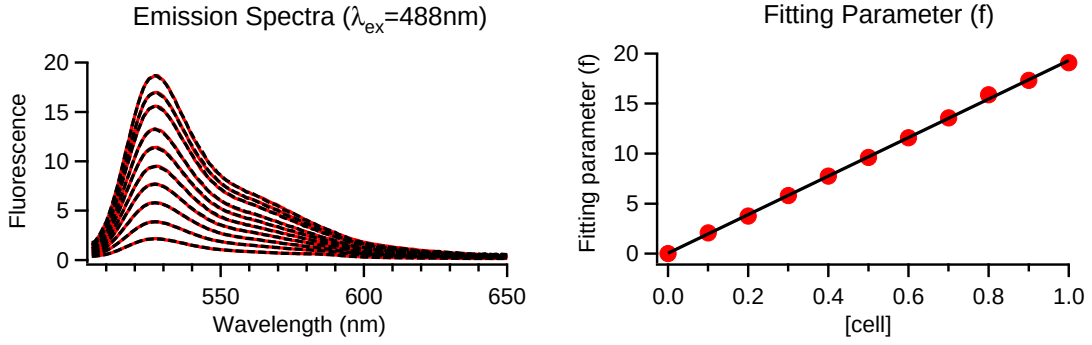

Figure 4.31: Dilution Series of YFP-expressing cells. YFP-expressing *E. coli* cells were serially diluted by substitution with *E. coli* cells. Emission spectra were measured at an excitation wavelength of YFP (488 nm) in PBS buffer. For more details see Fig. 4.30

Mixture series of CFP-expressing and YFP-expressing cells To check if the co-existence of CFP fluorescence and YFP fluorescence affect the performance of our fit, a mixture series of CFP-expressing and YFP-expressing cells was tested. CFP and YFP were expressed independently in *E. coli* cells. CFP-expressing cells and YFP-expressing cells were mixed at different ratios (Fig. 4.32, upper panel). Two different excitation wavelength were used (433 nm and 488 nm). The fitting results revealed a linear increase of CFP through the origin and a linear decrease of YFP through the point (1,0). (Fig. 4.32, lower panel). No offsets in both linear fits demonstrated that the difference in the relative ratio of CFP to YFP had no effect on the accuracy of the fit.

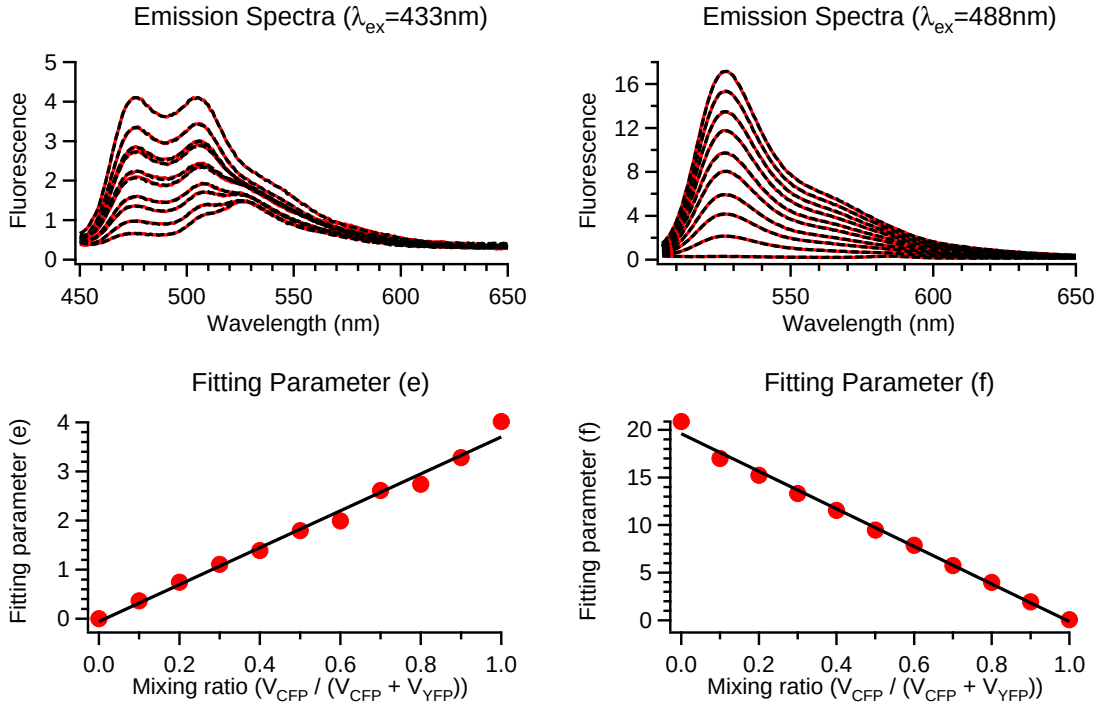

Figure 4.32: Mixture series of CFP-expressing cells and YFP-expressing cells. Stock solutions of CFP-expressing cells and YFP-expressing cells were mixed at different ratios ($\frac{V_{CFP}}{V_{CFP}+V_{YFP}}$). Samples were prepared with increasing V_{CFP} (volume of CFP-expressing cell solution) and decreasing V_{YFP} (volume of YFP-expressing cell solution) to a total volume ($V_{CFP}+V_{YFP}$) of 1 ml. Emission spectra were measured in PBS buffer, by excitation at 433 nm and 488 nm respectively. Measured spectra (red) were analyzed by FBS routine. The fitting results for parameter e (lower left, the contribution of CFP) and parameter f (lower right, the contribution of YFP) were plotted against mixing ratio ($\frac{V_{CFP}}{V_{CFP}+V_{YFP}}$).

Mixtures of *E. coli* cells (no D/A), CFP- and YFP-expressing cells To test if an additional *E. coli* background may affect the performance of our fitting function,

a fixed amount of *E. coli* cells was added to the mixture series of CFP-expressing cells and YFP-expressing cells (Fig. 4.33, upper panel). The fitting results revealed a linear increase of CFP and a linear decrease of YFP as expected (Fig. 4.33, lower panel), and the accuracy in the presence of additional *E. coli* background was comparable to that in the absence of additional *E. coli* background (Fig. 4.32), revealing that the additional *E. coli* background in the mixture series had no effect on the accuracy of the fitting function.

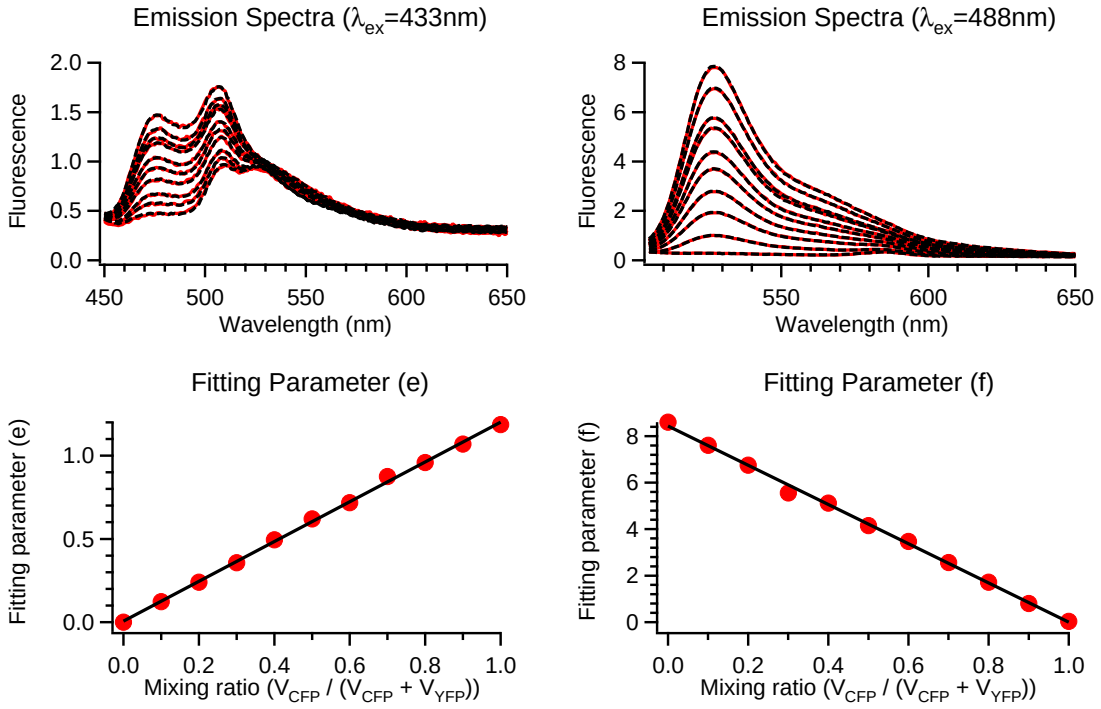

Figure 4.33: Mixture series of CFP-expressing cells and YFP-expressing cells containing a fixed amount of *E. coli* cells. In the presence of constant amount of non-FP-expressing *E. coli* cells (V_{Ecoli}), CFP-expressing cells and YFP-expressing cells were mixed at different ratios ($\frac{V_{CFP}}{V_{CFP}+V_{YFP}}$) to a total volume ($V_{CFP}+V_{YFP}+V_{Ecoli}$) of 1 ml. Conditions see Fig. 4.32

Similarly, the mixtures of fixed amount of CFP-expressing cells, and increased the amount of YFP-expressing cells in the mixtures were prepared (Fig. 4.34, upper panel). The fitting results revealed a constant level of CFP and a linear increase of YFP as expected (Fig. 4.34, lower panel).

Finally, the mixtures of fixed amount of YFP-expressing cells, and increased the amount of CFP-expressing cells in the mixtures were prepared (Fig. 4.35, upper panel). The fitting results revealed a constant level of YFP and a linear increase of CFP as expected (Fig. 4.34, lower panel).

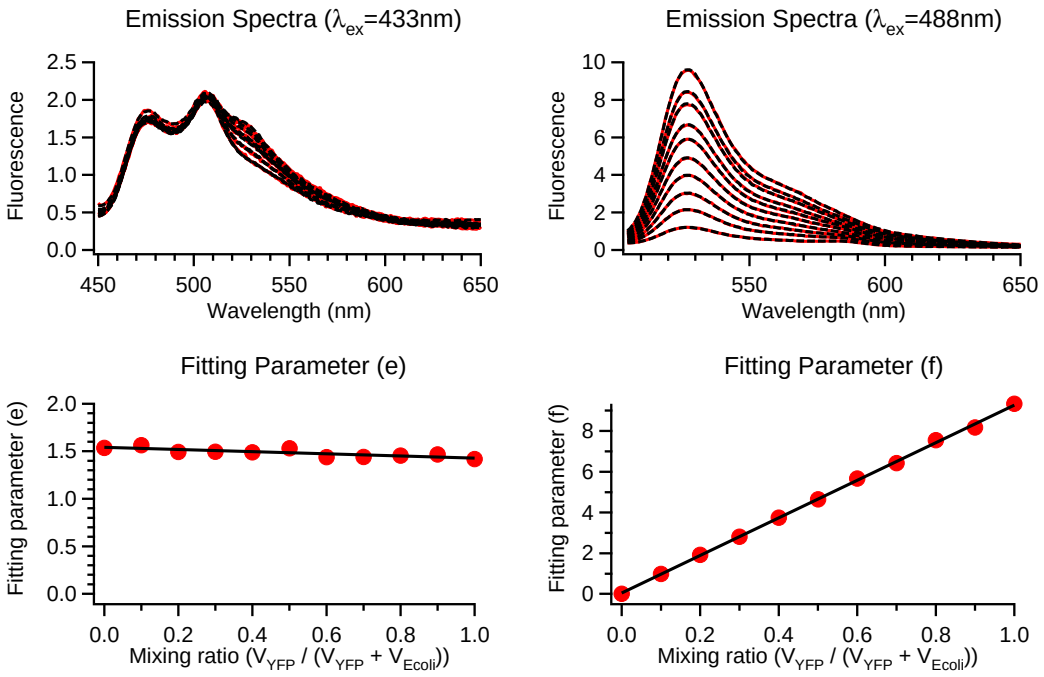

Figure 4.34: Mixture series of YFP-expressing cells and non-FP-expressing *E. coli* cells containing a fixed amount of CFP-expressing cells. In the presence of constant amount of CFP-expressing cells (V_{CFP}), YFP-expressing cells were mixed with *E. coli* cells at different ratios ($\frac{V_{YFP}}{V_{YFP}+V_{Ecoli}}$) to a total volume ($V_{CFP}+V_{YFP}+V_{Ecoli}$) of 1 ml. Conditions see Fig. 4.32

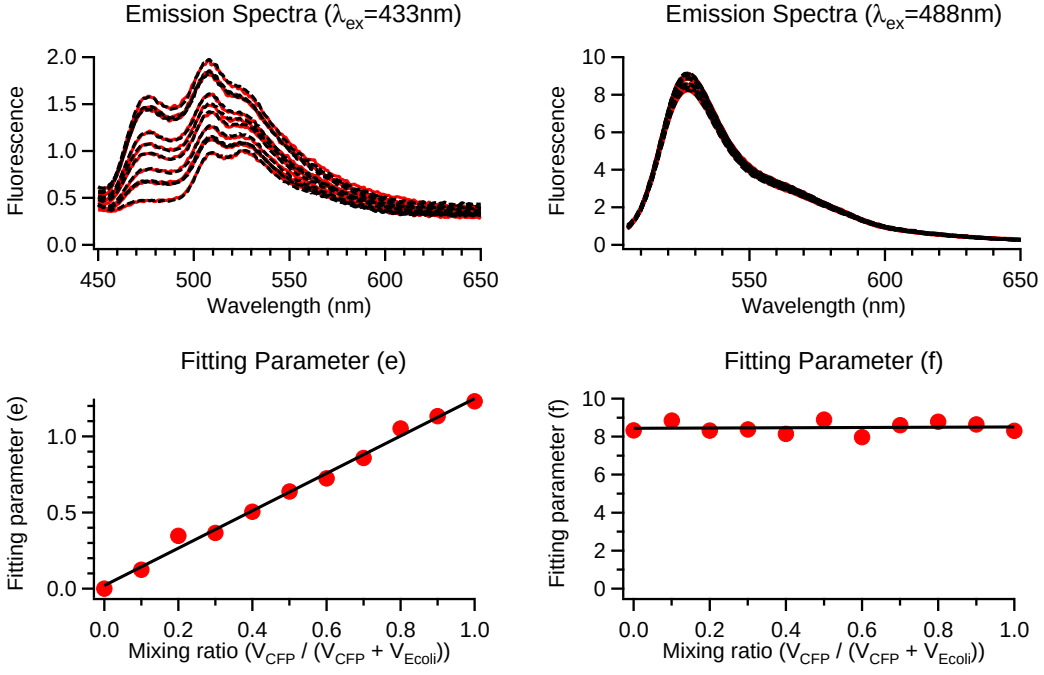

Figure 4.35: Mixture series of CFP-expressing cells and non-FP-expressing *E. coli* cells containing a fixed amount of YFP-expressing cells. In the presence of constant amount of YFP-expressing cells (V_{YFP}), CFP-expressing cells were mixed with *E. coli* cells at different ratios ($\frac{V_{CFP}}{V_{CFP}+V_{Ecoli}}$) to a total volume ($V_{CFP}+V_{YFP}+V_{Ecoli}$) of 1 ml. Conditions see Fig. 4.32

Conclusion The first step of our automatic FRET analysis, flexible background subtraction (FBS) based on a multi-parameter fitting, was verified theoretically and experimentally. The accuracy and consistency of our FBS routine was validated by Monte Carlo simulations. The applicability of it to our *in vivo* measurements was carefully examined by various defined dilution series and mixture series of FP-expressing cells. Our fitting function can accurately determine the amounts of CFP and YFP in living cells, even the absolute and relative fluorescence intensities in the samples are of different magnitudes. In conclusion, our flexible background subtraction (FBS) can accurately and effectively yield background-free spectra for the second step, subsequent calculation of FRET efficiency and fluorophore concentration indexes.

4.2.2 Step 2: Gordon's Equation

4.2.2.1 Adaptation for Fluorescence Spectroscopy

The second step of our FRET analysis is for the accurate determination of FRET efficiency and donor fraction based on the background-free FBS-corrected spectra obtained from step 1 (4.2.1). Gordon's equation (Eq. (2.10)) [48], originally developed for fluorescence microscopy, is a FRET quantification method combining the correction for spectral crosstalk with the normalization for variations in fluorescence concentrations.

The applicability of Gordon's equation was extended to fluorescence spectroscopy by the following adaptations to quantify FRET efficiency and donor fraction from measured spectra (Fig. 4.36):

- 3 values from spectra of samples containing both donor and acceptor (DA)
- 6 values from spectra of references containing either donor (D) or acceptor (A)
- G factor for FRET pair (see below)

The concept of filter sets (channels) in fluorescence microscopy was converted into excitation/detection wavelength pairs in fluorescence spectroscopy (Fig. 4.37). Gordon's equation is based on the detection of both quenched donor emission and sensitized acceptor emission. To apply Gordon's equation to fluorescence spectroscopy, two emission spectra of each sample were recorded by excitation of mainly donor or acceptor respectively. For the detection of FRET, donors are

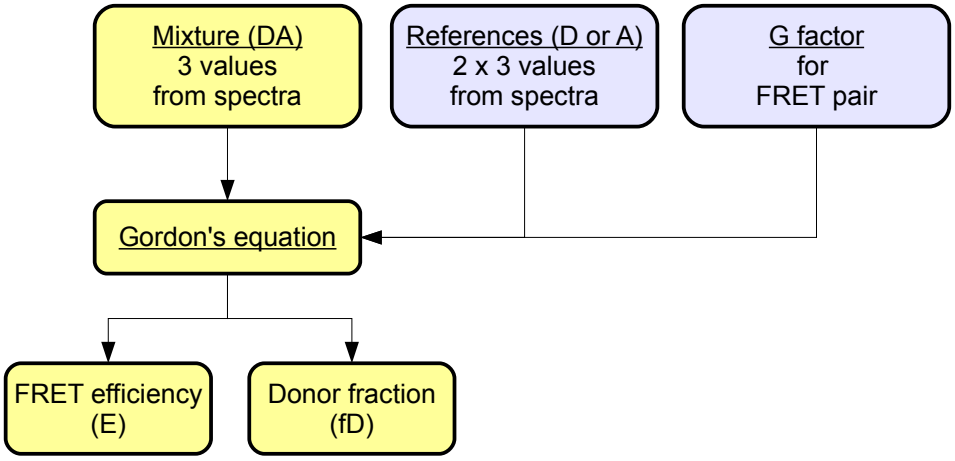

Figure 4.36: Adaptation of Gordon's equation for fluorescence spectroscopy. 3 values from samples containing both donor and acceptor were determined every times to quantify corresponding FRET efficiency and donor fraction in the presence of both donor and acceptor. 6 values from references (either donor or acceptor) and G factor were determined once for each FRET pair in this study.

excited at their absorption wavelength maximum, and FRET signals are detected at acceptor emission wavelength simultaneously. However, donors may not exclusively excited at their excitation wavelength. Due to the requirement of spectral overlap between donor emission and acceptor absorption for the occurrence of FRET, acceptors may also be excited at donor excitation wavelength and detected at acceptor emission wavelength. Therefore, not only FRET signals but other non-FRET signals (the direct excitation of acceptor at donor excitation wavelength and the detection of donor emission at acceptor emission wavelength) may also be detected at acceptor emission wavelength. For the separation of FRET and non-FRET signals, Gordon's equation corrects these cross talk by three filter sets in fluorescence microscopy. In our cases for spectroscopy, three values were extracted from two measured spectra mentioned above by the following three excitation/detection wavelength pairs (Fig. 4.37):

- Donor (D): excitation at the wavelength of donor excitation maximum (λ_{ex}^{D}) / detection at the wavelength of donor emission maximum (λ_{em}^{D}), hereafter cited as λ_D/λ_D
- FRET (F): λ_{ex}^{D} / detection at the wavelength of acceptor emission maximum (λ_{em}^{A}), hereafter cited as λ_D/λ_A
- Acceptor (A): excitation at the wavelength of donor excitation maximum (λ_{ex}^{A}) / λ_{em}^{A}, hereafter cited as λ_A/λ_A

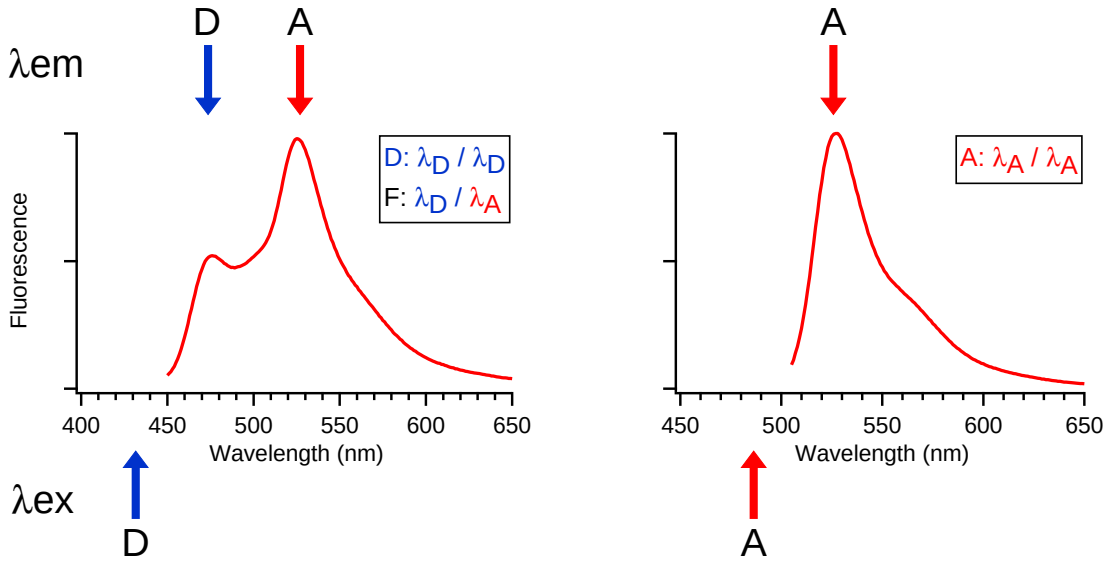

Figure 4.37: Fluorescence intensity values taken from the recorded and corrected emission spectra for analysis with Gordon's equation. For each sample, two spectra are recorded and three signals are extracted. The arrows indicate the spectral positions of excitation and detection for the three signals.

Table. 4.3 summarizes the spectral positions of three excitation/detection wavelength pairs for each FRET pair in this study.

	Wavelength pair (λ_{ex} / λ_{em}) in nm		
FRET pair	D	F	A
PDI / TDI	480 / 535	480 / 665	580 / 665
Alexa 488 / Alexa 594	480 / 517	480 / 620	580 / 620
IAF / TMRIA	480 / 520	480 / 575	530 / 575
CFP / YFP	433 / 477	433 / 527	488 / 527

Table 4.3: Spectral positions of three excitation/detection wavelength pairs (λ_{ex} / λ_{em}) for FRET pairs in this study. Wavelength pairs of D (λ_D / λ_D), F (λ_D / λ_A), and A (λ_A / λ_A) are as illustrated in Fig. 4.37, where λ_D or λ_A refer to the excitation (λ_{ex}) or detection wavelength (λ_{em}) of either donor (D) or acceptor (A).

In addition to 3 values from the spectra of sample containing both donor and acceptor (Fig. 4.36, upper left, DA), the spectra of references containing either donor or acceptor were also measured to get 6 values (Fig. 4.36, upper center, D or A). Taken together, 9 values will be extracted from 3 samples (donor-only, acceptor-only, or both donor and acceptor) by 3 excitation/detection wavelength pairs (Donor, FRET, and Acceptor).

G factor Moreover, G factor is required for Gordon's equation (Fig. 4.36, upper right). G factor is relating the loss of donor emission due to FRET in the Donor set (D: λ_D /λ_D) to the gain of acceptor emission due to FRET in the FRET set (F: λ_D/λ_A). Here, equation (2.11) is repeated.

$$G = \frac{QY_a}{QY_d} \times \frac{\Phi_a}{\Phi_d} \times \frac{T_F}{T_D} \tag{4.5}$$

where QY is the fluorescence quantum yield of donor (d) or acceptor (a), Φ is the fraction of the fluorescence transmitted by the detection set (see below), and T is the detection efficiency for a given wavelength pair.

Determination of Φ is illustrated in Fig. 4.38. The quantity represents the fraction of the dye emission recorded at the emission wavelength (black bar) with respect to the total dye emission (shaded area). It was calculated for donor and acceptor of each FRET pair separately.

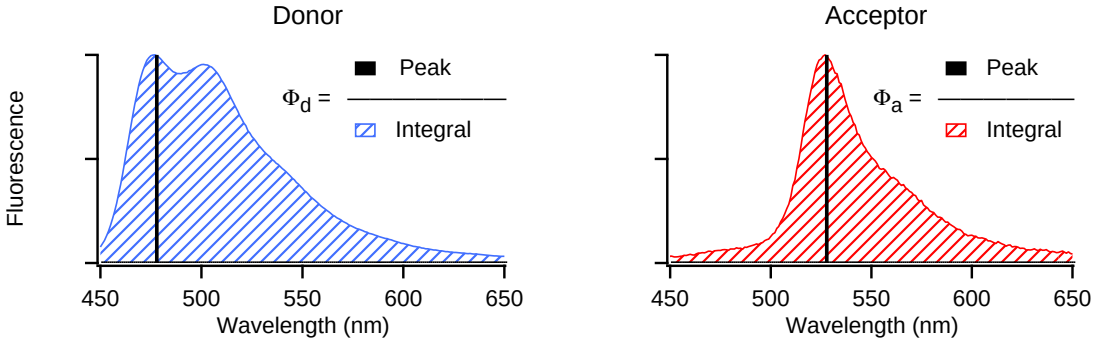

Figure 4.38: Determination of Φ. It represents the fraction of the fluorescence transmitted by the detection set. Donor-only sample was detected by the wavelength pair D (λ_D /λ_D), and acceptor-only sample was detected by the wavelength pair F (λ_D /λ_A). Based on the emission spectra of donor or acceptor respectively, Φ_d or Φ_a was calculated by dividing the fluorescence intensity (black bar) at selected emission wavelength (λ_{em} in Table. 4.3 and Fig. 4.37) by the fluorescence integral of the whole spectrum (shaded area).

The detection efficiency (T) usually depends on the emission wavelength. However, because the spectra were corrected for this dependency (Eq. (4.3)), T becomes wavelength-independent. Therefore, the ratio $\frac{T_F}{T_D}$ can be considered as 1. In consequence, Eq. (4.5) can be simplified as Eq. (4.6) to calculate G factor for fluorescence spectroscopy.

$$G_{spectroscopy} = \frac{QY_a}{QY_d} \times \frac{\Phi_a}{\Phi_d} \tag{4.6}$$

Table. 4.4 summarizes the required values and G factors of each FRET pair used in this study. Typically, the fluorescence quantum yield varies with the experimental conditions. For the FRET pairs (Alexa 488/Alexa 594 and IAF/TMRIA), quite different values are reported. Accordingly, the calculated G factor may vary by a factor of 2-3.

FRET pair	**PDI/TDI**	**Alexa488/Alexa594**	**IAF/TMRIA**	**CFP/YFP**
QY_a	0.73	0.36-0.57	0.26-0.28	0.61
QY_d	0.93	0.36-0.68	0.37-0.93	0.40
Reference	[62], [63]	[64]	[58], [65]	[66]
Φ_a	0.0198	0.013	0.0148	0.0187
Φ_d	0.021	0.02	0.019	0.0124
G factor (calculated)	**0.74**	0.34-1	0.22-0.59	**2.3**
G factor (empirical)		**1.3**	**0.25**	

Table 4.4: G factors of FRET pairs used in this study calculated by Eq. (4.6)**.** QY_d and QY_a: the quantum yields of donor and acceptor. Φ_d and Φ_a: the fractions of the fluorescence of donor or acceptor transmitted by the detection set (Fig. 4.38). G factors of FRET pairs with quite different reported quantum yields were adjusted experimentally. Finally, the values printed in bold were used for further FRET analysis.

In order to get more precise G factors, the G factors were determined for these FRET pairs experimentally. Donor and acceptor fluorophores were mixed at known concentrations and therefore known donor fractions (f_D= 0-1). These systems are very simple, do not contain any protein, do not reveal any background problems, and can be precisely prepared. Analysis with Gordon's equation should therefore accurately reproduce the used donor fractions. In a graph where the calculated donor fraction ($f_D(Gordon)$) is plotted against the experimental donor fraction ($f_D(exp)$), one has to expect a linear relationship going through the origin (Fig. 4.39).

In contrast, neither for Alexa 488/Alexa 594 nor for IAF/TMRIA the calculated G factors gave a straight line, but a bended curve was observed. Next, the G factors were modified to get the expected linear relationship. In the case of Alexa 488/Alexa 594, a G factor of 1.3 was obtained, and in the case of IAF/TMRIA a value of 0.25 gave an optimal result (Fig. 4.39). If the G factor is modified too strong, even a bending in the opposite direction can be observed. Unfortunately, such a test series as described above cannot be performed *in vivo*. Therefore, for CFP/YFP no empirical G factor could be determined. Finally, the G factors used for further FRET analysis were printed in bold in Table. 4.4.

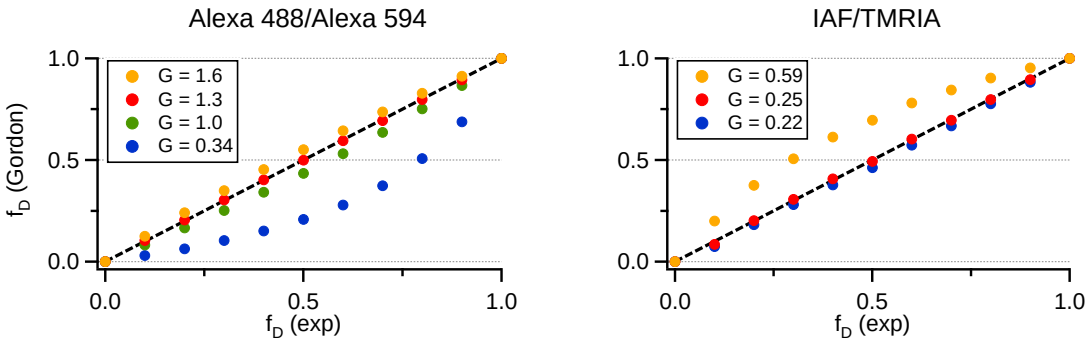

Figure 4.39: Effect of the G factor on the relationships between donor fractions determined by Gordon's equation ($f_D(Gordon)$) and experimentally defined ones ($f_D(exp)$). Stock solutions of each dye were 1 μM. Mixture series of donor and acceptor ($f_D(exp)$=0-1) were prepared in DcuS-labeling-buffer, and excited/detected at wavelength pairs given in Table. 4.3. Donor fractions ($f_D(Gordon)$) were determined by applying different values of G factor to Gordon's equation (Eq. (2.10)). In the case $f_D(Gordon)$ reproduces exactly $f_D(exp)$, one has to expect a linear relationship between both (black line).

Determination of donor fraction (f_D) Fluorescence intensity is proportional to the fluorophore concentration. Based on the G factor (Table. 4.4) combined with $\overline{Dfd}$ (Eq. (2.12)) and $\overline{Afa}$ (Eq. (2.13)), the donor-to-acceptor ratio ($ratio_{DA}$) was determined by Eq. (4.7).

$$ratio_{DA} = \frac{[D]}{[A]} = \frac{\overline{Dfd}}{\overline{Afa}} \times G \tag{4.7}$$

Finally, the donor fraction (f_D) was determined by Eq. (4.8).

$$f_D = \frac{ratio_{DA}}{1 + ratio_{DA}} = \frac{[D]}{[D] + [A]} \tag{4.8}$$

4.2.2.2 Experimental Validation by PDI-TDI Dyad

To test the applicability of Gordon's equation to fluorescence spectroscopy, a defined donor/acceptor dyad composed of a perylenediimide donor (PDI) and a terrylenediimide acceptor (TDI) linked by a hepta(phenylene) bridge containing a kink was used (Fig. 4.40) [51]. The covalent bonding between donor and acceptor ensures a constant 1:1 ratio of donor to acceptor in the dyad. Consequently, the donor fraction of the dyad has a fixed value of 0.5. The rigid linker ensures a fixed separation between donor and acceptor and by this a constant FRET efficiency over time.

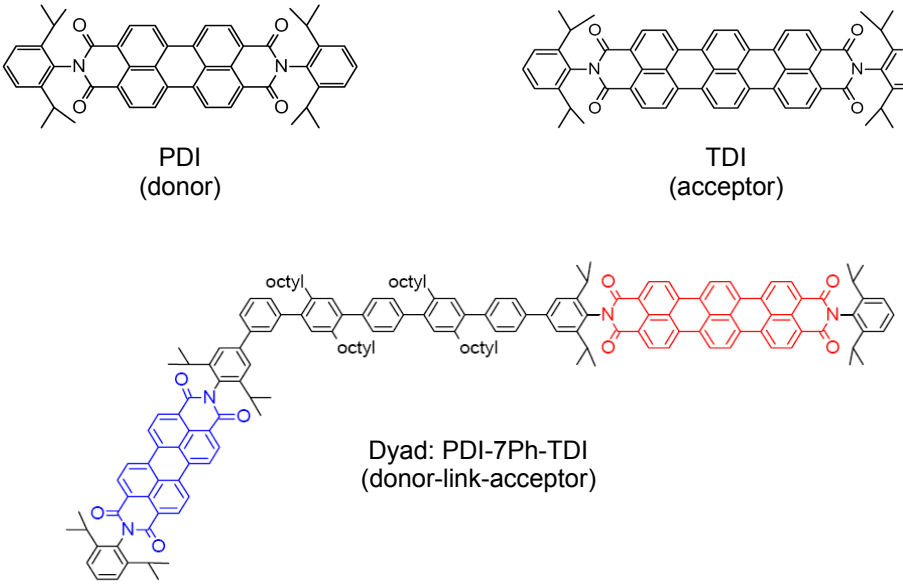

Figure 4.40: Chemical structure of perylenediimide donor (PDI), terrylenediimide acceptor (TDI), and donor/acceptor dyad.

Compared with the spectra of PDI donor and TDI acceptor (Fig. 4.41, left, blue and red), the spectrum of PDI-TDI dyad (Fig. 4.41, left black) reveals a strong FRET signal. The FRET efficiency of the dyad was reported as a value of 0.965 [51].

The PDI/TDI/dyad system also fulfills the prerequisites of Gordon's equation, such as: (1) no background fluorescence: background of toluene solvent can be easily subtracted from the measured spectra, (2) no autofluorescence: no existence of autofluorescence in organic dyes, (3) no photobleaching: no focused intense laser light for excitation. Moreover, strong fluorescence intensities of PDI and TDI ensure a high signal-to-noise ratio. These features are adequate to examine the performance of Gordon's equation in fluorescence spectroscopy.

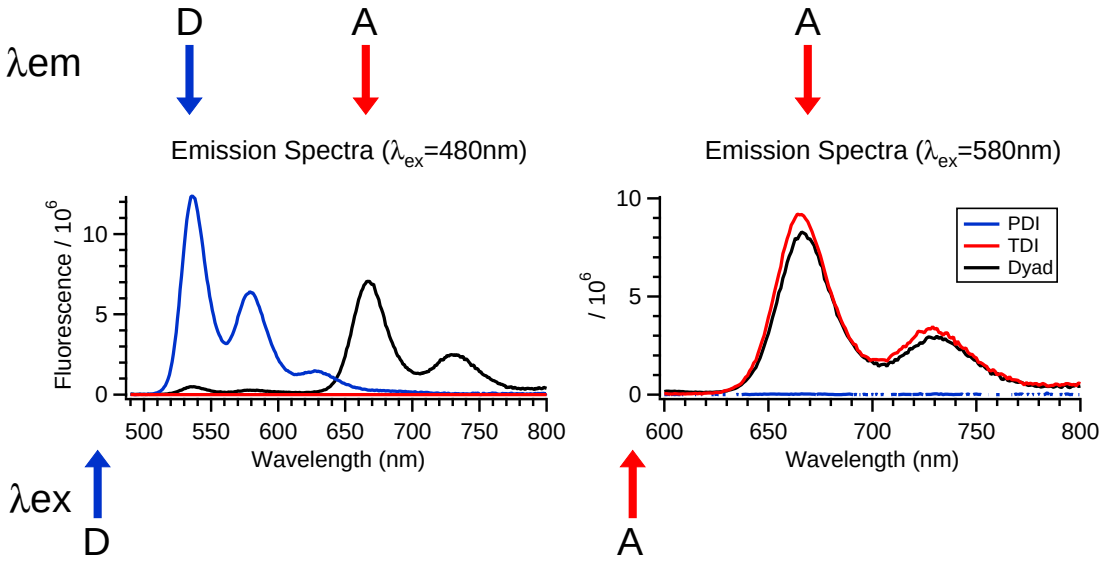

Figure 4.41: Emission spectra of PDI donor, TDI acceptor, and dyad (PDI-TDI). The excitation wavelengths were 480 nm and 580 nm. Compared to the emission spectrum of PDI (blue), dyad (black) excited at 480 nm revealed a TDI emission peak (665 nm) due to FRET.

To check if Gordon's equation can accurately determine donor fraction (f_D) and FRET efficiency (E) of dyad, two dilution series were tested as follows:

1. Titration series of TDI (A) and dyad (DA)
2. Titration series of PDI (D) and dyad (DA)

1. Titration series of TDI (A) and dyad (DA) TDI acceptor (A, $f_D = 0$) and PDI-TDI dyad (DA, $f_D = 0.5$) were mixed at different ratios (Fig. 4.42, upper panel). Based on the known donor fractions of dyad and TDI, the donor fractions in the mixtures were expected to be in the range of f_D = 0-0.5. These mixtures were excited at different wavelengths of PDI and TDI (480 nm and 580 nm, respectively). 3 values were extracted from the spectra of samples (Table. 4.3). Combined with G factor for PDI/TDI pair and 6 values obtained from the spectra of references, donor fraction (f_D) and FRET efficiency (E) were quantified by Gordon's equation (Fig. 4.36). The measured values of donor fraction (Fig. 4.42, lower left $f_{D(Gordon)}$ = 0-0.5) were in good agreement with the expected ones ($f_{D(expected)}$). Moreover, the presence of TDI acceptor should have no effect on the observed FRET efficiency of dyad, because TDI acceptors in the mixtures contribute no FRET efficiency. As expected, the linear fit of measured FRET efficiencies (E_{Gordon}) was always constant at the level of 0.96 (Fig. 4.42, lower right), in good agreement with the reported value of 0.965 [51].

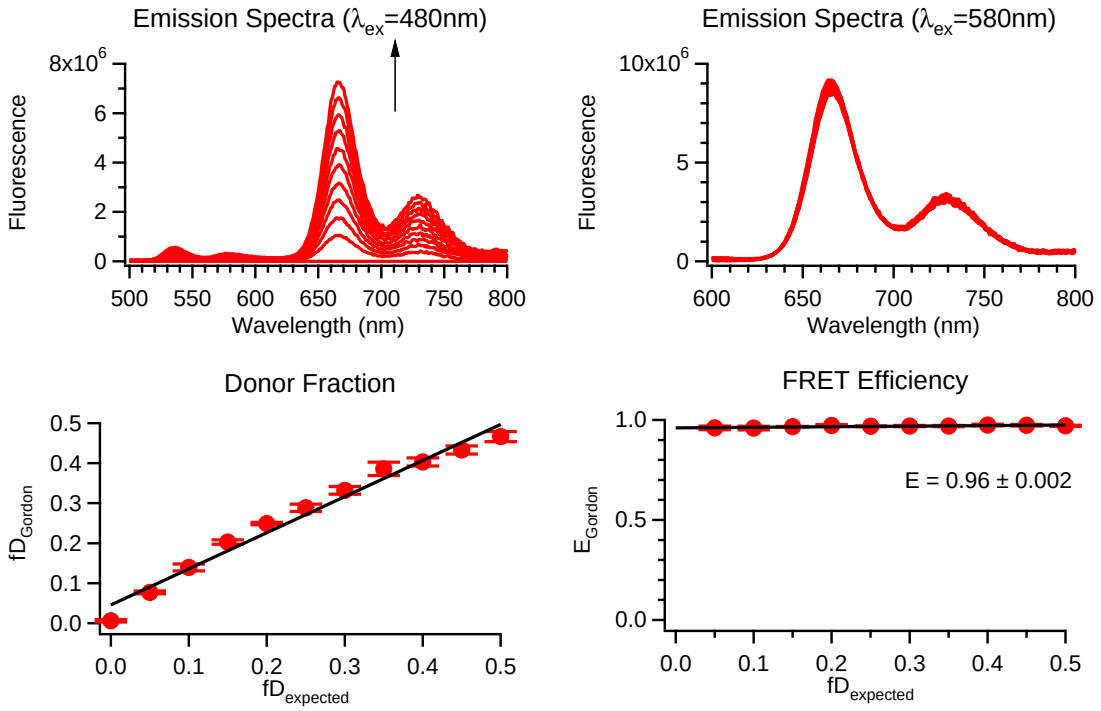

Figure 4.42: Titration series of TDI acceptor (A) and dyad (DA). Each compound was dissolved in toluene as an initial concentration of 10 nM. Emission spectra of different mixtures (f_D = 0-0.5) were measured at excitation wavelengths of PDI (480 nm) or of TDI (580 nm) respectively. Measured spectra were subtracted by toluene emission, and then analyzed by Gordon's equation to determine donor fraction (f_D) and FRET efficiency (E). Data were shown as the means $\pm$ standard deviations of three independent experiments, and the linear fits were indicated by black solid lines.

2. Titration series of PDI (D) and dyad (DA) Similarly, titration series of PDI donor (D, $f_D = 1$) and PDI-TDI dyad (DA, $f_D = 0.5$) were prepared at different ratios (Fig. 4.43, upper panel). These mixtures were expected to yield a linear increase of the donor fractions from $f_D = 0.5$ to $f_D = 1$. The measured donor fractions ($f_{D(Gordon)}$) were also in good agreement with the expected ones (Fig. 4.43, lower left). Based on the known FRET efficiency of PDI donor ($E = 0$) and dyad ($E = 0.96$), the increase of PDI donor ($f_D = 1$) in the mixtures should decrease the FRET efficiencies(from $E = 0.96$ to $E = 0$). A decrease of measured FRET efficiencies (Fig. 4.43, lower right, E_{Gordon}) was in a linear relationship to increasing donor fraction as expected.

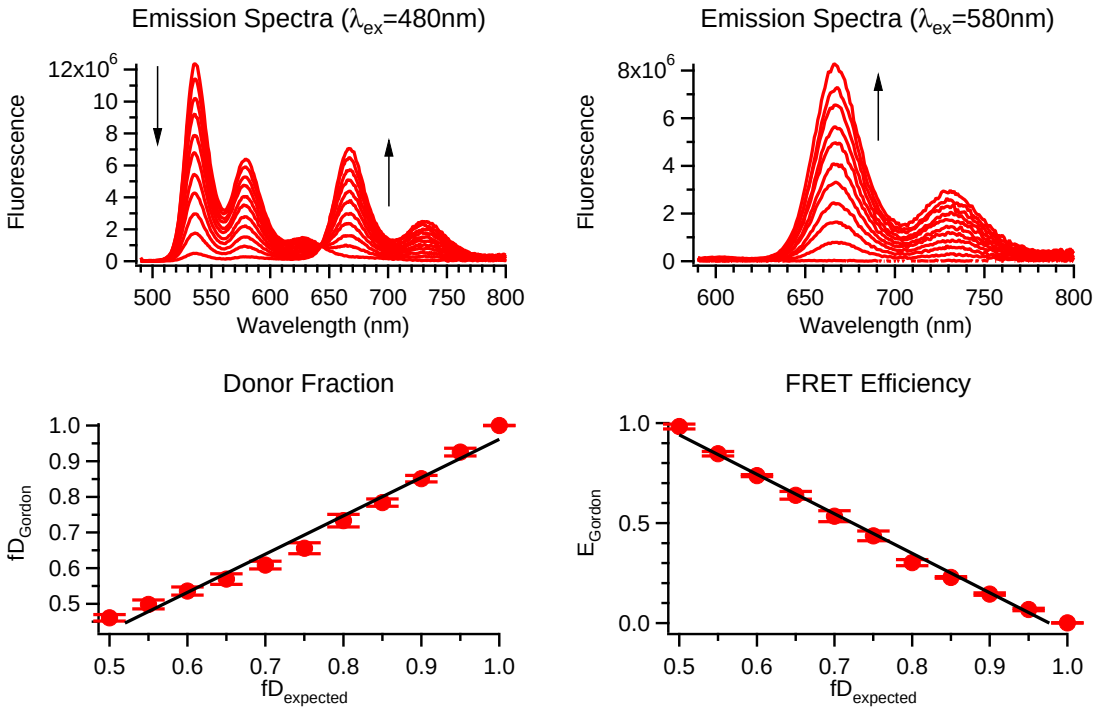

Figure 4.43: Titration series of PDI donor (D) and dyad (DA). For more details see Fig. 4.42

Conclusion The second step of our automatic FRET analysis, Gordon's equation to determine FRET efficiency (E) and donor fraction (f_D), was experimentally tested by a well-defined PDI-TDI dyad. The accuracy and applicability in fluorescence spectroscopy of Gordon's equation was verified by two titration series of the dyad with either PDI donor or TDI acceptor. In conclusion, Gordon's equation can accurately determine the FRET efficiency (E) and donor fraction (f_D) by analyzing background-free spectra.

4.2.3 Combining steps 1 and 2

The applicability of the analysis (combining steps 1 and 2) to our experimental systems both *in vitro* and in living cells was examined. As shown in Fig. 4.44, measured spectra were corrected by step 1 (spectral correction and background subtraction), and subsequently analyzed by step 2 (FRET determination by Gordon's equation) to yield FRET efficiency (E) and donor fraction (f_D).

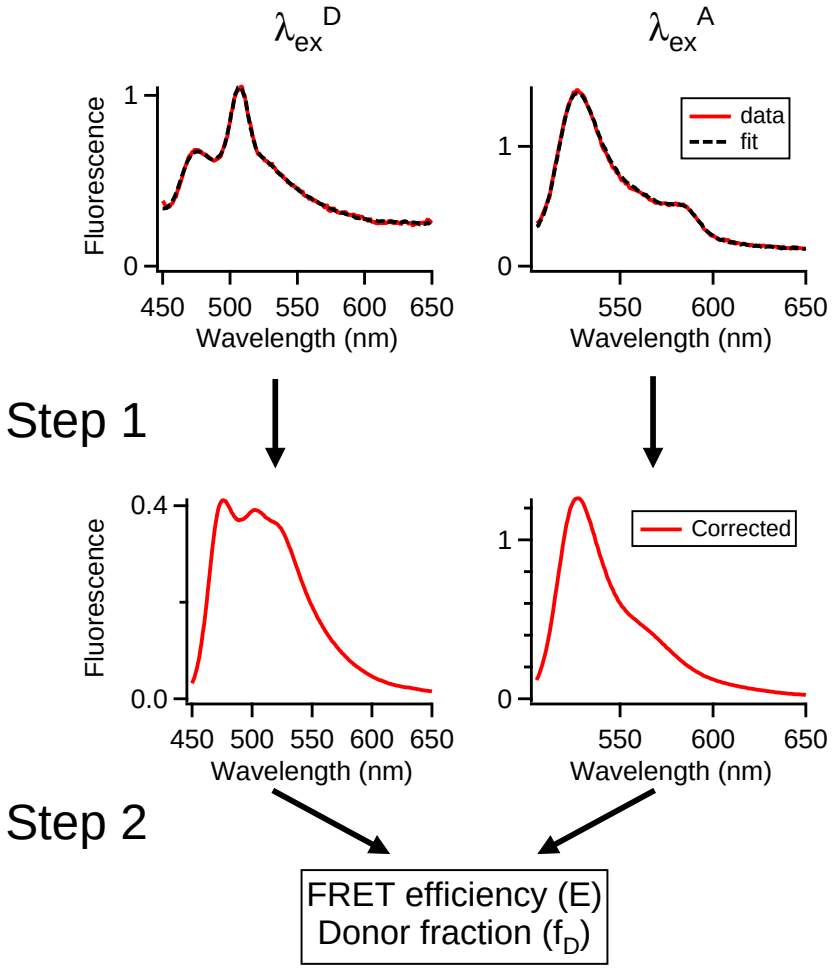

Figure 4.44: Combining steps 1 and 2. Sample containing both donor and acceptor were excited at wavelengths of donor and acceptor, respectively (upper panel, red lines). After general spectral correction and individual fitting (upper panel, black dashed lines), background-free corrected spectra (lower panel) were analyzed by Gordon's equation to determine FRET efficiency (E) and donor fraction (f_D).

4.2.3.1 Applicability and Accuracy (*in vitro*)

First, the applicability *in vitro* by a mixture series of Alexa 488-labeled (donor) and Alexa594-labeled DcuS (acceptor) at different ratios (f_D = 0-1) was tested. Because of the existing background (scattering, Sec. 4.2.1.2), the spectra of these mixtures were background subtracted in step 1 and then quantified in step 2. As shown in Fig. 4.45, the measured values of donor fraction ($f_{D(Gordon)}$) or FRET efficiency (E_{Gordon}) determined by Gordon's equation were plotted against the known experimental values of donor fraction ($f_{D(expected)}$) respectively. Measured donor fraction (Fig. 4.45, left) were in the expected range of $f_D = 0-1$, and most of the data points distributed on a diagonal with a slope of 1 which revealed a good agreement between measured and expected values. The Alexa-labeled DcuS mixtures were assumed monomeric in detergent. As expected, no FRET (Fig. 4.45, right, $E = 0$) was observed in the measured FRET efficiencies. These results confirm that the analysis (combining steps 1 and 2) can accurately determine donor fraction ($f_D = 0-1$) and work at least to determine no interaction ($E = 0$) in Alexa-labeled DcuS mixtures (*in vitro*).

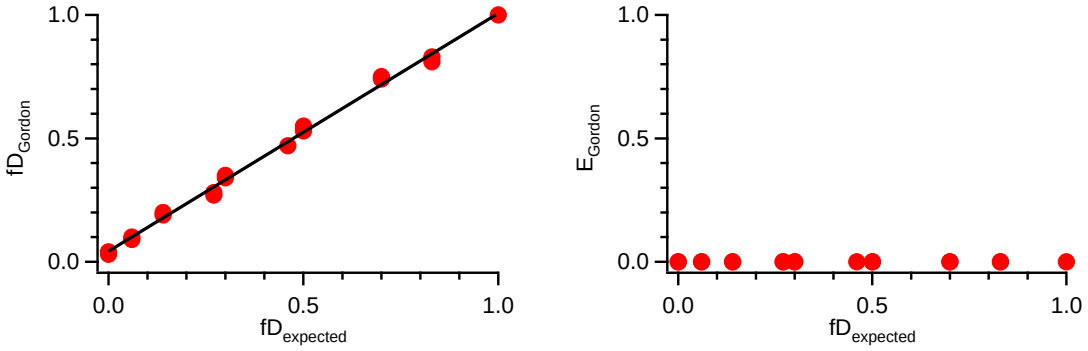

Figure 4.45: Series of DcuS labeled with either Alexa 488 (donor) or Alexa 594 (acceptor) and mixed at different ratios (f_D = 0-1). Stock solutions of labeled DcuS were 1 μM in DcuS-labeling buffer. After combining steps 1 and 2, measured values of donor fraction (f_D) were plotted against expected values.

4.2.3.2 Applicability and Accuracy in living cells

Similarly, the applicability *in vivo* was examined by the following mixture series of CFP- and YFP-expressing cells:

1. Positive controls: CFP-YFP or YFP-CFP tandem fusions expressed in cells
2. Controls: CFP and YFP co-expressed in the same cell

3. Negative controls: CFP and YFP expressed in separate cells

The spectra of these samples were treated in step 1 to remove the background signals from cells (scattering and autofluorescence in Sec. 4.2.1.2), and then quantified in step 2 (Fig. 4.44).

1. Positive Controls As positive controls of FRET between CFP and YFP, tandem fusions of CFP-YFP or YFP-CFP were constructed (Fig. 4.46) to ensure the occurrence of FRET and a constant 1:1 ratio of donor to acceptor, i.e. constant donor fraction ($f_{D(expected)} = 0.5$).

Figure 4.46: Tandem fusions of CFP-YFP (left) and YFP-CFP (right) containing a linker of 10 amino acid residues between CFP and YFP moieties.

Even the actual FRET efficiencies of these fusions are unknown, the observed FRET efficiencies can be estimated based on the distance between donor and acceptor (r) and the Förster radius between CFP and YFP (R_0 = 4.92 nm) [46]. Based on the X-ray structure of GFP [44, 45], the chromophore is buried in the center of the GFP barrel. The length of an individual CFP or YFP protein is around 4 nm. If CFP and YFP moieties are covalently linked without a spacer in the tandem fusions, the distance between chromophores of CFP and YFP (r) is roughly 4 nm, which is smaller than the Förster distance (R_0) and can result in a FRET efficiency ($E = \frac{1}{1+(\frac{r}{R_0})^6}$) of 0.78 as most. However, a link of 10 amino acid residues between CFP and YFP in these tandem fusions increases the distance (r) by at most 3.85 nm (based on the distance between amino acid residues, 0.15 nm in α-helix or 0.35 nm in β-strand [67]) which lowers the FRET efficiency to 0.06 at least. The linker should have a random conformation which leads to a FRET efficiency between ($E_{expected}$ = 0.06$\sim$0.78). After analysis (Fig. 4.44), measured and expected values were compared in Table. 4.5. The measured donor fraction ($f_{D(Gordon)} = 0.5 \pm 0.02$) was accurately determined and the occurrence of FRET was observed in the reasonable range (Table. 4.5, $E_{Gordon} = 0.6 \pm 0.1$).

2. Controls: CFP and YFP co-expressed in the same cell CFP and YFP were co-expressed in the same cell, and presumed non-interacting even co-localized in the cells (Table. 4.6, $E_{expected} = 0$). Because the copy number of expression vectors

Positive control	f_D	E
expected	0.5	0.06∼0.78
measured	0.5 ± 0.02	0.6 ± 0.1

Table 4.5: Positive controls (CFP-YFP or YFP-CFP fusions in cells, n = 8) analyzed by combining steps 1 and 2 (Fig. 4.44).

of CFP and YFP are of similar magnitude but not identical, co-expression of CFP and YFP should result in a donor fraction close to a value of $f_{D(expected)} \sim 0.5$. The measured donor fraction (Table. 4.6, $f_{D(Gordon)} = 0.4 \pm 0.06$) was in the expected range, but a minor FRET ($E_{Gordon} = 0.07 \pm 0.02$) was observed. Therefore, the extent of non-specific FRET between CFP and YFP co-localized in the same cells was evaluated with different expression levels of CFP and YFP. Even the inducer concentration and induction time were adjusted to increase the expression levels of CFP and YFP in these controls, the FRET signal was not increased with higher expression levels of CFP and YFP. The minor FRET efficiency ($E = 0.07 \pm 0.02$) observed in this control can estimate the error and rule out the false positive detection of FRET in the experimental system of living cells.

Negative control	f_D	E
expected	∼0.5	0
measured	0.4 ± 0.06	0.07 ± 0.02

Table 4.6: Controls (CFP and YFP co-expressed in the same cell, n = 6) analyzed by combining steps 1 and 2 (Fig. 4.44).

3. Negative controls: CFP and YFP in separate cells To check if the minor FRET observed in the above-mentioned controls (CFP and YFP co-expressed in the same cells, $E = 0.07 \pm 0.02$) was an artifact of our FRET analysis or of the sample (due to diffusion or interaction between CFP and YFP), controls in which FRET is not possible because of the spatial separation of donor and acceptor ($E_{expected} = 0$) were examined. Two defined mixture series of CFP-expressing cells, YFP-expressing cells and non-FP-expressing E. coli cells were tested as follows:

1. Mixture series of YFP-expressing cells and non-FP-expressing E. coli cells, containing a fixed amount of CFP-expressing cells
2. Mixture series of CFP-expressing cells and YFP-expressing cells, containing a fixed amount of non-FP-expressing *E. coli* cells

These mixture series (f_D = 0-1) were measured and analyzed (as illustrated in Fig. 4.44). The values of f_D were unknown, but the dilution steps are known.

Therefore, an arbitrary measure of fluorophore concentrations ($[D]$ and $[A]$) was used. $[D]$ and $[A]$ are represented as $\overline{Dfd}$ and $\overline{Afa}$ yielded by Eq. (2.12) and Eq. (2.13) [48]. $\overline{Dfd}$ refers to the donor signal (d) in the mixture of both donor and acceptor (f) detected by Donor excitation/detection wavelength pair (Fig. 4.37, D) in the absence of FRET (bar). $\overline{Afa}$ refers to the acceptor signal (a) in the mixture of both donor and acceptor (f) detected by Acceptor excitation/detection wavelength pair (Fig. 4.37, A) in the absence of FRET (bar). These measures ($\overline{Dfd}$ and $\overline{Afa}$ for the donor-only or acceptor-only signal in the mixture of both donor and acceptor in the absence of FRET) are immeasurable quantities which cannot be directly measured (in the mixture of both donor and acceptor in the presence of FRET) but can be computed by Eq. (2.12) and Eq. (2.13) instead.

Mixture series of YFP-expressing cells and non-FP-expressing E. coli cells, containing a fixed amount of CFP-expressing cells The mixture series of Fig. 4.34 were further analyzed (Fig. 4.47, upper panel: FBS-corrected). In the mixtures containing a fixed amount of CFP but increasing amount of YFP, a constant level of CFP and an increase of YFP were determined as expected (Fig. 4.47, lower panel). The measured fluorophore concentrations ($[D]$ and $[A]$) change as expected. Because CFP and YFP are expressed in separate cells, the occurrence of FRET is impossible ($E_{expected} = 0$). The measured FRET efficiency ($E_{Gordon} = 0 \pm 0.02$) was as expected.

Mixture series of CFP-expressing cells and YFP-expressing cells, containing a fixed amount of non-FP-expressing *E. coli* cells Spectra of the same mixture series as in Fig. 4.35 were further analyzed (Fig. 4.48, upper panel: FBS-corrected). The mixture series contains increasing CFP-expressing cells, decreasing YFP-expressing cells, but a fixed amount of non-FP-expressing *E. coli* cells. As expected, an increase of CFP and a decrease of YFP were obtained (Fig. 4.48, lower left), and no FRET was observed in these negative controls (Fig. 4.48, lower right).

These negative controls (Fig. 4.47 and Fig. 4.48) demonstrated the FRET efficiency ($E = 0$) can be accurately determined by the partial analysis (Fig. 4.44) even in such complex systems of mixture of FP-expressing and non-FP-expressing cells. Besides, these negative controls also suggested that the non-specific FRET observed in cells co-expressing CFP and YFP (Table. 4.6) should result from the sample intrinsically instead of our analysis.

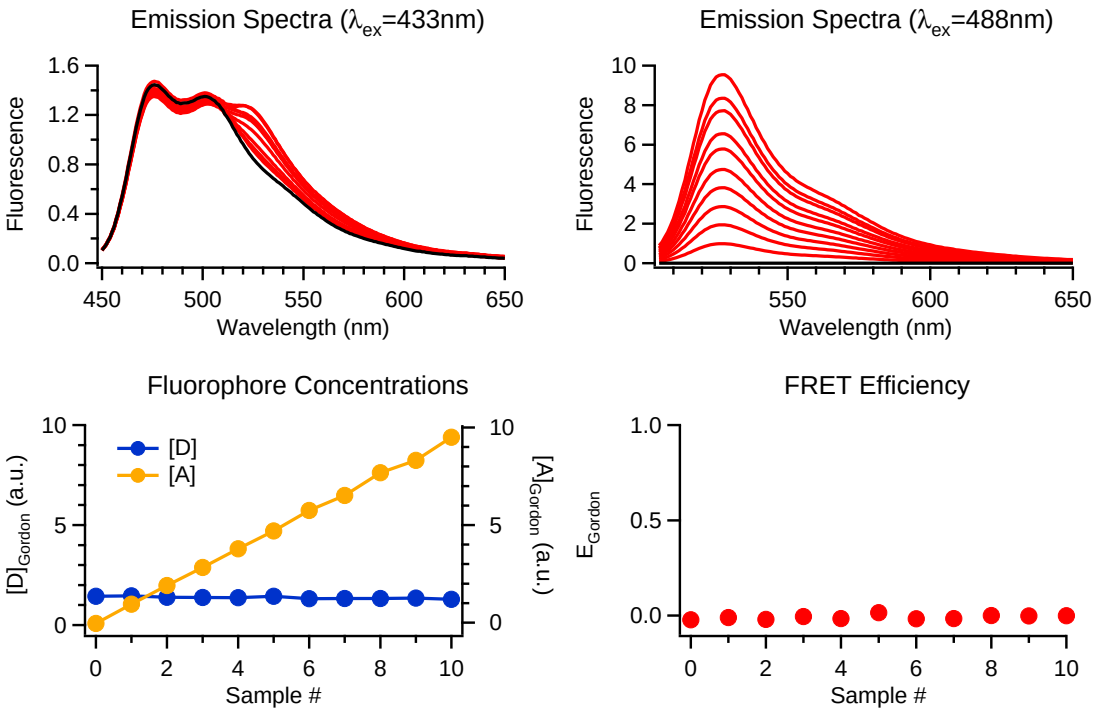

Figure 4.47: Mixture series of YFP-expressing cells and non-FP-expressing E. coli cells, containing a fixed amount of CFP-expressing cells. Measured spectra were corrected and analyzed by combining steps 1 and 2. Gordon's equation can compute a measure of fluorophore concentrations (lower panel). The raw data were the same as in Fig. 4.34

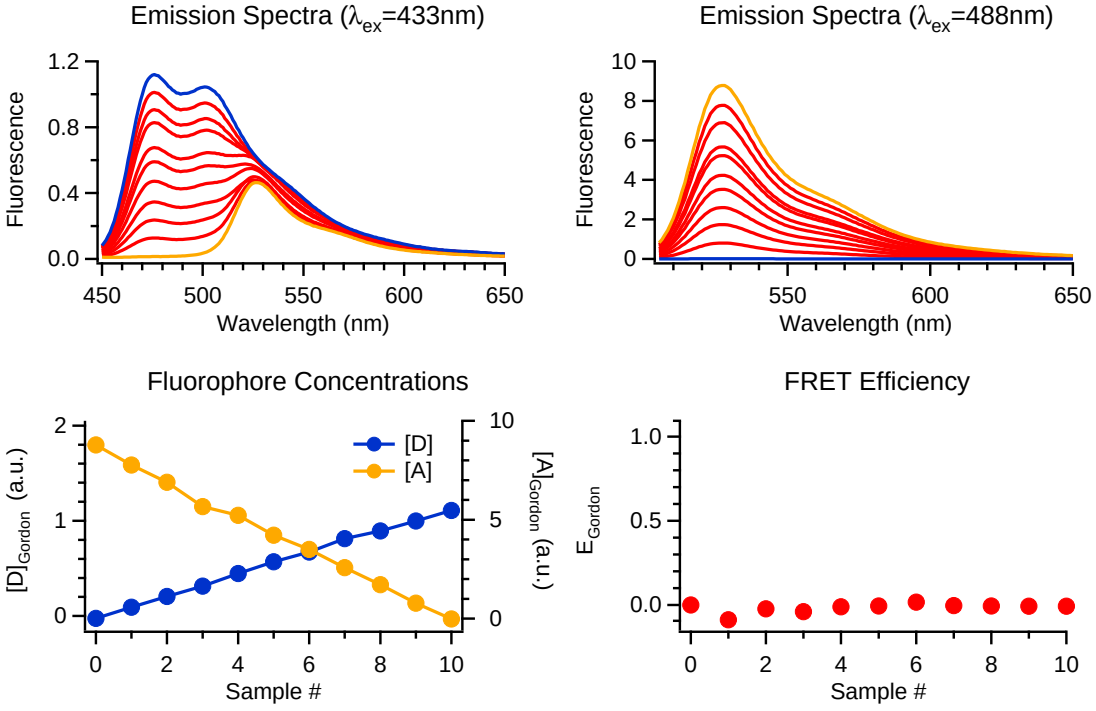

Figure 4.48: Mixture series of CFP-expressing cells and YFP-expressing cells, containing a fixed amount of non-FP-expressing *E. coli* cells. For more details see Fig. 4.47. The raw data were the same as in Fig. 4.35

The effect of G factor on E and f_D Gordon *et al.* [48] reported that using rough estimates of G factor should not be a problem in the FRET quantification, because FRET value is not very sensitive to the value of G factor. To test the influence of G factor on FRET quantification, the positive controls of constant donor fraction ($f_D = 0.5$) were used to reversely check the accuracy of calculated value of G factor for CFP/YFP ($G = 2.3$, Table. 4.4). By introducing different values of G factor (G = 1, 2.3, or 3.5) into Gordon's equation, it was demonstrated that the accuracy of G factor is critical to the accuracy of FRET efficiency (E) and donor fraction (f_D). In this case (Fig. 4.49), smaller G factor underestimated the donor fraction (f_D) and overestimated the FRET efficiency (E), and vice versa (larger G factor overestimated f_D and underestimated E). Moreover, the value of G factor we calculated ($G = 2.3$) yield the most accurate donor fraction ($f_D = 0.5$) among these three values tested, suggesting the accuracy of G factor we calculated was in the reasonable range.

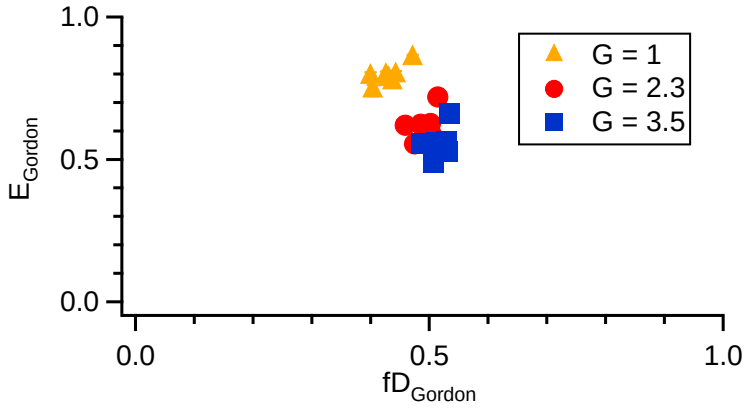

Figure 4.49: The effect of G factor on E and fD. Positive controls (CFP-YFP or YFP-CFP tandem fusions) were analyzed by using different values of G factor (G = 1, 2.3, or 3.5) for Gordon's equation to determine the FRET efficiencies (E) and donor fractions (f_D).

Conclusion The analysis combining steps 1 and 2 (Fig. 4.44) was demonstrated to accurately determine: donor fraction (f_D), FRET efficiency (E), and G factor (G), even under the complex experimental conditions in living cells. However, a minor FRET signal was observed in the negative controls (CFP and YFP co-expressed in the same cell), suggesting a 7% non-specific FRET may occur between CFP and YFP in our *in vivo* measurements, which should be originated from the sample instead of our analysis.

4.2.4 Combining steps 1, 2 and 3

The third step of our FRET analysis is for the accurate determination of the degree of oligomerization. A theoretical model of oligomeric states was reported as a fitting function combining FRET efficiency (E) with relative concentrations of donor and acceptor (f_D) in the oligomeric complex (Sec. 2.4).

$$E = E_{max} * (1 - f_D^{(oligo-1)}) \tag{4.9}$$

where E is the apparent FRET efficiency, E_{max} is the maximal FRET efficiency, f_D is donor fraction, and $oligo$ is the number of units in an oligomer.

Here, if the degree of oligomerization can be accurately determined by analysis (combining steps 1, 2, and 3) was tested both *in vitro* and *in vivo*. Mixture series of labeled DcuS monomers were prepared in different ratios of donor to acceptor (f_D = 0-1). After determining FRET efficiency (E) and donor fraction (f_D) in steps 1 and 2 (Fig. 4.44), FRET efficiency (E) was plotted against donor fraction (f_D) and fitted the data with the model of oligomeric states (Eq. (4.9)) to determine the degree of oligomerization (n) in step 3.

Alexa-labeled DcuS in detergent Alexa-labeled DcuS proteins were assumed as monomers in detergent-containing buffer. The mixture series of Alexa 488- and Alexa 594-labeled DcuS proteins analyzed were the same as those in Fig. 4.45. Fitting the data with the model of oligomeric states (Eq. (4.9)) revealed a horizontal line as expected and yielded an aggregation number $oligo = 1$, indicating that Alexa-labeled DcuS proteins exist as monomers in the presence of detergent (Fig. 4.50, left).

CFP and YFP expressed in separate cells Similarly, the applicability of the model of oligomeric states *in vivo* was tested by mixing CFP-expressing cells and YFP-expressing cells. FRET between CFP and YFP was impossible to occur because of the spatial separation among cells. Therefore, CFP or YFP in the cells was assumed as monomers. The mixture series of CFP- and YFP-expressing cells (same as those in Fig. 4.47 and Fig. 4.48) were analyzed by combining steps 1, 2, and 3. No FRET was observed ($E = 0$) as expected in these mixture series, and a fit as a horizontal line (monomer) was also as expected (Eq. (4.9)), confirming that FP-DcuS fusion proteins exist as monomers in separate cells (Fig. 4.50, right).

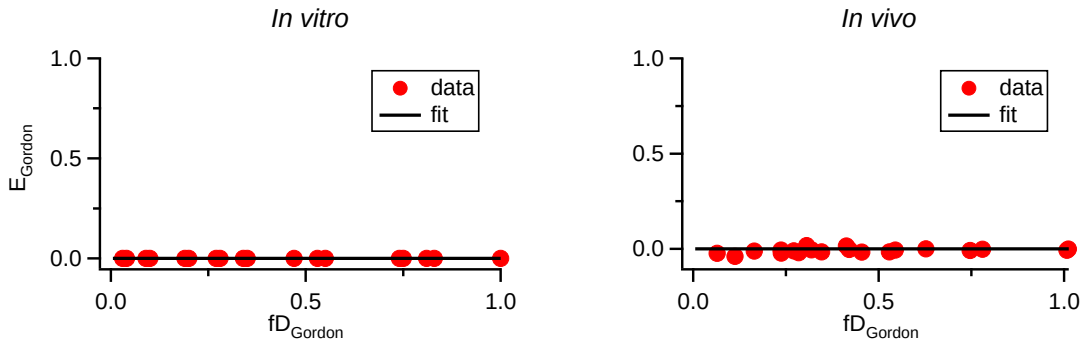

Figure 4.50: Degree of oligomerization *in vitro* and *in vivo*. Left: Mixture series of Alexa-labeled DcuS (n = 18, as in Fig. 4.45). The raw data were the same as in Fig. 4.45. Right: Mixture series of FP-expressing cells (n = 22). Mixture series were prepared in different ratios of donor to acceptor (f_D = 0-1). After combining steps 1 and 2, FRET efficiency (E) and donor fraction (f_D) were determined. Degree of oligomerization (step 3) was determined by fitting with Eq. (4.9). The aw data were the same as in Fig. 4.47 and Fig. 4.48.

Conclusion The analysis combining steps 1, 2 and 3 was demonstrated to accurately determine the oligomeric state of monomers both *in vitro* and *in vivo* (Fig. 4.50).

4.2.5 Conclusion

In conclusion, an automatic quantitative FRET analysis procedure was developed, including flexible background subtraction, Gordon's equation modified to robustly quantify FRET efficiency (E) and fluorophore concentrations (f_D), and a fitting model to determine the degree of oligomerization ($oligo$). The applicability of the automatic FRET analysis was verified by theoretical simulations and experimental validations, suggesting that this automatic analysis allows accurate, fast, and reproducible FRET quantification, even in living cells. This automatic FRET analysis will be executed routinely by homemade computer procedure (flowchart in Fig. 4.51) for robust and reliable quantification of inter-molecular FRET to study the oligomerization and protein-protein interactions of DcuS (Sec. 4.3).

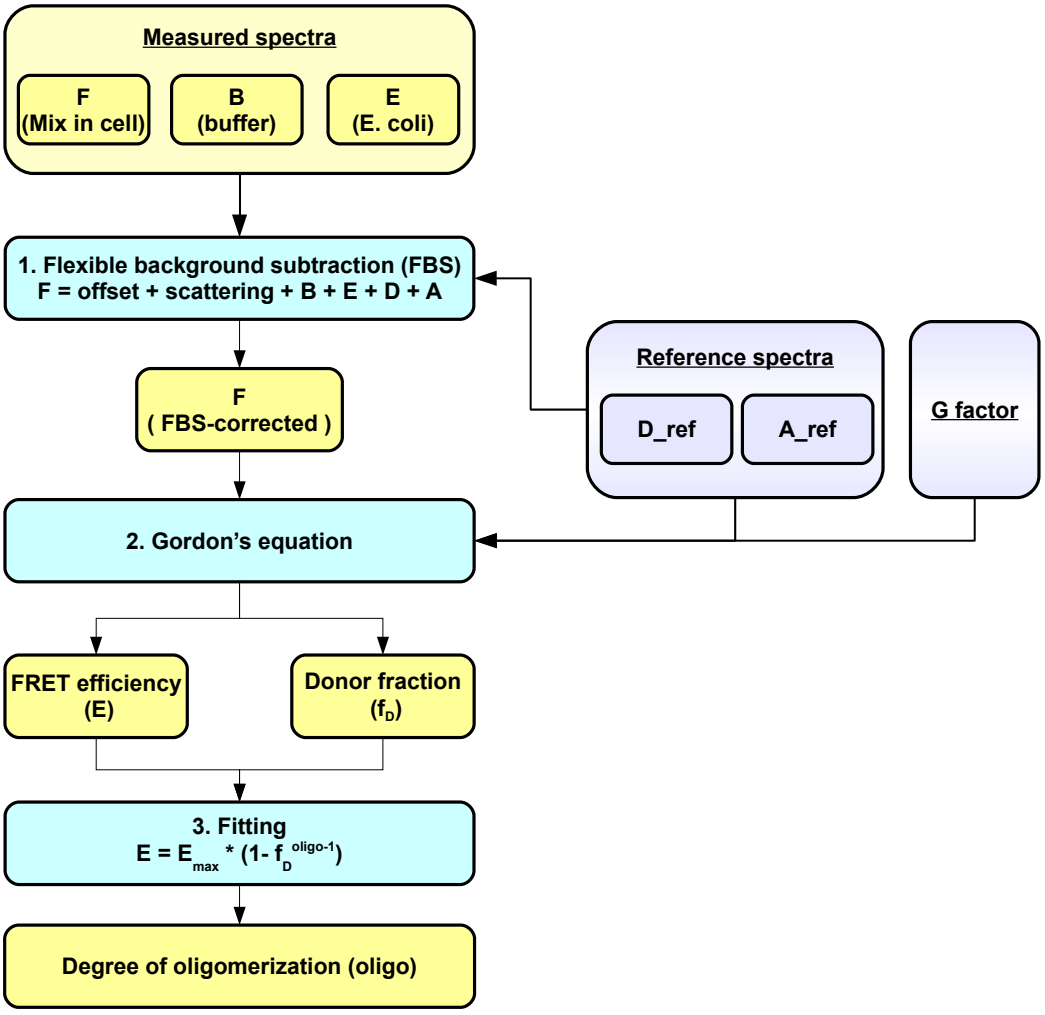

Figure 4.51: Flowchart of the automatic FRET analysis in this study. The spectra of the sample (a mixture containing donor and acceptor) are measured by exciting donor or acceptor respectively. As individual reference spectra for FBS, spectra of buffer (B) and E. coli (E) are recorded under the same conditions as the spectra of mixture sample (F). The measured spectra are then corrected by flexible background subtraction (FBS) to remove the background signals. A set of universal reference spectra, donor (D_{ref}) and acceptor (A_{ref}), are used for FBS and for Gordon's equation. By applying Gordon's equation to the FBS-corrected spectra, FRET efficiency (E) and donor fraction (f_D) can be accurately determined. FRET efficiency (E) is then plotted against donor fraction (f_D) to determine the degree of oligomerization (n) by fitting a theoretical model of oligomeric states to the plot of E vs. f_D .

4.3 Oligomerization and Protein-Protein Interaction of DcuS

The automatic FRET analysis was applied to investigate not only oligomerization of DcuS both *in vivo* and *in vitro* (aim 1) but protein-protein interactions of DcuS with relevant proteins *in vivo* (aim 2) as well.

4.3.1 Oligomerization (*in vivo*)

4.3.1.1 Oligomeric State of DcuS in Living Cells

To examine the oligomeric state of DcuS *in vivo*, DcuS was genetically fused with CFP (donor) in pBAD18 vector or YFP (acceptor) in pBAD30 vector respectively, and tested functional upon fusion (Sec. 3.2.2 and 4.1.1). Under the induction of arabinose inducer, DcuS-CFP (pBAD18) and DcuS-YFP (pBAD30) fusions could be co-expressed at relatively similar expression levels in the same cell. The inducer concentration was kept low but sufficient (133 μM or 333 μM) for moderate expression of DcuS-FP fusions at physiological level [68]. The induction temperature was kept at 30°C or 37°C for the proper folding of FP [43]. For determining the degree of oligomerization by Eq. (4.9) *in vivo*, different donor fractions (i.e. relative amounts of DcuS-CFP and DcuS-YFP co-expressed in the same cell) should be expressed in cells. Because DcuS-CFP and DcuS-YFP were expressed by different pBAD vectors, the expression levels of FP fusions may be induced differently by changing induction time. Therefore, cells co-expressing DcuS-CFP and DcuS-YFP were induced with increasing induction time as induction series, in order to test if donor fractions could be adjustable in cells. Measured spectra of each sample were quantified by automatic FRET analysis (Fig. 4.52). Both expression levels of DcuS-CFP and DcuS-YFP gradually increased with increasing induction time (Fig. 4.52, lower left), but donor fractions were limited in a range of f_D = 0.35-0.55 (Fig. 4.52, upper left) due to the similar inherent characteristics of expression vectors (pBAD18 and pBAD30). Substantial FRET signals ($E = 0.19 \pm 0.02$) were observed in five independent induction series (Fig. 4.52, upper right). The occurrence of FRET between DcuS-CFP and DcuS-YFP suggests an oligomeric state of DcuS in living cells. Moreover, the FRET efficiencies were detected at early induction time, indicating that the self-association of DcuS homo-oligomers already occurs during the early phase of biosynthesis. Even the limited distribution of

donor fractions (no data points at either lower or higher fraction) confined the application of the model of oligomeric states (Eq. (4.9)) to determine the oligomeric state of DcuS in cells, a pre-formed stable homo-oligomers (at least dimers) of DcuS in *E. coli* cells existed in the absence of fumarate (Fig. 4.52, lower panel), in contrast to the monomers observed in the controls (Fig. 4.50, right).

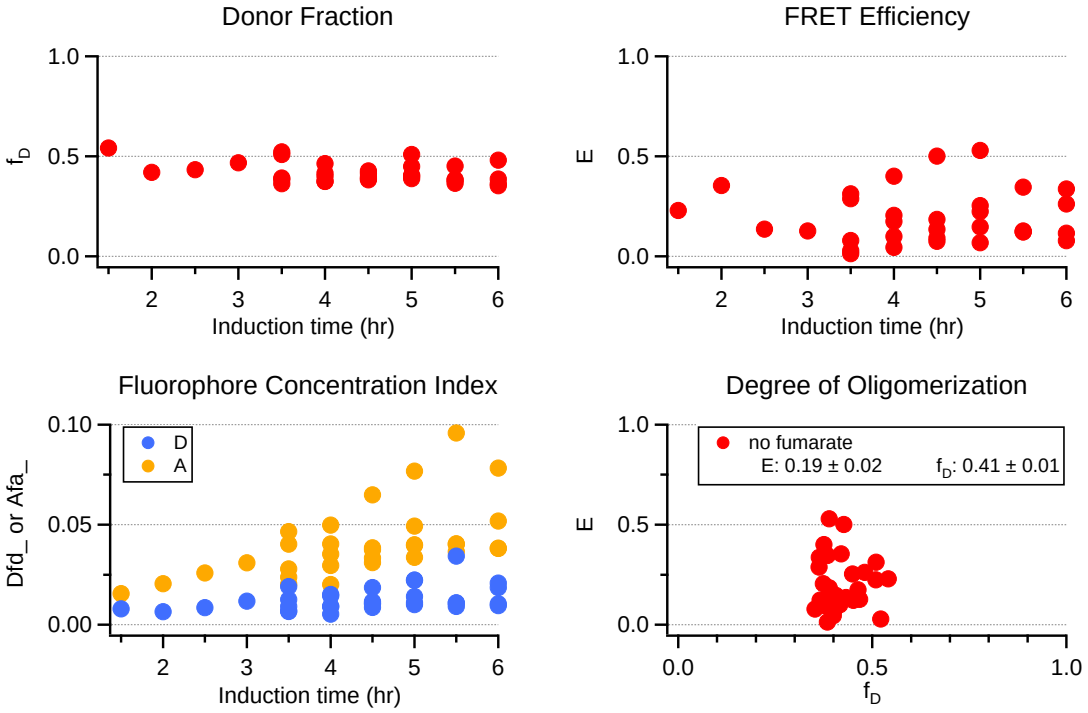

Figure 4.52: Oligomeric state of DcuS in cells (no fumarate). Co-expression of DcuS-CFP and DcuS-YFP was induced in *E. coli* cells by arabinose (133 μM) from 1.5 hr to 6 hr. Emission spectra of these samples were recorded by excitation at 433 nm and 488 nm respectively, and subsequently analyzed by the automatic FRET analysis (Fig. 4.51). Results are from five independent test series (in total n=30 data points). All samples were measured in PBS buffer.

4.3.1.2 Effect of Fumarate on the Oligomeric State

To test the effect of fumarate binding on the oligomeric state of DcuS, cells co-expressing DcuS-CFP and DcuS-YFP were treated in two different ways (Fig. 4.53, samples 1 and 2). Sample 1 (marked in triangle, no fumarate → with fumarate) was grown in the absence of fumarate for 6 hr-induction with arabinose but measured in the presence of fumarate (20 mM) over a time course of 50 min, whereas sample 2 (marked in circle, with fumarate → no fumarate) was grown in the presence of fumarate (20 mM) for 6 hr-induction with arabinose but measured in the absence of fumarate over a time course of 50 min. Even the expression levels

in sample 2 were higher than those in sample 1 (Fig. 4.53, lower left), donor fractions were similar in both samples (Fig. 4.53, upper left). Besides, FRET efficiencies were substantial and comparable in both samples (Fig. 4.53, upper right). However, the determination of oligomerization level was still limited because of the narrow range of donor fractions (Fig. 4.53, lower right).

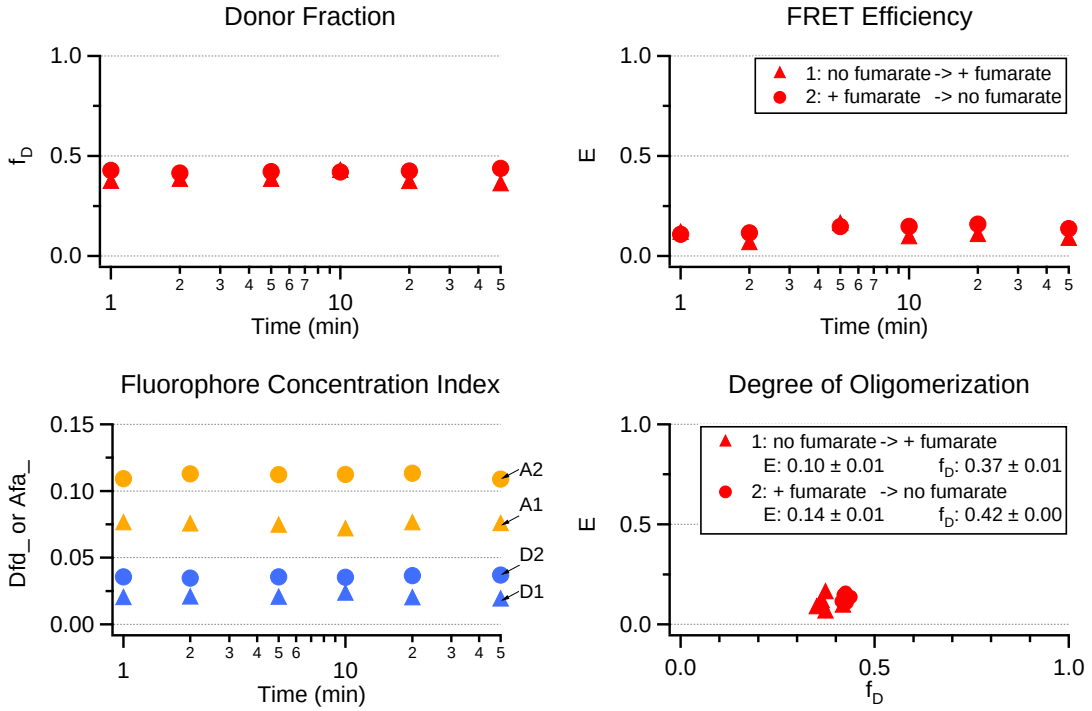

Figure 4.53: Oligomeric state of DcuS in cells (with fumarate). Co-expression of DcuS-CFP and DcuS-YFP was induced in *E. coli* cells by arabinose (133 μM) and treated in two different ways. Sample 1 (triangle, no fumarate → + fumarate): first grown in the absence of fumarate for 6 hr-induction with arabinose (133 μM), then measured in the presence of fumarate (20 mM) over a time-course of 50 min (n=6). Sample 2 (+ fumarate → no fumarate): first grown in the presence of fumarate (20 mM) for 6 hr-induction with arabinose (133 μM), then measured in the absence of fumarate over a time course of 50 min (n=6).

For comparison, data of both "degree of oligomerization" graphs were plotted in one graph (Fig. 4.54). By comparing the results in the absence of fumarate with those in the presence of fumarate, a slight difference in FRET efficiency was observed upon fumarate treatment (E: $0.19 \pm 0.02 \rightarrow E = 0.12 \pm 0.01$). The occurrence of FRET in the absence of fumarate (marked in blue) suggests a constitutive oligomeric state even in the absence of fumarate stimuli. No enhancement but decrease in FRET efficiency upon fumarate treatment (marked in red) imply that the signal transduction upon fumarate sensing may be followed by other mechanisms (e.g. conformational changes, hetero-oligomerization, and so on) instead of

altering the homo-oligomerization state. However, the exact oligomerization level *in vivo* could not be firmly determined because of the limitation of our expression vectors to a broader range of donor fraction. Therefore, the degree of oligomerization was subsequently determined *in vitro* by using DcuS labeled with organic dyes.

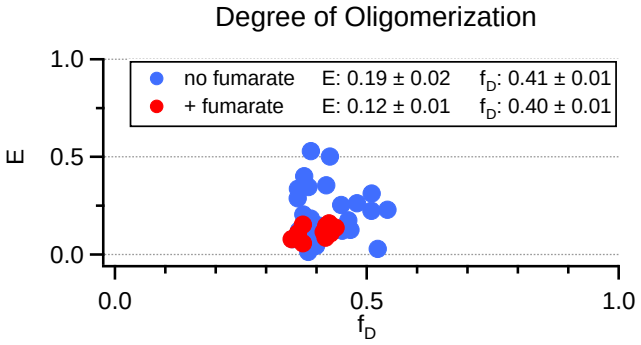

Figure 4.54: Effect of fumarate on the oligomeric state of DcuS in cells. Blue: no fumarate (n=30, as in Fig. 4.52). Red: with fumarate (n=12, as in Fig. 4.53).

4.3.2 Oligomerization (*in vitro*)

In contrast to the limited range of donor fraction in living cells (Sec. 4.3.1), DcuS labeled with organic dyes could be mixed in full range of donor fraction to determine the degree of oligomerization of DcuS *in vitro*. Two pairs of organic dyes suitable for FRET measurements, Alexa pair (Alexa 488 and Alexa 594) and IA pair (IAF and TMRIA), were used independently (Fig. 4.14). For each FRET pair, two aliquots of DcuS protein were labeled with either donor or acceptor (Sec. 4.1.2). Subsequently, donor- and acceptor-labeled DcuS could be mixed at different donor fractions (f_D = 0-1) as mixture series. Recorded spectra of these mixture series were quantified by automatic FRET analysis to examine the oligomeric state of DcuS either in detergent solution or in liposomes. Moreover, the dependence of oligomeric state of DcuS on fumarate binding, fumarate binding site, or protein amount in liposomes was tested respectively.

4.3.2.1 Oligomeric State of DcuS

Labeled DcuS in detergent solution (monomers) The oligomeric state of DcuS monomers was examined in detergent solution. Samples were prepared in sequence with stepwise increasing donor amounts and stepwise decreasing acceptor amounts. Because fluorophores conjugated on DcuS proteins in dilute solution (in nM range) were unlikely to interact with their FRET partners (E = 0), donor- or acceptor-labeled DcuS proteins in dilute solution were assumed to exist as monomers (oligo = 1). A horizontal line (E = 0, oligo = 1) was expected for the fitting of the oligomerization model to experimental data (for the fitting, data points of f_D = 0 (acceptor alone) were ruled out, because the FRET efficiencies in the absence of donor has no meaning at all). Independent mixture series using the two different FRET pairs were analyzed (Fig. 4.55 and 4.56). Donor fractions of the Alexa pair were nearly accurately determined, with a linear relationship passing through the origin as expected (Fig. 4.55, upper left). No FRET occurred as expected (E = 0 in Fig. 4.55, upper right). The concentration indexes of donor ($\overline{Dfd}$) and acceptor ($\overline{Afa}$) varied as expected (Fig. 4.55, lower left). The degree of oligomerization revealed a horizontal line (oligo = 1 in Fig. 4.55, lower right). An independent mixture series (IAF/TMRIA) yielded similar results (Fig. 4.56) as above-mentioned mixture series (Alexa 488/Alexa 594). Taken together, both mixture series revealed a monomeric state of labeled DcuS monomers in detergent solution.

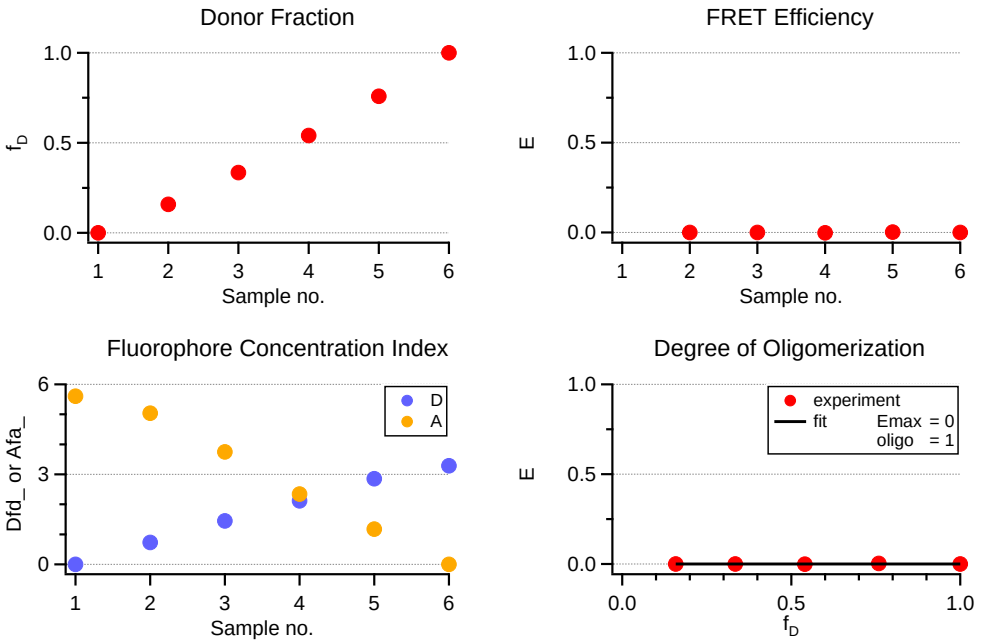

Figure 4.55: Oligomeric state of DcuS monomers (labeled with Alexa 488/Alexa 594). DcuS proteins labeled with either donor (Alexa 488) or acceptor (Alexa 594) in DcuS-labeling buffer containing detergent were mixed at various donor fraction (f_D = 0-1). Measured spectra were quantified by automatic FRET analysis (Fig. 4.51). Results are from one test series (in total n=6 data points, for the degree of oligomerization the point at f_D=0 was removed).

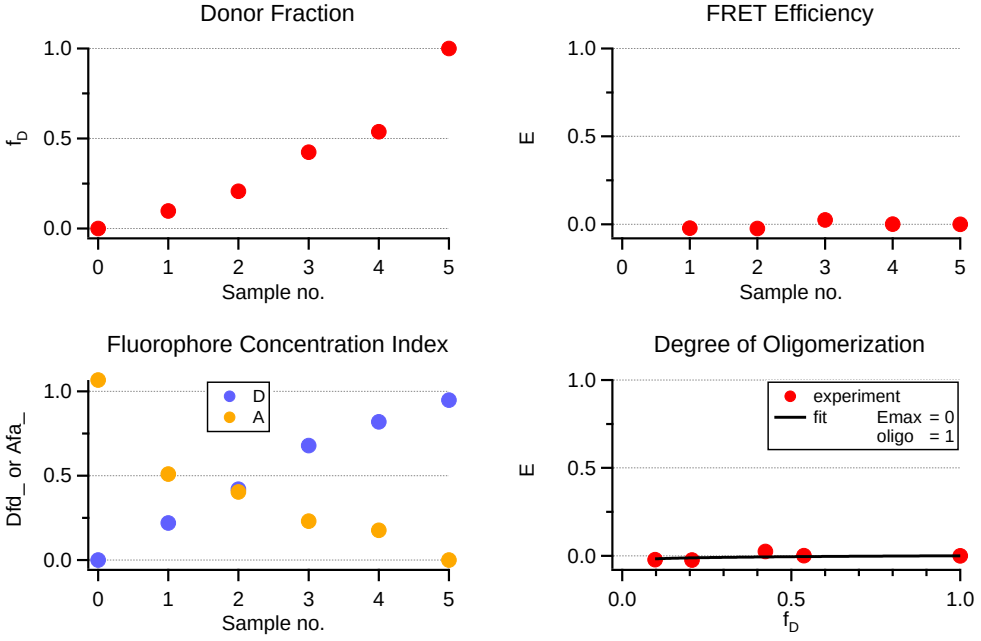

Figure 4.56: Oligomeric state of DcuS monomers (labeled with IAF/TMRIA). DcuS proteins labeled with either donor (IAF) or acceptor (TMRIA) in DcuS-labeling buffer containing detergent were mixed at various donor fraction (f_D = 0-1). Results are from one test series (in total n=6 data points.

Labeled DcuS in liposomes In contrast to the impaired function of DcuS solubilized in detergent, DcuS reconstituted into liposomes was reported functional for fumarate sensing and kinase activity [9]. Therefore, the functionally-relevant oligomeric state of DcuS in liposomes was investigated as follows. With the above-mentioned FRET pairs (Alexa 488/Alexa 594 or IAF/TMRIA), labeled DcuS were mixed at different donor fractions (f_D = 0-1). Samples were prepared in sequence with stepwise increasing donor amounts and stepwise decreasing acceptor amounts. Each sample of mixture series was reconstituted into liposomes respectively (Sec. 3.2.1). Measured spectra were quantified by automatic FRET analysis. According to five independent test series with the Alexa 488/Alexa 594 pair (Fig. 4.57), donor fractions and fluorophores concentration indexes varied as expected (Fig. 4.57, upper left and lower left). FRET signals were detected (Fig. 4.57, upper right), suggesting an oligomeric state of labeled DcuS in liposomes even in the absence of fumarate. Based on the fitting of oligomerization model to the data (Fig. 4.57, lower right), a dimeric state of labeled DcuS in liposomes was identified (oligo = 1.91 $\pm$ 0.17). Similar results were obtained from two independent test series with the IAF/TMRIA pair (Fig. 4.58). The observed FRET efficiencies with IAF/TMRIA pair were higher (E_{max} = 0.56) than those with Alexa pair (Fig. 4.57, E_{max} = 0.28), but yielded a dimeric state of labeled DcuS in liposomes as well (oligo = 1.67 $\pm$ 0.35). The difference in FRET efficiencies between IAF/TMR pair and Alexa pair may due to different labeling efficiencies.

4.3.2.2 Effect of Fumarate on the Oligomeric State

Fumarate To test the effect of fumarate binding on the oligomeric state of DcuS, samples of the above-mentioned test series (Fig. 4.57 and Fig. 4.58) were treated with fumarate (20 mM). Measured spectra in the presence of fumarate were quantified by automatic FRET analysis (Fig. 4.59 and Fig. 4.60). With the Alexa 488/Alexa 594 pair, donor fractions and fluorophore concentration indexes were insensitive to fumarate treatment as expected (Fig. 4.59, upper left and lower left), compared with those in the absence of fumarate (Fig. 4.57) Neither significant difference in FRET efficiency nor in degree of oligomerization were observed upon fumarate treatment (Fig. 4.59, lower right, E_{max} = 0.25, oligo = 1.92 $\pm$ 0.20), suggesting that the degree of oligomerization of DcuS is not enhanced or disrupted upon fumarate binding. With the IAF/TMRIA pair (Fig. 4.60), an increased FRET efficiency and a decreased degree of oligomerization were observed upon fumarate treatment (Fig. 4.60, lower right, E_{max} = 0.72, oligo = 1.38 $\pm$

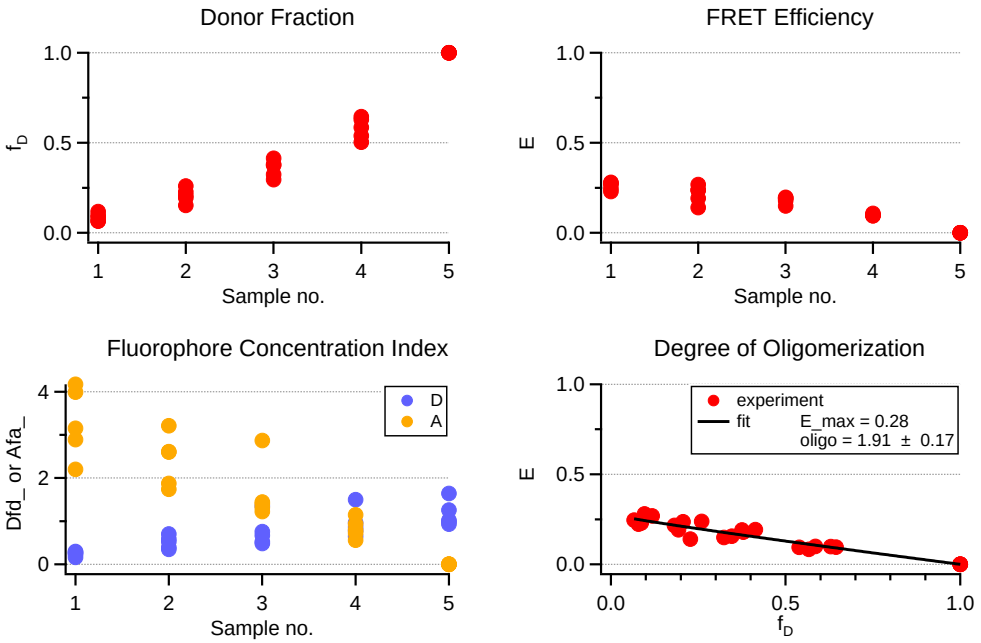

Figure 4.57: Oligomeric state of DcuS (labeled with Alexa 488/Alexa 594) in liposomes (no fumarate). Mixture series of Alexa 488- and Alexa 594-labeled DcuS were reconstituted in liposomes. Spectra were measured in Tris buffer (50 mM). Results are from five independent test series (in total n=25 data points).

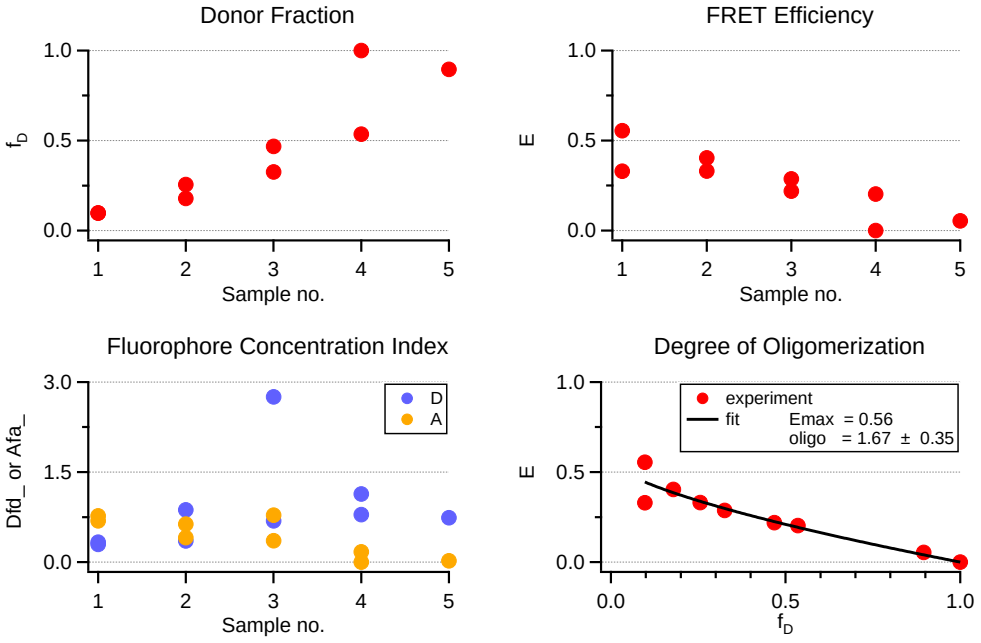

Figure 4.58: Oligomeric state of DcuS (labeled with IAF/TMRIA) in liposomes (no fumarate). Mixture series of IAF- and TMRIA-labeled DcuS were reconstituted in liposomes. Spectra were measured in Tris buffer (50 mM). Results are from two independent test series (in total n=10 data points).

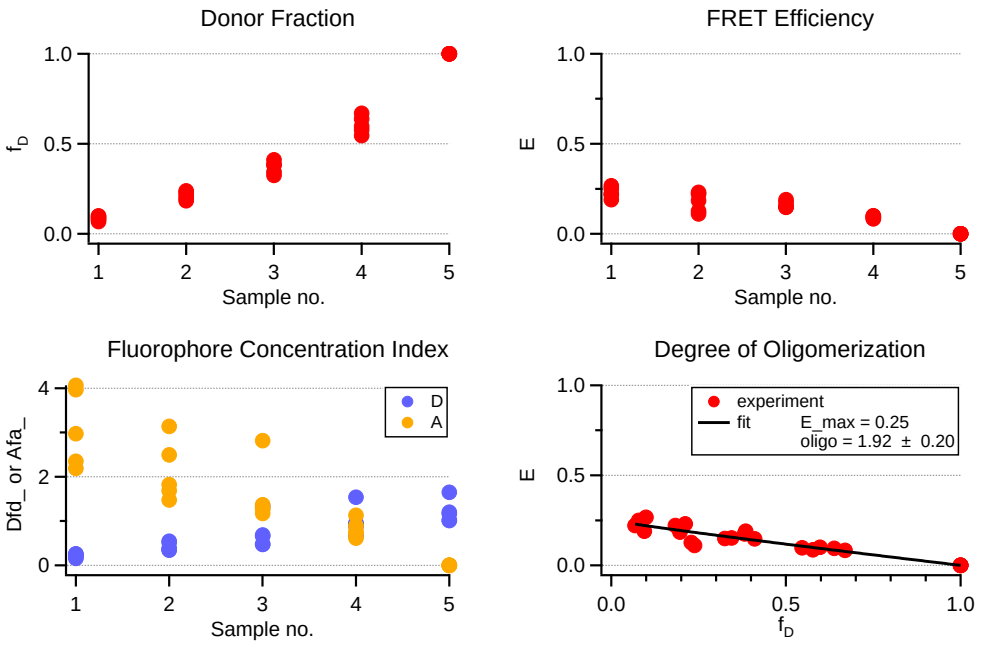

Figure 4.59: Oligomeric state of DcuS (labeled with Alexa 488/Alexa 594) in liposomes (with fumarate) Mixture series of Alexa 488- and Alexa 594-labeled DcuS were reconstituted in liposomes. Spectra were measured in Tris buffer (50 mM) containing fumarate (20 mM). Results are from five independent test series (in total n=25 data points).

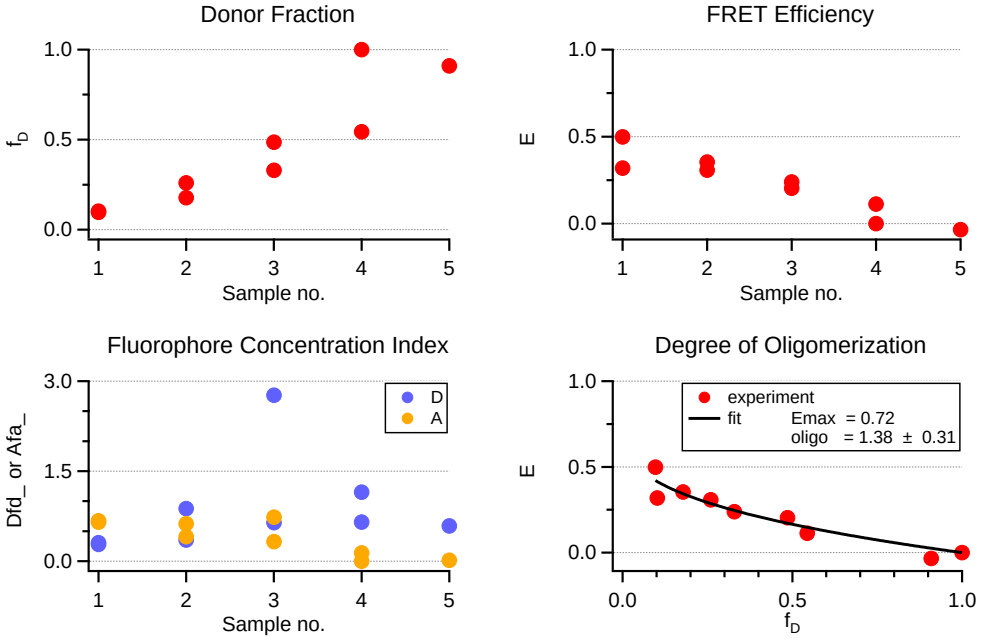

Figure 4.60: Oligomeric state of DcuS (labeled with IAF or TMRIA) in liposomes (with fumarate). Mixture series of IAF- and TMRIA-labeled DcuS were reconstituted in liposomes. All spectra were measured in Tris buffer containing fumarate (20 mM). Results are from two independent test series (in total n=10 data points).

0.31). The deviation in oligomerization level may result from limited data points in this case.

Freeze-and-thaw The sensory domain of DcuS is naturally outside the cell membrane, but reconstituted DcuS may have random orientation in liposomes, with the sensory domain toward either outside or inside liposomes. In principle, fumarate should be able to freely diffuse into liposomes. To ensure the full access of effector fumarate to the sensory domains of DcuS enclosed inside liposomes, labeled DcuS in liposomes in the presence of fumarate was subjected to freeze-and-thaw cycles leading to the breakdown and reformation of liposomes and exposure of all sensory domains of DcuS to fumarate. One of the test series in the presence of fumarate (Fig. 4.59) was additionally treated with three cycles of freeze-and-thaw (Fig. 4.61). By comparing the results before and after freeze-and-thaw (Fig. 4.61), only slight increase in FRET efficiency (E_{max}= 0.25 → 0.29) and slight decrease in degree of oligomerization (oligo = 1.82 ± 0.02 → 1.58 ± 0.12) was observed upon treatment of freeze-and-thaw (Fig. 4.61). The differences seem not related to the formation of higher-order oligomers, and may relate to other mechanism (e.g. intra-molecular conformational changes or other protein-protein interactions). The freeze-and-thaw for samples in the absence of fumarate was also performed, and no effect of freeze-and-thaw on FRET efficiency and degree of oligomerization was observed (not shown).

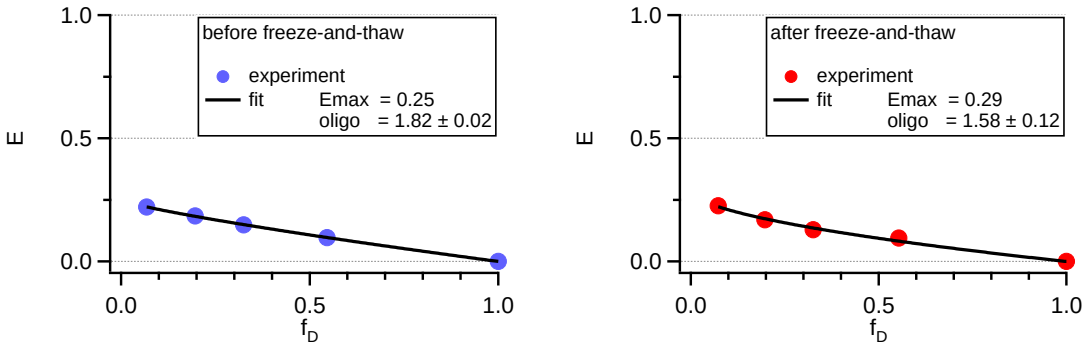

Figure 4.61: Effect of freeze-and-thaw on oligomeric state of DcuS in liposomes. One test series from Fig. 4.59 (in total n=5 data points) in the presence of fumarate (20 mM) were tested before (left) and after (right) 3 cycles of freeze-and-thaw.

4.3.2.3 Oligomeric State of a Binding-defect Mutant

To test the effect of the fumarate-binding site on the oligomeric state of DcuS, a binding-defect DcuS mutant, hereafter cited as DcuS (BD), was generated with a R147A mutation in fumarate binding site to abolish the fumarate-binding ability [15], and an additional C199S mutation for single cysteine-labeling site (Fig. 4.12). A 1:1 mixture of Alexa 488- and Alexa 594-labeled DcuS (BD) was reconstituted in liposomes. A significant FRET peak was observed in the spectrum of this mixture (Fig. 4.62, indicated by arrow). The disruption of fumarate binding ability of DcuS (BD) mutant had no effect on its oligomerization activity, and the oligomerization activity of DcuS is independent of the fumarate-binding site. Combined with the results upon fumarate treatment (Sec. 4.3.2.2), the oligomerization of DcuS may not be regulated by fumarate binding.

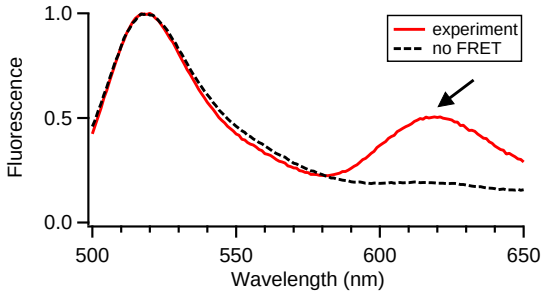

Figure 4.62: Oligomeric state of DcuS (binding defect mutant). Red: measured spectrum of a 1:1 mixture of Alexa 488- and Alexa 594 labeled binding-defect DcuS mutant (BD) in liposomes. The arrow indicates the FRET peak. Black dashed: simulated spectrum as a superposition of spectrum of Alexa 488-labeled DcuS in liposomes and that of Alexa 594-labeled DcuS in liposomes. The protein amount of each sample was 100 μg before reconstitution. All spectra were excited at 480 nm, and normalized to unity.

4.3.2.4 Effect of Protein Amount on the Oligomeric State

Protein amount in liposomes To confirm the specificity of observed FRET in liposomes (Sec. 4.3.2.1), the concentration-dependence of donor fraction and FRET efficiency was tested by a dilution series of labeled DcuS in liposomes. A stock solution (initial protein amount: 100 μg labeled DcuS) containing mixture of Alexa 488- and Alexa 594-labeled DcuS at a constant donor fraction ($f_D = 0.25$) was serially diluted to prepare a dilution series (6 samples of 2- to 50-fold dilution; final protein amounts: 2-100 μg labeled DcuS). Each reconstitution of this dilution series was performed at a fixed lipid-to-protein ratio (10:1) instead of the

ratio (20:1) used for previous reconstitutions, because lower lipid-to-protein ratio could lead to higher protein densities in liposomes. Because a high recovery (>90%) after reconstitution was confirmed by comparison with fluorescence intensity of labeled DcuS before reconstitution, the protein amount after reconstitution (in liposomes) should be comparable to that before reconstitution. Measured spectra of this dilution series were quantified by automatic FRET analysis. Donor fractions and FRET efficiencies were plotted against protein amounts before reconstitution (Fig. 4.63). The effect of protein amount on donor fraction (decrease with increasing protein amount) was stronger than that on FRET efficiency ($E = 0.22 \pm 0.04$). At lower protein amounts in liposomes, substantial FRET efficiencies were still observed even at more deviated donor fractions. In this study, the actual protein amount for each reconstitution was always kept in the range of 80-100 μg. Therefore, the observed FRET efficiency and the oligomerization of labeled DcuS in liposomes (Sec. 4.3.2.1) were confirmed specific and not an artifact due to molecular crowding in liposomes.

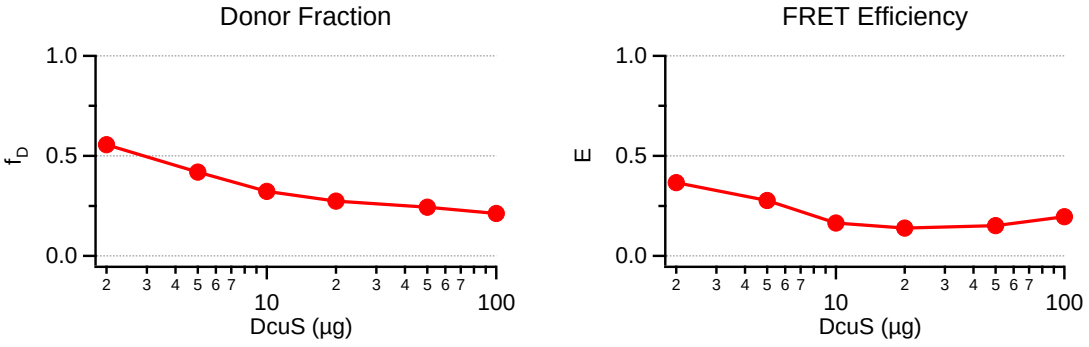

Figure 4.63: Effect of protein amount on oligomerization of DcuS. DcuS (labeled with Alexa 488/Alexa594) was mixed at fixed donor fraction (f_D=0.25) as stock solution. Dilution series (2- to 50-fold) of this stock solution were reconstituted in liposomes. In this study, the protein amount of labeled DcuS was always kept in the range of 80-100 μg before reconstitution. The recovery of protein amount after reconstitution was confirmed > 90% by comparing fluorescence intensities of conjugated fluorophores before and after reconstitution.

Theoretical Estimation of DcuS amount in Liposome The observed FRET efficiencies seem concentration-independent to rule out the artificial aggregation due to molecular crowding. In addition to the experimental validation, a theoretical estimation of DcuS amount in liposomes was estimated as follows. According to the average volume (V) of a glycerol head group of a lipid ($\sim$ 0.07 nm^3) [69], the average area per lipid molecule (A) covered by this head group is roughly 0.2 nm^2 (volume of a sphere (V) = $\frac{4}{3}\pi r^3$; calculated from this the average radius of

the head group (r) is 0.2557 nm; area of a circle (A) = πr^2). For a liposome of 100 nm in diameter, the surface area is around 31,000 nm^2 (with radius r = 50 nm; surface area of sphere $4\pi r^2$). For a lipid bilayer (with an inner and outer surface), the total surface covered by lipid molecules is around 60,000 nm^2. The average area per lipid is 0.2 nm^2 as above-mentioned. Therefore, around 300,000 lipid molecules are required to form a liposome of 100 nm in diameter (average number of lipid molecules per liposome). In this study, DcuS proteins were reconstituted in liposomes at a lipid-to-protein ratio (w/w) of 20:1. The molar mass of DcuS with His_6-tag is about 62.7 kDa, and the average molar mass of the lipid mixture used for reconstitution is 945 Da. Therefore, there are around 1,300 lipids per DcuS proteins (62,700 $\times$ 20 $\div$ 945 $\sim$ 1,300). If 300,000 lipid molecules form a liposome as above-mentioned, around 230 DcuS proteins could be incorporated in a liposome (average amount of DcuS proteins per liposome = 300,000 $\div$ 1,300 $\sim$ 230). If lipid-to-protein ratio (w/w) is decreased to 10:1 for reconstitution (as Fig. 4.63), around 460 DcuS proteins per liposome would be expected.

Conclusion: oligomeric state of labeled-DcuS *in vitro* The oligomeric state of DcuS was examined by using Alexa 488/Alexa 594 and IAF/TMRIA pairs independently. Novel finding in the functionally-relevant oligomerization of DcuS was examined upon reconstitution into liposomes. Both experimental systems showed evidence of FRET among labeled DcuS in liposomes, and the absence of FRET among labeled DcuS in detergent solution. Moreover, a dimeric state of labeled DcuS in liposomes was pre-formed in the absence of fumarate. Upon fumarate and freeze-and-thaw treatments, no significant changes in FRET efficiency and degree of oligomerization were observed in labeled DcuS reconstituted in liposomes. Besides, FRET observed in the binding-defect mutant of DcuS suggested that the oligomerization activity may be independent of fumarate binding. In the range of concentration of labeled DcuS we used for reconstitution (80-100 μg), no strong concentration-dependence of donor fraction and FRET efficiency was observed.

4.3.3 Protein-Protein Interactions of DcuS (*in vivo*)

In addition to the homo-oligomerization of DcuS, the protein-protein interactions of DcuS with other proteins (hetero-oligomerization) were examined in living cells as well. For *in vivo* FRET measurements, relevant proteins (CitA and DctA) and an irrelevant protein (Tar) were genetically tagged with YFP respectively. DcuS-CFP and YFP-tagged protein of interest were co-expressed in *E. coli* cells (Fig. 4.64). Measured spectra of these cells were quantified by automatic FRET analysis as above-mentioned for oligomerization of DcuS (Sec. 4.3.1). The binding of FP-tagged proteins may result in the occurrence of FRET between CFP and YFP, providing direct evidences for protein-protein interactions *in vivo*.

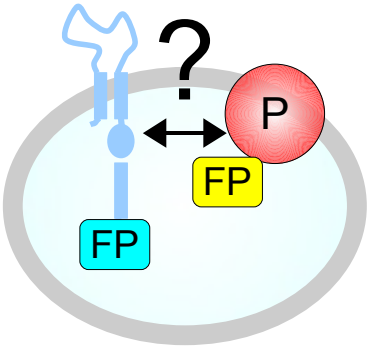

Figure 4.64: Biological Aim 2: Is there an interaction between DcuS and its relevant proteins (P) in *E. coli*?

4.3.3.1 Interaction between DcuS and CitA

To study the interaction between DcuS and CitA, CitA-YFP in pBAD30 vector was constructed and tested for CitA function and YFP fluorescence (Fig. 4.8). Co-expression of DcuS-CFP and CitA-YFP fusions were induced in *E. coli* cells by arabinose from 3.5 hr to 6 hr. From five independent induction series (in total n=20 data points), measured spectra were quantified by automatic FRET analysis (Fig. 4.65). Donor fractions (Fig. 4.65, upper left, $f_D = 0.40 \pm 0.02$) were similar to previous co-expression of pBAD18 and pBAD30 vectors for DcuS-FP fusions (Fig. 4.52, upper left, $f_D = 0.41 \pm 0.01$). Substantial FRET efficiencies were detected between DcuS-CFP and CitA-YFP (Fig. 4.65, upper right, $E = 0.15 \pm 0.02$), suggesting that an interaction or co-localization of DcuS-CFP and CitA-YFP in cells already occurs during the early phase of biosynthesis. Because of the difficulty to reach lower or higher donor fractions (Fig. 4.65, lower right), it can be concluded that a hetero-complex (at least hetero-dimer) between DcuS-CFP and CitA-YFP

was formed in *E. coli* cells, but the exact oligomerization level could not be determined in this case.

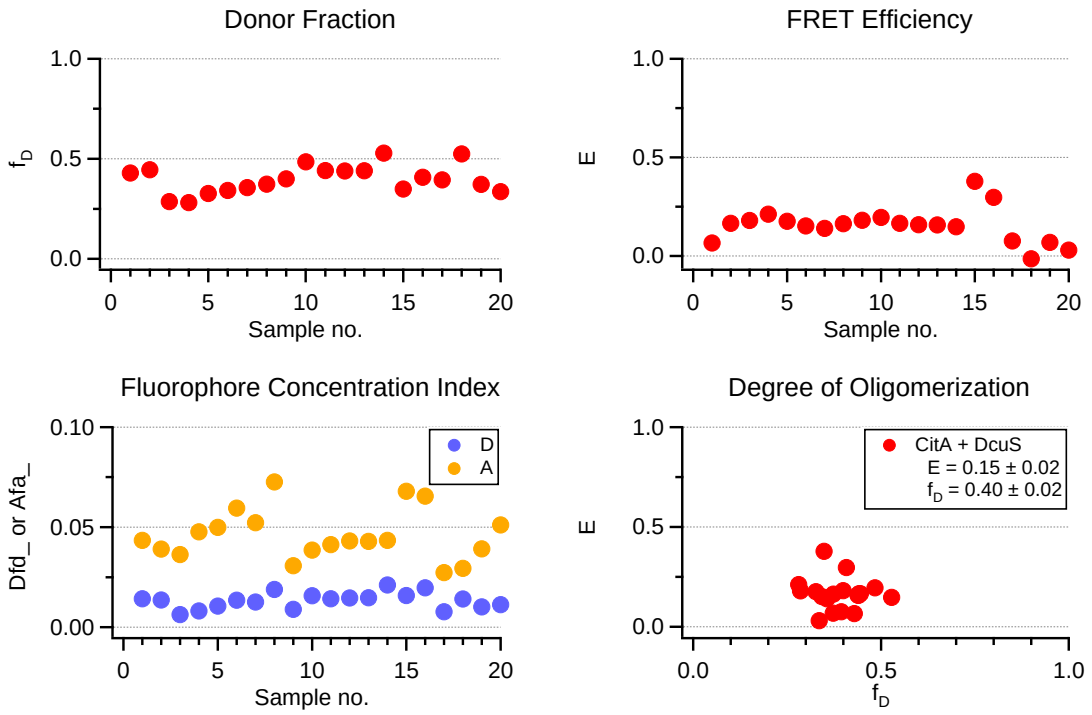

Figure 4.65: Interaction between DcuS and CitA. DcuS-CFP (pBAD18) and CitA-YFP (pBAD30) were co-expressed in *E. coli* cells by arabinose (133 μM) from 3.5 to 6 hr. Results are from five independent induction series (in total n=20 data points).

4.3.3.2 Interaction between DcuS and DctA

To study the interaction between DcuS and DctA *in vivo*, DctA-YFP in pBAD30 vector was generated and tested for functional activities (Fig. 4.9). DcuS-CFP and DctA-YFP fusions were co-expressed in *E. coli* cells by 3.5-6 hr of induction with arabinose. Measured spectra of cells from six independent induction series (in total n=35 data points) were quantified by automatic FRET analysis (Fig. 4.66). Donor fractions were also limited to a narrow range (Fig. 4.66, upper left, f_D = 0.48 $\pm$ 0.01), similar to those observed in previous induction series co-expressed by pBAD18 and pBAD30 vectors (Fig. 4.52 and Fig. 4.65). Substantial FRET signals were observed between DcuS-CFP and DctA-YFP (Fig. 4.66, upper right, E = 0.28 $\pm$ 0.03), which suggest an interaction between DcuS-CFP and DctA-YFP in cells. The stoichiometry of the interaction between DcuS and DctA was also hard to determine in this case because of the limited distribution of donor fractions (Fig.

4.66, lower right). Therefore, it can only be concluded that at least hetero-dimers were formed for the interaction between DcuS-CFP and DctA-YFP in living cells.

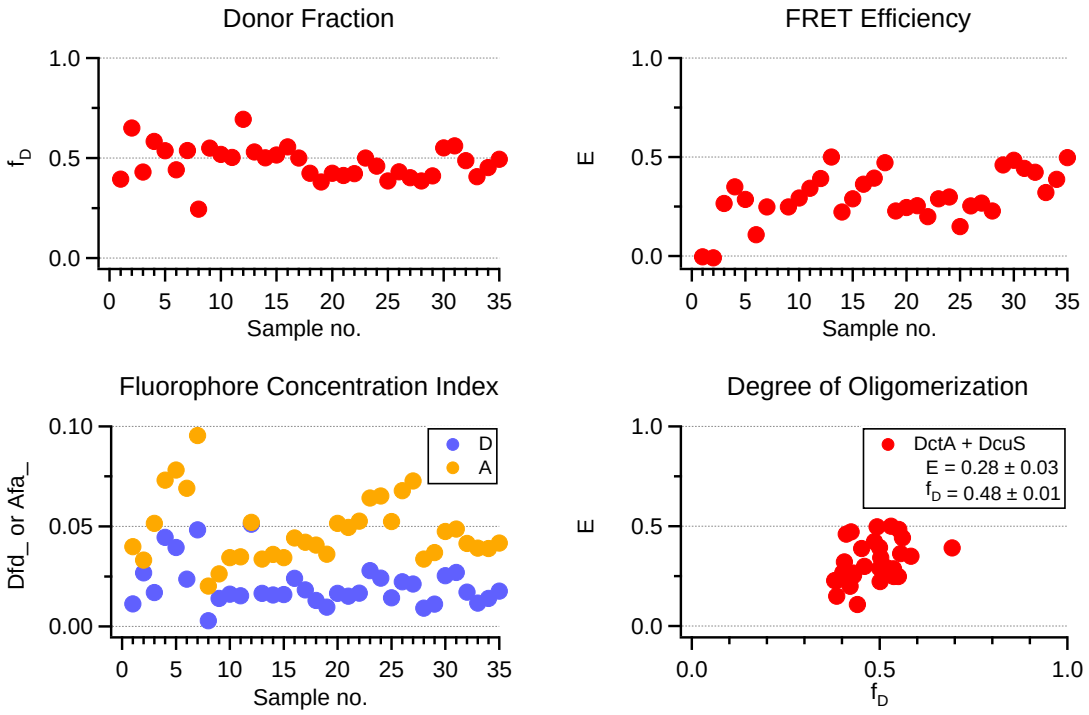

Figure 4.66: Interaction between DcuS and DctA. DcuS-CFP (pBAD18) and DctA-YFP (pBAD30) were co-expressed in *E. coli* cells by arabinose (133 μM) from 3.5 to 6 hr. Results are from six independent test series (in total n=35 data points).

4.3.3.3 Interaction between DcuS and Tar

To confirm the specificities of above-mentioned hetero-oligomerization of DcuS-CitA and DcuS-DctA, an irrelevant membrane protein (Tar) was tested as a non-interacting control for protein-protein interaction of DcuS while co-localized in the membrane. Tar functions as a membrane-bound chemotaxis receptor. The YFP fusion of a C-terminal truncated Tar^{1-331} is homogeneously distributed in the cell membrane [54]. Because DcuS and Tar are not functionally relevant, no direct interaction between DcuS and Tar was assumed as a negative control for FRET occurrence upon protein-protein interaction. As a non-interacting protein with DcuS-CFP in the membrane, Tar^{1-331}-YFP was generated and expressed under the control of pTrc99a induced by IPTG (from Dr. V. Sourjik, ZMBH, Heidelberg, Germany) [54]. The YFP fluorescence of Tar-YFP fusion protein was comparable to that of YFP (Fig. 4.67).

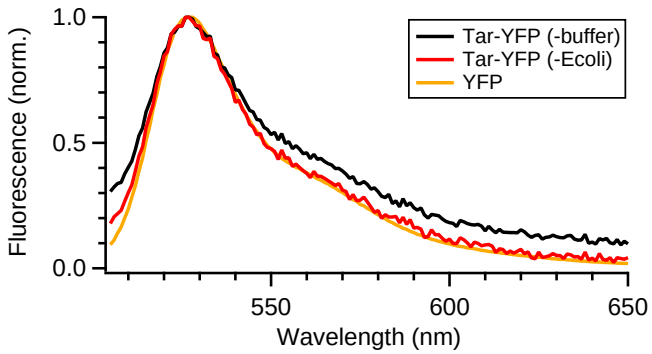

Figure 4.67: YFP fluorescence of Tar$^{1-331}$-YFP. Emission spectra (λ_{ex}= 488 nm) of cells expressing Tar$^{1-331}$-YFP fusion (black: buffer-subtracted; red: *E. coli*-subtracted) in comparison with YFP reference spectra (yellow). Spectra were normalized by peak intensity.

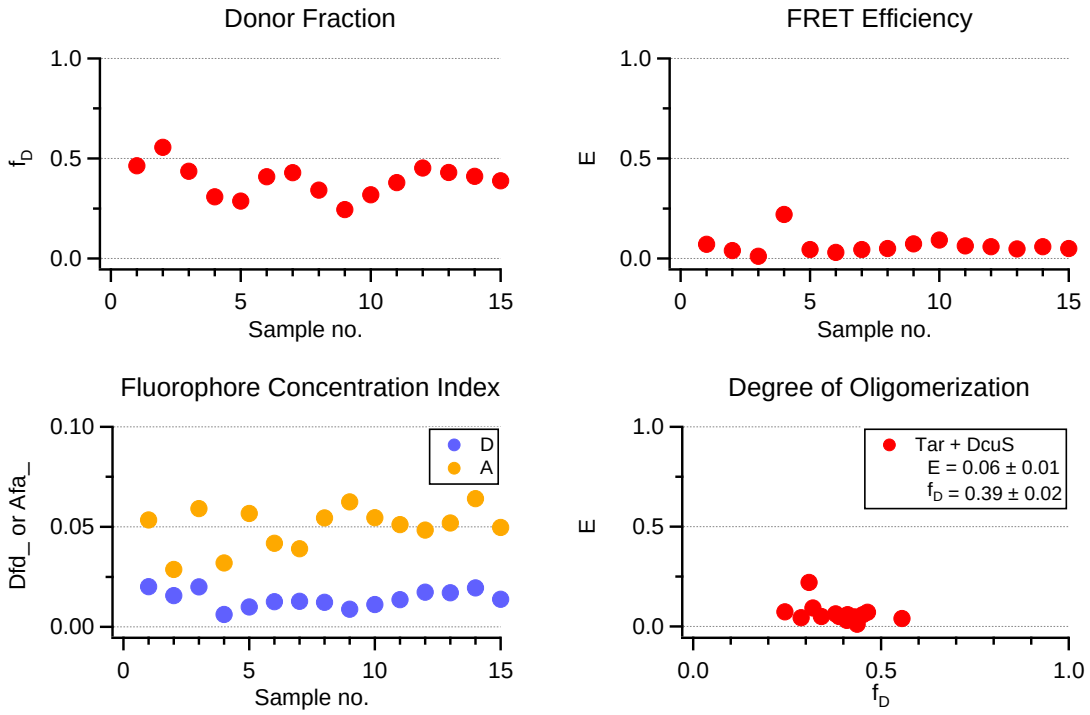

Figure 4.68: Interaction between DcuS and Tar. DcuS-CFP (pBAD18) and Tar$^{1-331}$-YFP (pTrc99a) were co-expressed in *E. coli* cells by arabinose (133 μM) and IPTG (1 mM) from 3 to 6 hr. Results are from four independent test series (in total n=15 data points).

DcuS-CFP and Tar-YFP fusions were co-expressed in *E. coli* cells in the presence of both arabinose and IPTG. For four independent induction series (in total n=15 data points), measured spectra were quantified by automatic FRET analysis (Fig. 4.68). The expression level of Tar^{1-331}-YFP in pTrc99a (medium-copy-number vector) were slightly higher than that of above-mentioned YFP fusions in pBAD (low-copy-number vector) (Fig. 4.68, lower left, acceptor concentration index ($\overline{Afa}$) marked in yellow), and thus donor fractions were slightly lower than other above-mentioned induction series under the control of pBAD vectors induced by arabinose (Fig. 4.68, upper left, $f_D = 0.39 \pm 0.02$). FRET efficiencies were detected between Tar^{1-331}-YFP and DcuS-CFP (Fig. 4.68, upper right, $E = 0.06 \pm 0.01$), but much lower compared with other substantial FRET signals observed in other co-expression of FP-fusions, such as DcuS-DcuS (Fig. 4.52), DcuS-CitA (Fig. 4.65), and DcuS-DctA (Fig. 4.66). A possible explanation for the minor FRET signals observed between DcuS-CFP and Tar^{1-331}-YFP could be the higher expression of Tar^{1-331}-YFP compared to DcuS-CFP which may result in locally crowded fluorophore concentrations and thus increase the possibility of non-specific FRET between non-interacting FP fusions. However, even higher FRET efficiencies should be expected at relatively lower donor fractions in this case. Therefore, another possible explanation could be the direct interaction between CFP and YFP moieties of fusion proteins in the membrane. Therefore, the minor FRET ($E = 0.06 \pm 0.01$) could be an estimate of error of FRET detection which may exist between CFP- and YFP-tagged fusions while co-localized in membrane.

5 Discussion

DcuS is a membranous sensor kinase of *E. coli* involved in signal transduction pathways to regulate C_4-dicarboxylate metabolism [6, 25]. The mechanism of signal transmission across the membrane is not clear. Several modes were proposed in the literature, e.g. ligand-induced conformational changes [29], changes of oligomerization level [70, 71], or interactions with other proteins [72]. Partial structures of DcuS have been reported on truncated domains, e.g. sensory domain [12, 13, 15, 16] and PAS domain of DcuS [19]. However, the structure-function relationship of DcuS is little understood based on the full-length membrane protein. Isolated DcuS monomers show no phosphorylation activity [9]. Therefore, in this study the oligomeric state and protein-protein interactions of full-length DcuS was investigated by quantitative Fluorescence Resonance Energy Transfer (FRET) spectroscopy both in living cells and *in vitro*.

5.1 Method: Quantitative FRET Analysis

To determine the interaction stoichiometry of protein complexes, a new quantitative FRET method was developed for fluorescence spectroscopy. The sensitivity of fluorescence methods allows oligomerization or protein-protein interaction to be studied at low concentration or expression levels much closer to physiological conditions than the over-expression for *in vitro* assays. Combined with genetically encoded fluorescent protein fusions as site-specific probes and nondestructive tools in living cells [43, 66, 73–75], fluorescence methods can monitor dynamic molecular complexes as direct *in vivo* evidences for protein-protein interactions in living cells. FRET measurements performed both *in vitro* and *in vivo* allow comparisons between FRET results of both more controlled or more physiological conditions. Many fluorescence/bioluminescence methods are applicable for studying association/interaction of proteins, and each has its own advantages and disadvantages. Lifetime-based measurements can determine the FRET efficiency accurately, but require sophisticated instrumentation. Because fluorescence

lifetime is concentration-independent, lifetime measurements are incapable of differentiating relative concentrations of the donor and acceptor [76–78]. Acceptor photobleaching methods is destructive because of the high laser power needed, and may result in an error of FRET efficiency due to incomplete photobleaching of acceptor or simultaneous photobleaching of donor [79–81]. Bioluminescence resonance energy transfer (BRET) method requires substrates to generate BRET signals, and BRET signals are usually weaker than FRET signals [82]. Bimolecular fluorescence complementation (BiFC) method sensitively detects a new fluorescence signal, whereas FRET method detects the dynamic changes in fluorescence that already exists [83]. Fluorescence cross correlation spectroscopy (FCCS) method can determine oligomerization, but requires a specialized apparatus and nontrivial data analysis [84]. Fluorescence spectroscopy records fluorescence spectra under equilibrium conditions in solution without any separation or fixation, and provides non-destructive detection in the absence of photobleaching and phototoxicity from laser excitation. Therefore, FRET spectroscopy was used to investigate the oligomerization and protein-protein interactions of DcuS in this study.

Since FRET efficiency (E) depends on the relative concentrations of donor (D) and acceptor (A) fluorophores (donor fraction $f_D = \frac{[D]}{[D]+[A]}$) as shown in Fig. 5.1, knowledge of FRET efficiency (E) without the corresponding donor fraction (f_D) is of very limited use. It is important to consider the dependence of FRET efficiency on the stoichiometry of donors and acceptors for intra-experiment and inter-experiment comparisons [85–87].

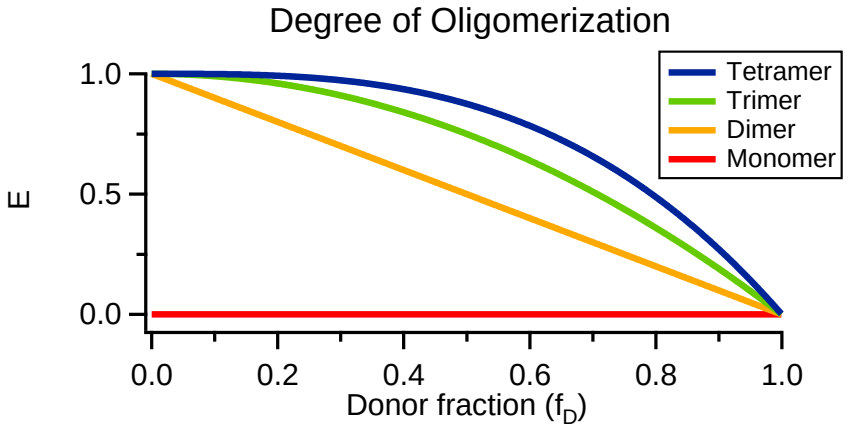

Figure 5.1: FRET efficiency as a function of donor fraction and degree of oligomerization. Model for oligomerization state: $E = E_{max} \times (1 - f_D^{(oligo-1)})$. E: FRET efficiency; f_D: donor fraction; $oligo$: degree of oligomerization

However, donor fraction (f_D) or fluorophore concentrations ($[D]$ or $[A]$) are hard

to determine directly, in particular in living cells. Even FRET methods have been widely used to study oligomerization or protein-protein interactions, the FRET efficiency in living cells has not always been carefully quantified or even neglected the dependence on the stoichiometry of donor and acceptors in protein complexes in many studies.

In this study, a quantitative method originally described for fluorescence microscopy [48] was modified for fluorescence spectroscopy by using two different excitation wavelengths to yield E and f_D simultaneously (hereafter cited as Gordon's equation). Based on the FRET efficiency (E) as a function of donor fraction (f_D), data were fitted to a model of oligomeric states [49, 50] to determine the degree of oligomerization (Fig. 5.1, $E = E_{max} \times (1 - f_D^{(oligo-1)})$). The reliability of determined degree of oligomerization depends on the accuracy of FRET efficiency (E) and donor fraction (f_D) determined by Gordon's equation.

The occurrence of FRET requires the spectral overlap between the emission spectrum of donor and the absorption spectrum of acceptor. Because of the spectral overlap, the observed FRET signal is likely accompanied with the direct excitation of donor detected at acceptor emission wavelength, or with the direct excitation of acceptor at donor excitation wavelength. To correct the spectral crosstalk, various FRET determination methods were proposed in the literature [48, 88–93]. Gordon's equation was reported as a relatively reliable approach for FRET quantification in comparison with other methods [90], because Gordon's equation provides more rigorous cross talk correction (by removing the non-FRET contributions of donor and acceptor) to yield more stable and reproducible FRET efficiencies as well as measures of fluorophore concentrations (even donor-only and acceptor-only signals can not be directly measured in the presence of both donor and acceptor). For the comparison among biological samples containing variable ratios of donor to acceptor, the FRET efficiencies has to be normalized for variation in fluorophore concentrations to confirm the statistically significant values of FRET efficiency.

For each FRET pair, Gordon's equation requires a proportionality constant termed G factor which represents the ratio of sensitized acceptor emission to the reduced donor emission due to FRET occurrence [48]. In this study, the values of G factor were first calculated from literature values and then -if possible- validated experimentally (Table. 4.4) by mixing donor and acceptor fluorophores at known concentrations and therefore known donor fractions (f_D= 0-1). Based on the calculated values of G factor, the empirical values of G factor were optimized by

checking the linear relationship between donor fractions determined by Gordon's equation and the expected ones. In the literature, G factors (also called ξ or α) for CFP/YFP pair have been determined by using CFP-YFP tandem fusions, such as fusion of known lifetime [94] (estimated G: 0.022, measured: 0.012), fusion under different extent of photobleaching (G, measured: 3.50) [80], or fusions of different linker lengths (i.e. different FRET efficiencies, G =5.7 and 0.615) [95], or fusion of other GFP variants (Cerulean and Venus, $G = 1.815 \pm 0.067$) [96]. Even for the same FRET pair, the values of G factor showed instrument-dependent deviations [95]. Therefore, G factor (or other equivalent terms for this measure) is critical to be determined before FRET quantification. The advantages of our calibration method for G factor is rather simple, readily applicable to other FRET pairs, and needs no specialized instrumentation.

This method based on Gordon's equation requires background-free spectra. However, living cells usually contain strong background, such as scattering and autofluorescence [61]. In this study, the background problem was handled by using flexible background subtraction (FBS). A multi-parameter fitting for FBS was developed to subtract individual background among cells instead of subtraction by a fixed background, which ensures background-free spectra for further FRET quantifications. The quality of reference spectra used for FBS was improved by sequential steps of centrifugation and ultracentrifugation to remove the cellular autofluorescence from flavins (FAD, FMN, and riboflavin) and NADH molecules [61]. Validated by theoretical simulations and experimental controls, FBS can accurately determine contributions of spectral components, and then efficiently extract donor and acceptor signals from background, even at low signal-to-noise ratios. Despite the inevitable instrument-based noise, FBS allows robust and reliable extraction of fluorescence signals from background as an automated background subtraction for spectroscopy in complex biological samples. In contrast, numerous FRET studies in the literature neglected the variations among samples, and performed background correction by subtracting a constant background (the signal from a reference containing neither donor nor acceptor). While cellular autofluorescence varies from cells to cells, the general background subtraction may not ensure background-free data for further FRET analysis. Surprisingly, individual deviations in background fluorescence were seldom taken into account. Only a few studies handled cell-based background individually, e.g. removal of flavin autofluorescence components by spectral unmixing in fluorescence microscopy [97], estimation of autofluorescence by using reference spectra/images of cells containing neither donor nor acceptor [87, 98, 99].

For the accurate determination of FRET efficiency, many factors must be taken into account, such fluorophore concentrations and signal-to-noise ratios. In this study, the accuracy and applicability of our method for quantitative FRET analysis was validated step by step with different donor-acceptor pairs, even under complex experimental conditions in living cells. Therefore, this method can be routinely employed by software to study the oligomeric states of homo- or hetero-complexes with almost each donor-acceptor pair either *in vitro* or *in vivo*. This method was subsequently applied to study the oligomerization and protein-protein interactions of DcuS.

5.2 Interaction between CFP and YFP

To apply the above-mentioned quantitative method for *in vivo* FRET measurements, GFP variants were used as fluorescent probes which have been widely used to study homo- or hetero- protein complexes in living cells [100–104]. To interpret FRET data adequately, the accuracy and precision of determination of FRET efficiency should be carefully evaluated by FRET controls [85]. The FRET pair of GFPs has a tendency to form a dimer, the dissociation constant for a GFP homodimer has been estimated to be 0.1 mM measured by analytical ultracentrifugation [105, 106]. Even many crystal structures of GFPs exist as dimers [44, 45, 107], purified GFP reveals a diffusion coefficient of consistent monomers at low protein concentrations by fluorescence correlation microscopy [108]. The tendency to form dimers of GFP and its variants depends on the local concentration of GFPs. In this study, different controls were tested to evaluate the interaction between CFP and YFP moieties of fusions in living cells. First, (1) **a 1:1 CFP-YFP tandem fusion was generated as a positive control**. Not only positive FRET efficiency ($E = 0.6 \pm 0.1$) but accurate donor fraction ($f_D = 0.5 \pm 0.02$) was observed as expected. Secondly, (2) **CFP and YFP were co-expressed in the same cells**. A minor FRET efficiency ($E = 0.07 \pm 0.02$ for $f_D = 0.4 \pm 0.06$) was observed that suggest a weak interaction between cytosolic CFP and YFP. Thirdly, (3) **CFP and YFP were separately expressed in different cells**. FRET between CFP and YFP was impossible to occur because of the spatial separation among cells. No FRET occurrence ($E = 0 \pm 0.02$ for $f_D =$ 0-1) was observed as expected in this negative control. (4) DcuS is a membrane protein, but CFP and YFP are cytosolic in the absence of DcuS fusion. Therefore, above-mentioned controls only demonstrated the interaction between CFP and YFP in the cytosol. To further evaluate the

interaction between CFP and YFP in the cell membrane, a YFP fusion with a non-interacting membrane protein, a truncated form of the chemotaxis receptor Tar (Tar^{1-331}) was used to check the interaction with DcuS-CFP in cell membrane. **FP fusions of non-interacting membrane proteins** were co-expressed in the same cells. The co-localization of DcuS-CFP and Tar^{1-331}-YFP in the membrane results in a minor FRET efficiency ($E = 0.06 \pm 0.01$ for $f_D = 0.39 \pm 0.02$), which is an estimate of background FRET signal in our experimental system. In other words, if the observed FRET efficiency is clearly above the background FRET (i.e. the interaction of target proteins is stronger than the direct association of CFP and YFP), it can be concluded that the FRET occurrence is specific due to the interaction of investigated proteins instead of the false-positive FRET results (nonspecific FP interaction or random collisions because of local accumulation of proteins).

5.3 Oligomerization / Protein-Protein Interactions of DcuS

Oligomerization of DcuS In this study, oligomerization of DcuS was investigated both in living cells and *in vitro*. The FRET efficiency observed *in vivo* between DcuS-CFP and DcuS-YFP ($E = 0.19 \pm 0.02$ for $f_D = 0.41 \pm 0.01$) was clearly above the background of $E = 0.06$. However, the range of f_D was very limited because of the similar expression vectors (pBAD30 vector is a lower-copy-number derivative of pBAD18 vector) [68]. Even the degree of oligomerization is hard to determine because of limited range of f_D, it can be concluded that DcuS exists at least as an oligomer. Only a minor effect of fumarate on the oligomerization level ($E = 0.12 \pm 0.01$ for $f_D = 0.40 \pm 0.01$) was observed, which suggest a constitutive oligomeric state of DcuS in living cells. Options to solve the problem of limited f_D could be using different expression vectors or performing *in vitro* measurements. Accordingly, oligomerization of DcuS was examined *in vitro*. Here, no direct donor-acceptor interaction of conjugated dye molecules was observed (i.e. no background FRET signal). Donor fractions of labeled DcuS mixtures could be adjusted in the full range of f_D = 0-1. The dependence of observed FRET efficiencies on the corresponding donor fractions allowed the determination of degree of oligomerization by fitting with the model of oligomeric state. Consistent results from two independent FRET pairs *in vitro* revealed that DcuS is mainly a dimer. No significant effect of fumarate on the oligomerization level was observed. The binding defect mutant of DcuS which retains the kinase activity [15] also revealed

the oligomerization ability. Therefore, the oligomerization of DcuS seems independent of fumarate or fumarate binding site. Besides, no significant concentration-dependence of FRET efficiency was observed in the range of DcuS concentration less than 0.1 μM, which can exclude the formation of artificial aggregates of reconstituted DcuS in liposomes. The consistent FRET occurrence *in vitro* and *in vivo* provides evidence for homo-dimerization of DcuS as full-length protein for the first time. So far, all structures of DcuS as well as structural and functional homologues in two-component systems were reported in truncated domains or *in vitro*. Examples are the periplasmic sensory domains (DcuS and DctB [30, 31], PhoQ [14]) and PAS domain (DcuS [19]). Solution structure of the homodimeric core domain of *Escherichia coli* histidine kinase EnvZ was reported as the first structure of the dimerization domain of an orthodox Histidine protein kinase which shows a close relationship to the CheA structure, and the periplasmic C-terminal core domain is critical for homo-dimerization [109–112]. Other examples are histidine kinases of two-component systems in *E. coli* (e.g. turgor sensor KdpD [113], EvgS in phosphorelay system [34]) as well as those from other species (e.g. LuxQ in the marine bacterium *Vibrio harveyi* [114] and VirA in plant-Agrobacterium signal transduction [115]). Crystal structure revealed a dimer interface of the PhoQ sensor domain [30, 116]. Compared with these *in vitro* structural studies on truncated domains, the oligomerization of DcuS was confirmed by stable FRET signals of full-length DcuS protein fusions in living cells, as a more functionally-relevant native state of DcuS.

Interaction of DcuS with CitA The *in vivo* binding between DcuS and citrate-specific sensor kinase CitA was newly found. The observed FRET efficiencies between DcuS-CFP and CitA-YFP ($E = 0.15 \pm 0.02$ for $f_D = 0.41 \pm 0.01$) were above the background. DcuS is structurally related to CitA [13], but recognizes a broader range of substrates than CitA [15, 16]. Both DcuS and CitA regulate metabolic processes without obvious polar function, but exhibit polar accumulation [53]. The binding between DcuS and CitA may suggest a crosstalk between functionally similar two-component systems DcuSR and CitAB. Crosstalk between two non-cognate two-component systems is rarely published [117] (e.g. two distinct two-component systems, CpxA-CpxR and EnvZ-OmpR, converge at the porin promoters [118], PmrD protein connecting two distinct two-component systems PhoP-PhoQ and PmrA-PmrB [119]). The crosstalk may promote signal amplification and persistence of expression [120].

Interaction of DcuS with DctA A novel interaction between DcuS and the aerobic dicarboxylate transporter DctA was found by *in vivo* FRET for the first time. The observed FRET efficiencies between DcuS-CFP and DctA-YFP ($E = 0.28 \pm 0.03$ for $f_D = 0.48 \pm 0.01$) were clearly above the background, as an evidence for hetero-oligomerization at the protein level. At gene level, the gene regulation of aerobic dicarboxylate carrier (*dctA*) by DcuS was reported controversially: negatively regulated [6] or induced by the DcuSR system in the presence of C_4-dicarboxylates [25, 33]. In addition to the transcriptional regulation of *dctA* gene expression by DcuSR system demonstrated by *in vitro* binding of DcuR to the promoter of *dctA* gene [7] (at gene level, from a genomic perspective), our *in vivo* FRET evidence suggests a post-transcriptional regulation of DctA by DcuSR system may be mediated through protein-protein interactions between DcuS and DctA (at protein level, from a proteomic perspective). For the functionally similar two-component system CitAB and cognate carrier CitS, transcriptional regulation of citrate carrier *citS* gene by CitAB system was also revealed by the *in vitro* binding of CitB to the *citS* operon [121], but no direct interaction between CitA and CitS was reported yet.

5.4 Outlook

In this study, an automatic quantitative FRET analysis was developed for fluorescence spectroscopy, and successfully applied to study the oligomerization and protein-protein interactions of DcuS. This analysis can be widely applicable to determine the interaction stoichiometry of protein complexes for other proteins of interest labeled with adequate fluorophores *in vitro* or *in vivo*. To achieve a broader range of donor fraction (f_D) in living cells, different expression vectors can be employed (e.g. different magnitude of copy number or different inducers) to adjust the donor fraction for determining the degree of oligomerization in living cells. With respect to the role of DcuS in the transmembrane signal transduction, the oligomerization of DcuS seems not to be fumarate-dependent, suggesting that signal transduction of DcuS is unlikely to be mediated by changes of the oligomerization state. Therefore, interactions of DcuS with other proteins could be responsible for signal transduction. Here, we could reveal that such interactions exist, but the effect of fumarate on these interactions has not been studied yet.

Abbreviations

Glossary of Acronyms

Alexa 488	Alexa Fluor 488-C_5-Maleimide
Alexa 594	Alexa Fluor 594-C_5-Maleimide
C	Single-letter code for Cysteine
CFP	Cyan Fluorescence Protein
Cys	Cysteine
Dct	dicarboxylate transport
Dcu	dicarboxylate uptake
E. coli	Escherichia coli
FP	Fluorescent Protein
FRET	Fluorescence Resonance Energy Transfer
GFP	Green Fluorescence Protein
His	Histidine
HK	Histidine Protein Kinase
IAF	5-(Iodoacetamido)fluorescein
PBS	Phosphate Buffered Saline
PD	Periplasmic Sensory Domain
PDI	Perylenediimide
RR	Response Regulator Protein
S	Single-letter code for Serine
TAMRIA	Tetramethylrhodamine-5-iodoacetamide
TDI	Terrylenediimide
TM	Transmembrane Helix
Trp	Tryptophan
W	Single-letter code for tryptophan
XFP	CFP or YFP
YFP	Yellow Fluorescence Protein

Glossary of Mathematical Terms

A	Acceptor
	Absorption
$\overline{Afa}$	Concentration index of acceptor
c	Concentration
D	Donor
$\overline{Dfd}$	Concentration index of donor
E	Energy transfer efficiency / FRET efficiency
F	Steady state intensity or fluorescence
F(λ)	Emission spectrum
f_D	Donor fraction ($\frac{[D]}{[D]+[A]}$)
FI	Fluorescence intensity
h	Hour
J	Spectral overlap
L	Liter
M	Molar
min	Minute
M.W.	Molecular weight / Molar mass
n	Refractive index
QY	Quantum yield
R_0	F*ö*ster distance
r	Distance between donor and acceptor
T	the detection efficiency for a given wavelength pair
t	Time
V	Volume
WT	Wild-type
ε	Extinction coefficient
Φ	the fraction of the fluorescence transmitted by the detection set
κ^2	Orientation factor
λ	Wavelength
λ_{em}	Emission wavelength
λ_{ex}	Excitation wavelength
λ_{max}	Emission maximum
τ	Fluorescence lifetime / Decay time
τ_D	Donor decay time

Bibliography

[1] A. M. Stock, V. L. Robinson, and P. N. Goudreau. Two-component signal transduction. *Annu. Rev. Biochem.*, 69:183–215, 2000.

[2] A. H. West and A. M. Stock. Histidine kinases and response regulator proteins in two-component signaling systems. *Trends Biochem Sci*, 26(6):369–376, Jun 2001.

[3] T. Mascher, J. D. Helmann, and G. Unden. Stimulus perception in bacterial signal-transducing histidine kinases. *Microbiol. Mol. Biol. Rev.*, 70(4):910–938, Dec 2006.

[4] M.Y. Galperin and M. Gomelsky. Bacterial Signal Transduction Modules: from Genomics to Biology. *ASM News*, 71:326–333, 2005.

[5] M. T. Laub and M. Goulian. Specificity in two-component signal transduction pathways. *Annu Rev Genet*, 41:121–145, 2007.

[6] E. Zientz, J. Bongaerts, and G. Unden. Fumarate regulation of gene expression in Escherichia coli by the DcuSR (dcuSR genes) two-component regulatory system. *J. Bacteriol.*, 180(20):5421–5425, Oct 1998.

[7] A. E. Abo-Amer, J. Munn, K. Jackson, M. Aktas, P. Golby, D. J. Kelly, and S. C. Andrews. DNA interaction and phosphotransfer of the C4-dicarboxylate-responsive DcuS-DcuR two-component regulatory system from Escherichia coli. *J. Bacteriol.*, 186(6):1879–1889, Mar 2004.

[8] I. G. Janausch, I. Garcia-Moreno, D. Lehnen, Y. Zeuner, and G. Unden. Phosphorylation and DNA binding of the regulator DcuR of the fumarate-responsive two-component system DcuSR of Escherichia coli. *Microbiology*, 150(Pt 4):877–883, Apr 2004.

[9] I. G. Janausch, I. Garcia-Moreno, and G. Unden. Function of DcuS from Escherichia coli as a fumarate-stimulated histidine protein kinase in vitro. *J Biol Chem*, 277(42):39809–39814, Oct 2002.

[10] B. L. Taylor and I. B. Zhulin. PAS domains: internal sensors of oxygen, redox potential, and light. *Microbiol Mol Biol Rev*, 63(2):479–506, Jun 1999.

[11] M. H. Hefti, K.-J. Francoijs, S. C. de Vries, R. Dixon, and J. Vervoort. The PAS fold. A redefinition of the PAS domain based upon structural prediction. *Eur J Biochem*, 271(6):1198–1208, Mar 2004.

[12] T. N. Parac, B. Coligaev, E. Zientz, G. Unden, W. Pet, and C. Griesinger. Assignment of 1H, 13C and 15N resonances to the sensory domain of the membraneous two-component fumarate sensor (histidine protein kinase) DcuS of Escherichia coli. *J Biomol NMR*, 19(1):91–92, Jan 2001.

[13] L. Pappalardo, I. G. Janausch, V. Vijayan, E. Zientz, J. Junker, W. Peti, M. Zweckstetter, G. Unden, and C. Griesinger. The NMR structure of the sensory domain of the membranous two-component fumarate sensor (histidine protein kinase) DcuS of Escherichia coli. *J Biol Chem*, 278(40):39185–39188, Oct 2003.

[14] J. Cheung and W. A. Hendrickson. Crystal structures of C4-dicarboxylate ligand complexes with sensor domains of histidine kinases DcuS and DctB. *J Biol Chem*, Aug 2008.

[15] H. Kneuper, I. G. Janausch, V. Vijayan, M. Zweckstetter, V. Bock, C. Griesinger, and G. Unden. The nature of the stimulus and of the fumarate binding site of the fumarate sensor DcuS of Escherichia coli. *J Biol Chem*, 280(21):20596–20603, May 2005.

[16] J. Krämer, J. D. Fischer, E. Zientz, V. Vijayan, C. Griesinger, A. Lupas, and G. Unden. Citrate sensing by the C4-dicarboxylate/citrate sensor kinase DcuS of Escherichia coli: binding site and conversion of DcuS to a C4-dicarboxylate- or citrate-specific sensor. *J. Bacteriol.*, 189(11):4290–4298, Jun 2007.

[17] T. Tanaka, S. K. Saha, C. Tomomori, R. Ishima, D. Liu, K. I. Tong, H. Park, R. Dutta, L. Qin, M. B. Swindells, T. Yamazaki, A. M. Ono, M. Kainosho, M. Inouye, and M. Ikura. NMR structure of the histidine kinase domain of the E. coli osmosensor EnvZ. *Nature*, 396(6706):88–92, Nov 1998.

[18] A. Marina, C. D. Waldburger, and W. A. Hendrickson. Structure of the entire cytoplasmic portion of a sensor histidine-kinase protein. *EMBO J.*, 24(24):4247–4259, Dec 2005.

[19] M. Etzkorn, H. Kneuper, P. Dünnwald, V. Vijayan, J. Krämer, C. Griesinger,

S. Becker, G. Unden, and M. Baldus. Plasticity of the PAS domain and a potential role for signal transduction in the histidine kinase DcuS. *Nat Struct Mol Biol*, Sep 2008.

[20] I. G. Janausch, E. Zientz, Q. H. Tran, A. Kröger, and G. Unden. C4-dicarboxylate carriers and sensors in bacteria. *Biochim. Biophys. Acta*, 1553(1-2):39–56, Jan 2002.

[21] B. L. Wanner. Is cross regulation by phosphorylation of two-component response regulator proteins important in bacteria? *J Bacteriol*, 174(7):2053–2058, Apr 1992.

[22] K. Yamamoto, K. Hirao, T. Oshima, H. Aiba, R. Utsumi, and A. Ishihama. Functional characterization in vitro of all two-component signal transduction systems from Escherichia coli. *J Biol Chem*, 280(2):1448–1456, Jan 2005.

[23] E.-B. Goh, P. J. Bledsoe, L.-L. Chen, P. Gyaneshwar, V. Stewart, and M. M. Igo. Hierarchical control of anaerobic gene expression in Escherichia coli K-12: the nitrate-responsive NarX-NarL regulatory system represses synthesis of the fumarate-responsive DcuS-DcuR regulatory system. *J. Bacteriol.*, 187(14):4890–4899, Jul 2005.

[24] T. Oyamada, K. Yokoyama, M. Morinaga, M. Suzuki, and K. Makino. Expression of Escherichia coli DcuS-R two-component regulatory system is regulated by the secondary internal promoter which is activated by CRP-cAMP. *J Microbiol*, 45(3):234–240, Jun 2007.

[25] P. Golby, S. Davies, D. J. Kelly, J. R. Guest, and S. C. Andrews. Identification and characterization of a two-component sensor-kinase and response-regulator system (DcuS-DcuR) controlling gene expression in response to C4-dicarboxylates in Escherichia coli. *J. Bacteriol.*, 181(4):1238–1248, Feb 1999.

[26] S. Kaspar, R. Perozzo, S. Reinelt, M. Meyer, K. Pfister, L. Scapozza, and M. Bott. The periplasmic domain of the histidine autokinase CitA functions as a highly specific citrate receptor. *Mol. Microbiol.*, 33(4):858–872, Aug 1999.

[27] S. Kaspar and M. Bott. The sensor kinase CitA (DpiB) of Escherichia coli functions as a high-affinity citrate receptor. *Arch Microbiol*, 177(4):313–321, Apr 2002.

[28] S. Reinelt, E. Hofmann, T. Gerharz, M. Bott, and D. R. Madden. The structure of the periplasmic ligand-binding domain of the sensor kinase CitA reveals the first extracellular PAS domain. *J Biol Chem*, 278(40):39189–39196, Oct 2003.

[29] M. Sevvana, V. Vijayan, M. Zweckstetter, S. Reinelt, D. R. Madden, R. Herbst-Irmer, G. M. Sheldrick, M. Bott, C. Griesinger, and S. Becker. A Ligand-Induced Switch in the Periplasmic Domain of Sensor Histidine Kinase CitA. *J Mol Biol*, Jan 2008.

[30] J. Cheung, C. A. Bingman, M. Reyngold, W. A. Hendrickson, and C. D. Waldburger. Crystal Structure of a Functional Dimer of the PhoQ Sensor Domain. *J Biol Chem*, 283(20):13762–13770, May 2008.

[31] Y.-F. Zhou, B. Nan, J. Nan, Q. Ma, S. Panjikar, Y.-H. Liang, Y. Wang, and X.-D. Su. C(4)-Dicarboxylates Sensing Mechanism Revealed by the Crystal Structures of DctB Sensor Domain. *J Mol Biol*, Aug 2008.

[32] I. G. Janausch, O. B. Kim, and G. Unden. DctA- and Dcu-independent transport of succinate in Escherichia coli: contribution of diffusion and of alternative carriers. *Arch Microbiol*, 176(3):224–230, Sep 2001.

[33] S. J. Davies, P. Golby, D. Omrani, S. A. Broad, V. L. Harrington, J. R. Guest, D. J. Kelly, and S. C. Andrews. Inactivation and regulation of the aerobic C(4)-dicarboxylate transport (dctA) gene of Escherichia coli. *J. Bacteriol.*, 181(18):5624–5635, Sep 1999.

[34] A. L. Perraud, K. Rippe, M. Bantscheff, M. Glocker, M. Lucassen, K. Jung, W. Sebald, V. Weiss, and R. Gross. Dimerization of signalling modules of the EvgAS and BvgAS phosphorelay systems. *Biochim Biophys Acta*, 1478(2):341–354, May 2000.

[35] C. Shi, M. Paige, J. Maley, and M. C. Loewen. In vitro characterization of ligand-induced oligomerization of the S. cerevisiae G-protein coupled receptor, Ste2p. *Biochim Biophys Acta*, Oct 2008.

[36] W. Vollmer, M. von Rechenberg, and J. V. Höltje. Demonstration of molecular interactions between the murein polymerase PBP1B, the lytic transglycosylase MltA, and the scaffolding protein MipA of Escherichia coli. *J Biol Chem*, 274(10):6726–6734, Mar 1999.

[37] R. J. F. Haft, E. G. Gachelet, T. Nguyen, L. Toussaint, D. Chivian, and

B. Traxler. In Vivo Oligomerization of the F Conjugative Coupling Protein TraD? *Journal of Bacteriology*, 189(18):6626–6634, 2007.

[38] D. Hilger, H. Jung, E. Padan, C. Wegener, K.-P. Vogel, H.-J. Steinhoff, and G. Jeschke. Assessing oligomerization of membrane proteins by four-pulse DEER: pH-dependent dimerization of NhaA Na+/H+ antiporter of E. coli. *Biophys J*, 89(2):1328–1338, Aug 2005.

[39] B. N. G. Giepmans, S. R Adams, M. H. Ellisman, and R. Y. Tsien. The fluorescent toolbox for assessing protein location and function. *Science*, 312(5771):217–224, Apr 2006.

[40] N. C. Shaner, P. A. Steinbach, and R. Y. Tsien. A guide to choosing fluorescent proteins. *Nat Methods*, 2(12):905–909, Dec 2005.

[41] O. Shimomura, F. H. Johnson, and Y. Saiga. Extraction, purification and properties of aequorin, a bioluminescent protein from the luminous hydromedusan, Aequorea. *J Cell Comp Physiol*, 59:223–239, Jun 1962.

[42] M. Chalfie, Y. Tu, G. Euskirchen, W. W. Ward, and D. C. Prasher. Green fluorescent protein as a marker for gene expression. *Science*, 263(5148):802–805, Feb 1994.

[43] R. Y. Tsien. The green fluorescent protein. *Annu Rev Biochem*, 67:509–544, 1998.

[44] F. Yang, L. G. Moss, and G. N. Phillips. The molecular structure of green fluorescent protein. *Nat Biotechnol*, 14(10):1246–1251, Oct 1996.

[45] M. Ormö, A. B. Cubitt, K. Kallio, L. A. Gross, R. Y. Tsien, and S. J. Remington. Crystal structure of the Aequorea victoria green fluorescent protein. *Science*, 273(5280):1392–1395, Sep 1996.

[46] G. H. Patterson, D. W. Piston, and B. G. Barisas. Förster distances between green fluorescent protein pairs. *Anal. Biochem.*, 284(2):438–440, Sep 2000.

[47] J. R. Lakowicz. *Principles of Fluorescence Spectroscopy. 3rd*. Plenum, New York, 2006.

[48] G. W. Gordon, G. Berry, X. H. Liang, B. Levine, and B. Herman. Quantitative fluorescence resonance energy transfer measurements using fluorescence microscopy. *Biophys. J.*, 74(5):2702–2713, May 1998.

[49] B. D. Adair and D. M. Engelman. Glycophorin A helical transmembrane

domains dimerize in phospholipid bilayers: a resonance energy transfer study. *Biochemistry*, 33(18):5539–5544, May 1994.

[50] B. H. Meyer, J.-M. Segura, K. L. Martinez, R. Hovius, N. George, K. Johnsson, and H. Vogel. FRET imaging reveals that functional neurokinin-1 receptors are monomeric and reside in membrane microdomains of live cells. *Proc. Natl. Acad. Sci. U. S. A.*, 103(7):2138–2143, Feb 2006.

[51] G. Hinze, R. Métivier, F. Nolde, K. Müllen, and Th Basché. Intramolecular electronic excitation energy transfer in donor/acceptor dyads studied by time and frequency resolved single molecule spectroscopy. *J Chem Phys*, 128(12):124516, Mar 2008.

[52] C. Yanisch-Perron, J. Vieira, and J. Messing. Improved M13 phage cloning vectors and host strains: nucleotide sequences of the M13mp18 and pUC19 vectors. *Gene*, 33(1):103–119, 1985.

[53] P. Scheu, S. Sdorra, Y.-F. Liao, M. Wegner, T. Basché, G. Unden, and W. Erker. Polar accumulation of the metabolic sensory histidine kinases DcuS and CitA in Escherichia coli. *Microbiology*, 154(Pt 8):2463–2472, Aug 2008.

[54] D. Kentner, S. Thiem, M. Hildenbeutel, and V. Sourjik. Determinants of chemoreceptor cluster formation in Escherichia coli. *Mol Microbiol*, 61(2):407–417, Jul 2006.

[55] J. Sambrook, E.F. Fritsch, and T. Maniatis. *Molecular cloning: a laboratory manual*. Cold Spring Harbor Laboratory Press, Cold Spring Harbor, NY, 1989.

[56] U. K. Laemmli. Cleavage of structural proteins during the assembly of the head of bacteriophage T4. *Nature*, 227(5259):680–685, Aug 1970.

[57] H. Towbin, T. Staehelin, and J. Gordon. Electrophoretic transfer of proteins from polyacrylamide gels to nitrocellulose sheets: procedure and some applications. *Proc Natl Acad Sci U S A*, 76(9):4350–4354, Sep 1979.

[58] R. P. Haugland. *The Handbook: A Guide to Fluorescent Probes and Labeling Technologies*. Molecular Probes, 10th edition, 2005.

[59] Institute of Nuclear Research of the Hungarian Academy of Sciences (ATOMKI). Pulse-Loss Corrections. `http://www.atomki.hu/atomki/Electr/deadtime.htm`.

[60] Association of Universities for Research in Astronomy. Calibration Algorithms. http://www.stsci.edu/documents/dhb/webvol2/c16_hspcalib.fm3.html.

[61] N. Billinton and A. W. Knight. Seeing the wood through the trees: a review of techniques for distinguishing green fluorescent protein from endogenous autofluorescence. *Anal Biochem*, 291(2):175–197, Apr 2001.

[62] Anne Boos. Spektroskopische Untersuchung der Rylenfarbstoffe Perylendiimid und Perylenmonoimid: Bestimmung der Fluoreszenzquantenausbeuten. Wahlpflichtmodul Physikalische Chemie: Optische Spektroskopie und Mikroskopie, 2007.

[63] Florian A. Feist. Spektroskopische Charakterisierung von bi- und multichromophoren Rylenfarbstoffen - Bestimmung von Fluoreszenzquantenausbeuten. Wahlpflichtmodul Physikalische Chemie: Optische Spektroskopie und Mikroskopie, 2005.

[64] N. Panchuk-Voloshina, R. P. Haugland, J. Bishop-Stewart, M. K. Bhalgat, P. J. Millard, F. Mao, W. Y. Leung, and R. P. Haugland. Alexa dyes, a series of new fluorescent dyes that yield exceptionally bright, photostable conjugates. *J Histochem Cytochem*, 47(9):1179–1188, Sep 1999.

[65] R.Y. Tsien, A. Waggoner, and JB Pawley. *Handbook of Biological Confocal Microscopy*. Plenum Press, New York, 1995.

[66] G. Patterson, R. N. Day, and D. Piston. Fluorescent protein spectra. *J Cell Sci*, 114(Pt 5):837–838, Mar 2001.

[67] L. Stryer, J. M. Berg, and J. L. Tymoczko. *Biochemistry*. W.H.Freeman, 5th edition, 2002.

[68] L. M. Guzman, D. Belin, M. J. Carson, and J. Beckwith. Tight regulation, modulation, and high-level expression by vectors containing the arabinose PBAD promoter. *J Bacteriol*, 177(14):4121–4130, Jul 1995.

[69] R. S. Armen, O. D. Uitto, and S. E. Feller. Phospholipid component volumes: determination and application to bilayer structure calculations. *Biophys J*, 75(2):734–744, Aug 1998.

[70] I. C. Koo and R. S. Stephens. A developmentally regulated two-component signal transduction system in Chlamydia. *J Biol Chem*, 278(19):17314–17319, May 2003.

[71] I. L. Budyak, V. Pipich, O. S. Mironova, R. Schlesinger, G. Zaccai, and J. Klein-Seetharaman. Shape and oligomerization state of the cytoplasmic domain of the phototaxis transducer II from Natronobacterium pharaonis. *Proc Natl Acad Sci U S A*, 103(42):15428–15433, Oct 2006.

[72] V. L. Robinson, D. R. Buckler, and A. M. Stock. A tale of two components: a novel kinase and a regulatory switch. *Nat. Struct. Biol.*, 7(8):626–633, Aug 2000.

[73] B. J. Feilmeier, G. Iseminger, D. Schroeder, H. Webber, and G. J. Phillips. Green fluorescent protein functions as a reporter for protein localization in Escherichia coli. *J Bacteriol*, 182(14):4068–4076, Jul 2000.

[74] N. C. Shaner, G. H. Patterson, and M. W. Davidson. Advances in fluorescent protein technology. *J Cell Sci*, 120(Pt 24):4247–4260, Dec 2007.

[75] S. B. VanEngelenburg and A. E. Palmer. Fluorescent biosensors of protein function. *Curr Opin Chem Biol*, 12(1):60–65, Feb 2008.

[76] V. Sourjik and H. C. Berg. Localization of components of the chemotaxis machinery of Escherichia coli using fluorescent protein fusions. *Mol Microbiol*, 37(4):740–751, Aug 2000.

[77] P. J. Verveer, F. S. Wouters, A. R. Reynolds, and P. I. Bastiaens. Quantitative imaging of lateral ErbB1 receptor signal propagation in the plasma membrane. *Science*, 290(5496):1567–1570, Nov 2000.

[78] A. Periasamy, M. Elangovan, E. Elliott, and D. L. Brautigan. Fluorescence lifetime imaging (FLIM) of green fluorescent fusion proteins in living cells. *Methods Mol Biol*, 183:89–100, 2002.

[79] A. K. Kenworthy. Imaging protein-protein interactions using fluorescence resonance energy transfer microscopy. *Methods*, 24(3):289–296, Jul 2001.

[80] T. Zal and N. R. J. Gascoigne. Photobleaching-corrected FRET efficiency imaging of live cells. *Biophys J*, 86(6):3923–3939, Jun 2004.

[81] Y. Gu, W. L. Di, D. P. Kelsell, and D. Zicha. Quantitative fluorescence resonance energy transfer (FRET) measurement with acceptor photobleaching and spectral unmixing. *J. Microsc.*, 215(Pt 2):162–173, Aug 2004.

[82] S. Angers, A. Salahpour, E. Joly, S. Hilairet, D. Chelsky, M. Dennis, and M. Bouvier. Detection of beta 2-adrenergic receptor dimerization in living

cells using bioluminescence resonance energy transfer (BRET). *Proc Natl Acad Sci U S A*, 97(7):3684–3689, Mar 2000.

[83] C.-D. Hu, Y. Chinenov, and T. K. Kerppola. Visualization of interactions among bZIP and Rel family proteins in living cells using bimolecular fluorescence complementation. *Mol Cell*, 9(4):789–798, Apr 2002.

[84] J. Lippincott-Schwartz, E. Snapp, and A. Kenworthy. Studying protein dynamics in living cells. *Nat Rev Mol Cell Biol*, 2(6):444–456, Jun 2001.

[85] S. S. Vogel, C. Thaler, and S. V. Koushik. Fanciful FRET. *Sci. STKE*, 2006(331):re2, Apr 2006.

[86] H. Wallrabe, M. Elangovan, A. Burchard, A. Periasamy, and M. Barroso. Confocal FRET microscopy to measure clustering of ligand-receptor complexes in endocytic membranes. *Biophys J*, 85(1):559–571, Jul 2003.

[87] H. Wallrabe, Y. Chen, A. Periasamy, and M. Barroso. Issues in confocal microscopy for quantitative FRET analysis. *Microsc Res Tech*, 69(3):196–206, Mar 2006.

[88] Z. Xia and Y. Liu. Reliable and global measurement of fluorescence resonance energy transfer using fluorescence microscopes. *Biophys. J.*, 81(4):2395–2402, Oct 2001.

[89] M. G. Erickson, B. A. Alseikhan, B. Z. Peterson, and D. T. Yue. Preassociation of calmodulin with voltage-gated Ca(2+) channels revealed by FRET in single living cells. *Neuron*, 31(6):973–985, Sep 2001.

[90] C. Berney and G. Danuser. FRET or no FRET: a quantitative comparison. *Biophys. J.*, 84(6):3992–4010, Jun 2003.

[91] J. van Rheenen, M. Langeslag, and K. Jalink. Correcting confocal acquisition to optimize imaging of fluorescence resonance energy transfer by sensitized emission. *Biophys. J.*, 86(4):2517–2529, Apr 2004.

[92] V. Raicu, D. B. Jansma, R. J. Dwayne Miller, and J. D. Friesen. Protein interaction quantified in vivo by spectrally resolved fluorescence resonance energy transfer. *Biochem. J.*, 385(Pt 1):265–277, Jan 2005.

[93] J. Wlodarczyk, A. Woehler, F. Kobe, E. Ponimaskin, A. Zeug, and E. Neher. Analysis of FRET signals in the presence of free donors and acceptors. *Biophys J*, 94(3):986–1000, Feb 2008.

[94] A. Hoppe, K. Christensen, and J. A. Swanson. Fluorescence resonance energy transfer-based stoichiometry in living cells. *Biophys. J.*, 83(6):3652–3664, Dec 2002.

[95] P. Nagy, L. Bene, W. C. Hyun, G. Vereb, M. Braun, C. Antz, J. Paysan, S. Damjanovich, J. W. Park, and J. Szöllsi. Novel calibration method for flow cytometric fluorescence resonance energy transfer measurements between visible fluorescent proteins. *Cytometry A*, 67(2):86–96, Oct 2005.

[96] H. Chen, H. L. Puhl, S. V. Koushik, S. S. Vogel, and S. R. Ikeda. Measurement of FRET efficiency and ratio of donor to acceptor concentration in living cells. *Biophys. J.*, 91(5):L39–L41, Sep 2006.

[97] D. Chorvat, J. Kirchnerova, M. Cagalinec, J. Smolka, A. Mateasik, and A. Chorvatova. Spectral unmixing of flavin autofluorescence components in cardiac myocytes. *Biophys J*, 89(6):L55–L57, Dec 2005.

[98] P. Nagy, G. Vámosi, A. Bodnár, S. J. Lockett, and J. Szöllösi. Intensity-based energy transfer measurements in digital imaging microscopy. *Eur Biophys J*, 27(4):377–389, 1998.

[99] P. S. Salonikidis, A. Zeug, F. Kobe, E. Ponimaskin, and D. W. Richter. Quantitative Measurement of cAMP Concentration Using an Exchange Protein Directly Activated by a cAMP-Based FRET-Sensor. *Biophys J*, 95(11):5412–5423, Dec 2008.

[100] M. Li, L. G. Reddy, R. Bennett, N. D. Silva, L. R. Jones, and D. D. Thomas. A fluorescence energy transfer method for analyzing protein oligomeric structure: application to phospholamban. *Biophys. J.*, 76(5):2587–2599, May 1999.

[101] E. Biener, M. Charlier, V. K. Ramanujan, N. Daniel, A. Eisenberg, C. Bjorbaek, B. Herman, A. Gertler, and J. Djiane. Quantitative FRET imaging of leptin receptor oligomerization kinetics in single cells. *Biol. Cell.*, 97(12):905–919, Dec 2005.

[102] K. D. G. Pfleger and K. A Eidne. Monitoring the formation of dynamic G-protein-coupled receptor-protein complexes in living cells. *Biochem J*, 385(Pt 3):625–637, Feb 2005.

[103] V. Balannik, R. A. Lamb, and L. H. Pinto. The oligomeric state of the active BM2 ion channel protein of influenza B virus. *J Biol Chem*, 283(8):4895–4904, Feb 2008.

[104] F. Kobe, U. Renner, A. Woehler, J. Wlodarczyk, E. Papusheva, G. Bao, A. Zeug, D. W. Richter, E. Neher, and E. Ponimaskin. Stimulation- and palmitoylation-dependent changes in oligomeric conformation of serotonin 5-HT1A receptors. *Biochim Biophys Acta*, 1783(8):1503–1516, Aug 2008.

[105] G. N. Phillips. Structure and dynamics of green fluorescent protein. *Curr Opin Struct Biol*, 7(6):821–827, Dec 1997.

[106] D. A. Zacharias, J. D. Violin, A. C. Newton, and R. Y. Tsien. Partitioning of lipid-modified monomeric GFPs into membrane microdomains of live cells. *Science*, 296(5569):913–916, May 2002.

[107] A. Rekas, J.-R. Alattia, T. Nagai, A. Miyawaki, and M. Ikura. Crystal structure of venus, a yellow fluorescent protein with improved maturation and reduced environmental sensitivity. *J Biol Chem*, 277(52):50573–50578, Dec 2002.

[108] B. R. Terry, E. K. Matthews, and J. Haseloff. Molecular characterisation of recombinant green fluorescent protein by fluorescence correlation microscopy. *Biochem Biophys Res Commun*, 217(1):21–27, Dec 1995.

[109] C. Tomomori, T. Tanaka, R. Dutta, H. Park, S. K. Saha, Y. Zhu, R. Ishima, D. Liu, K. I. Tong, H. Kurokawa, H. Qian, M. Inouye, and M. Ikura. Solution structure of the homodimeric core domain of Escherichia coli histidine kinase EnvZ. *Nat Struct Biol*, 6(8):729–734, Aug 1999.

[110] A. M. Bilwes, L. A. Alex, B. R. Crane, and M. I. Simon. Structure of CheA, a signal-transducing histidine kinase. *Cell*, 96(1):131–141, Jan 1999.

[111] P. M. Wolanin, P. A. Thomason, and J. B. Stock. Histidine protein kinases: key signal transducers outside the animal kingdom. *Genome Biol*, 3(10):REVIEWS3013, Sep 2002.

[112] A. Khorchid, M. Inouye, and M. Ikura. Structural characterization of Escherichia coli sensor histidine kinase EnvZ: the periplasmic C-terminal core domain is critical for homodimerization. *Biochem J*, 385(Pt 1):255–264, Jan 2005.

[113] R. Heermann, K. Altendorf, and K. Jung. The turgor sensor KdpD of Escherichia coli is a homodimer. *Biochim Biophys Acta*, 1415(1):114–124, Dec 1998.

[114] M. B. Neiditch, M. J. Federle, A. J. Pompeani, R. C. Kelly, D. L. Swem, P. D.

Jeffrey, B. L. Bassler, and F. M Hughson. Ligand-induced asymmetry in histidine sensor kinase complex regulates quorum sensing. *Cell*, 126(6):1095–1108, Sep 2006.

[115] S. Q. Pan, T. Charles, S. Jin, Z. L. Wu, and E. W. Nester. Preformed dimeric state of the sensor protein VirA is involved in plant–Agrobacterium signal transduction. *Proc Natl Acad Sci U S A*, 90(21):9939–9943, Nov 1993.

[116] S. D. Goldberg, C. S. Soto, C. D. Waldburger, and W. F. Degrado. Determination of the physiological dimer interface of the PhoQ sensor domain. *J Mol Biol*, 379(4):656–665, Jun 2008.

[117] J. J. E. Bijlsma and E. A. Groisman. Making informed decisions: regulatory interactions between two-component systems. *Trends Microbiol*, 11(8):359–366, Aug 2003.

[118] E. Batchelor, D. Walthers, L. J. Kenney, and M. Goulian. The Escherichia coli CpxA-CpxR envelope stress response system regulates expression of the porins ompF and ompC. *J Bacteriol*, 187(16):5723–5731, Aug 2005.

[119] Y. Eguchi and R. Utsumi. A novel mechanism for connecting bacterial two-component signal-transduction systems. *Trends Biochem. Sci.*, 30(2):70–72, Feb 2005.

[120] A. Kato, A. Y. Mitrophanov, and E. A. Groisman. A connector of two-component regulatory systems promotes signal amplification and persistence of expression. *Proc Natl Acad Sci U S A*, 104(29):12063–12068, Jul 2007.

[121] M. Meyer, P. Dimroth, and M. Bott. In vitro binding of the response regulator CitB and of its carboxy-terminal domain to A + T-rich DNA target sequences in the control region of the divergent citC and citS operons of Klebsiella pneumoniae. *J Mol Biol*, 269(5):719–731, Jun 1997.

Publications and Presentations

P. Scheu, S. Sdorra, **Y.-F. Liao**, Wegner M., T. Basché, G. Unden, W. Erker
Polar accumulation of the metabolic sensory histidine kinases DcuS and CitA in *Escherichia coli*.
Microbiology, 2008, 154, 2463-72

Y.-F. Liao, P. Scheu, W. Erker, G. Unden, T. Basché
Oligomerization of Fumarate Sensor DcuS in *Escherichia coli* investigated with Quantitative FRET Spectroscopy.
manuscript in preparation

Posters

Y.-F. Liao, P. Scheu, W. Erker, G. Unden, T. Basché
Oligomerization of Fumarate Sensor DcuS in *Escherichia coli*.
Annual Meeting of the German Biophysical Society, Mainz, Germany
September 24-27, 2006

S. Sdorra, P. Scheu, **Y.-F. Liao**, G. Unden, T. Basché, W. Erker
Polar localisation of the fumarate sensory kinase DcuS in *Escherichia coli*.
Annual Meeting of the German Biophysical Society, Mainz, Germany
September 24-27, 2006

P. Scheu, W. Erker, S. Sdorra, **Y.-F. Liao**, T. Basché, G. Unden
Polar localization of the C_4-Dicarboxylate sensor DcuS in *E. coli*.
27th Symposium on Mechanisms of Gene Regulation, Burg Ludwigstein, Germany
October 10-12, 2008

J. Bauer, W. Erker, **Y.-F. Liao**, T. Basché, G. Unden
DctA of *Escherichia coli* interacts with the DcuSR two component system.
General and Applied Microbiology (VAAM). Bochum, Germany
March 8-11, 2009